TWO DIMENSIONAL TRANSPORT COEFFICIENTS FOR THE PWR'S THERMAL/HYDRAULIC ANALYSIS

by

CHONG CHIU

Bachelor of Science
Tsing-hua University
Taiwan (Republic of China)

(1974)

Submitted in Partial Fulfillment of
the Requirements for the
Degree of Master of Science

at the

MASSACHUSETTS INSTITUTE OF TECHNOLOGY

(May, 1976)

Signature of Author _____
Department of Nuclear Engineering,
May, 1976

Certified by _____
Thesis Supervisor

Accepted by _____
Chairman, Departmental Committee on Graduate Students

TWO DIMENSIONAL TRANSPORT COEFFICIENTS FOR THE PWR'S THERMAL/HYDRAULIC ANALYSIS

by

Chong Chiu

Submitted to the Department of Nuclear Engineering, May 1976, in partial fulfillment of the requirements for the Degree of Master of Science.

ABSTRACT

For typical PWR open lattice core configurations, detailed core analyses are performed in a cascade fashion. In this approach, crossflows between fuel assemblies are first determined by treating each fuel assembly as a homogenized region and these crossflows are subsequently imposed as boundary conditions in the subchannel analysis of the hot assembly. The common requirement of these procedures is for transport or coupling coefficients to represent exchange in momentum and energy between the homogenized regions. These coefficients are developed from the conservation equations and examined in this thesis.

Thesis Supervisor: Neil E. Todreas

Title: Professor of Nuclear Engineering

ACKNOWLEDGEMENTS

The author wishes to express his sincere gratitude to all people who assisted him during the preparation of this thesis. In particular, to the following people:

Professor Neil E. Todreas, who, as my thesis advisor, has so generously given his time and advice. His valuable guidance and careful thought have contributed much to this work and are sincerely appreciated.

Mr. Robert W. Bowring for his valuable assistance and advice on the problems that occurred during the preparation of this thesis.

To Pablo Moreno for his helpful suggestions and comments on Appendix B and during the course of this work.

To Mrs. Lynda DuVall and Ms. Irene Battalen who patiently typed this thesis.

To my wife, Wendy, for her encouragement through the period of this work.

This work was initiated under the sponsorship of the Electric Power Research Institute. It was completed as part of the Nuclear Reactor Safety Research Program under the Electric Power Program sponsored by New England Electric System and Northeast Utilities Service Company.

TABLE OF CONTENTS

TABLE OF CONTENTS(continued)

TABLE OF CONTENTS(continued)

LIST OF FIGURES

LIST OF FIGURES(continued)

LIST OF TABLES

LIST OF APPENDICES

LIST OF APPENDICES(continued)

NOMENCLATURE

A_i	cross-section area for subchannels i, (L^2)
A_s	cross-section area for any subchannel (L^2)
A_k	cross-section area for homogenized subchannels k (L^2)
$c_{i,j}$	thermal conduction coefficient for subchannels i and j $(H/T\theta L)$
$C_{L,R}$	thermal conduction coefficient for homogenized subchannels L and R $(H/T\theta L)$
c_i	crossflow friction force for subchannel i (F)
C	crossflow friction force for homogenized subchannels (F)
Δx	axial elevation increment, (L)
$\Delta \dagger h$	axial change of radially averaged enthalpy in the multi-subchannel representation, (H)
ΔH	axial change of radially averaged enthalpy in the homogenized representation, (H)
F	axial friction force per unit length (F/L)
F_R	Flow ratio
$\overline{F}$	average flow rate
g	gravitational constant, (L/T^2)
g_i	mass flux of channel i
$\overline{G}$	averaged mass flux
h_i	enthalpy for subchannel i, (H)

h^*	effective enthalpy carried by diversion crossflow (H)
$\overline{h}_k$	radially averaged multi-subchannel enthalpy, (H)
H_k	homogenized enthalpy for region k, (H)
H_R	inlet enthalpy ratio
K	crossflow resistance coefficient
L	channel length, (L)
m_i	flow rate for subchannel i (M/T)
M_k	flow rate for homogenized region k, (M/T)
N	Total number of subchannels
$N_H, N_U, N_{TP}, N_{TF}, N_{TU}$	coupling coefficients
$\overline{N}_H$	averaged coupling coefficient
N'	N/2 for N even
	$\frac{N}{2} + \frac{1}{2}$ for N odd
p_i	pressure for subchannel i (F/L^2)
P_k	pressure for homogenized region k (F/L^2)
P_R	power ratio
q'_i	heat addition per unit length, for subchannel i (H/L)
$\overline{q}$	averaged heat addition per unit length (H/L)
Q_k	heat addition per unit length for homogenized region k (H/L)
R_H, R_p	ratio of $\overline{N_H}$ in the FLOW UPSET CASE
S	rod spacing (L)
u^*	effective velocity carried by diversion
$\overline{u}$	effective averaged velocity for adjacent channels

u_i	effective momentum velocity for subchannel i, (L/T)
U_k	effective momentum velocity for homogenized region k, (L/T)
$\bar{U}$	effective averaged velocity for homogenized region L and R
$w_{i,j}$	diversion crossflow between adjacent subchannels (M/TL)
$W_{L,R}$	diversion crossflow between homogenized region L and R (M/TL)
$w'_{i,j}$	turbulent interchange between adjacent subchannels i and j (M/TL)
$W'_{L,R}$	turbulent interchange between adjacent homogenized region L and R (M/TL)
ρ^*	density carried by the diversion crossflow (M/L3)
β	turbulent mixing parameter

Subscripts

i	subchannel identification number
k	homogenized region identification number

Variables

J	axial elevation node along the subchannels

CHAPTER 1

INTRODUCTION

1.1 Background

Thermal hydraulic design studies of Pressurized Water Reactor (PWR) core performance are carried out using lumped parameter computational methods typified by the COBRA[1] and THINC[2] developments. In analyses of these cores the smallest homogenized segment is a subchannel which is characterized by properties of interest such as enthalpy, flow rate and pressure. For typical PWR open lattice core configurations, detailed core analyses are performed in a cascade fashion. In this approach, crossflows between fuel assemblies are first determined by treating each fuel assembly as a homogenized region and these crossflows are subsequently imposed as boundary conditions in the subchannel analysis of the hot assembly. Alternatively, some analyses are performed by representing the core by increasing coarsely homogenized regions around the hot subchannel of interest.

The common requirement of each of these procedures is for transport or coupling coefficients to represent exchange of momentum and energy between the homogenized regions. These coefficients are properly developed

when they produce properties in a homogenized region which are equivalent to those obtained by averaging local distributions of the same properties over the same region. The work of France and Ginsberg[3] and Ramm, Johannsen and Todreas[4] on developing transport coefficients for adjacent subchannels from local property distributions within a subchannel represents the solution to an analogous problem. In our case the smallest region is the subchannel so that our homogenized representation of the individual subchannels comprising an assembly becomes analogous to the earlier France et al. homogenized representation of the subchannel. However, as opposed to this previous work, in the case we now address, crossflows between subchannels exist and must be considered in the analysis.

1.2 General Problem Statement

We desired to represent a PWR assembly comprised of a square array of N by N rods as a single node in a corewide lumped parameter analysis. We seek those transport coefficients which when used in the lumped analysis will yield node enthalpies for all axial stations equivalent to those obtained by averaging the subchannel enthalpies over all subchannels comprising the single node. It is assumed that the axial enthalpy dis-

tribution of every subchannel in the N by N array is known. In our example we obtain this known distribution from analysis of the N by N assembly using arbitrary coefficients for interaction between subchannels. This known axial enthalpy distribution of course is ultimately to be derived from experiment. Interpretation of such experiments to yield coefficients and this known distribution is a topic separate from the task of this work.

1.3 Cases of Interest

Let us identify cases of interest and test the usefulness of our hypothesis in solving these cases.

a) Case 1: The prime case of interest is that of adjacent heated bundles with different linear power ratings and different inlet mass flow rates. Within each bundle the linear power and mass flow rate is taken constant. We identify this case as the POWER/FLOW UPSET CONDITION. This case has been studied for the condition leading to the maximum crossflow which occurs when the higher power and lower inlet flow exist together in the same bundle. Other variables in this case are the power and flow ratios between assemblies. These ratios were both taken as 1.2, the maximum anticipated in practice.

b) Case 2: A degenerate version of Case 1 is that of linear power upset but the same inlet mass flow to each assembly. This case was studied since crossflow is reduced versus Case 1 and is only due to radial enthalpy gradients between assemblies. This case is called the POWER UPSET CONDITION.

The following two non-prototypic reactor cases were also examined. These cases permitted almost complete separation of the enthalpy and crossflow effects. Additionally, they are of interest in themselves since experiments based on these cases may be performed since they are considerably less complex and costly than heated, multipin assembly tests. These cases are:

c) Case 3: Unheated rods with all subchannels in each of the two adjacent assemblies at a uniform inlet enthalpy. Each assembly however, has a different inlet enthalpy. Both assemblies have the same inlet mass flux to each subchannel. This case is called the ENTHALPY UPSET CONDITION.

d) Case 4: Same as Case 3 except the upset condition is in inlet mass flux plus the inlet enthalpy. This case is called the ENTHALPY/FLOW UPSET CONDITION.

For each case of interest, a range of bundle sizes, $N' = f(N)$ and subchannel mixing rates, β, were investi-

gated spanning the range of interest to PWR application. The input parameters K and S/L for the crossflow resistance and the control volume of the crossflow are kept constant as 0.5.

CHAPTER 2

METHODS OF PROBLEM SOLUTION

2.1 Detailed Problem Definition

Figure 1 illustrates a typical N by N assembly of interest (N odd) surrounded by neighboring assemblies. We develop a one dimensional solution by selecting adjacent strips of N' subchannels where for N odd, $N' = \frac{N}{2} + \frac{1}{2}$, the edge subchannel being half the size of the interior subchannels (for N even, $N' = \frac{N}{2}$ and the edge subchannel is equal to the interior subchannel). The selected adjacent strips shown in Figure 2 are assumed to be bounded by adiabatic, impervious boundaries. The homogenized representation of Figure 2 is shown in Figure 3 which has flow area, wetted perimeter, heat flux and mass flow equivalent to that of the strip of N' subchannels. It should be recognized that many equivalent pictorial homogenized representations satisfying these conditions are possible. However, since the following prescribed prediction technique does not utilize the distance between subchannel centroids of Figure 2, any equivalent pictorial representation can be adopted.

We require that at every axial position of the homogenized region, the total flow, the energy content and

the pressure drop from inlet should be the same as those obtainable by averaging the values of the individual subchannels. These conditions are met if the mass, heat and momentum transfer across the boundary between the adjacent strips at every axial position are the same in both cases. In calculating the boundary transport, we use subchannel values of the pressure and enthalpy differences in the multi-subchannel case but the difference in the averaged values in the homogenized representation.

For the homogenized representation calculation, we require a method of calculating the lateral transport in terms of what would have been the local parameter difference while knowing only the average differences.

2.2 Problem Solution by Analysis of the Differential Form of the Conservation Equations

We postulate that this can be accomplished by applying suitable coefficients to the terms in the conservation equations of the homogenized representation. The form of these coefficients which transform average (homogenized representation) parameter differences to local (multi-channel representation) differences are derived in Appendix A from the differential expression of the conservation equations. These forms are

$$N_H \equiv \frac{H_L - H_R}{h_C - h_D}$$

$$N_U \equiv \frac{U_L - U_R}{u_C - u_D}$$

$$N_{TU} \equiv \frac{\frac{\partial(\bar{U}W_{L,R})}{\partial x}}{\sum_{i=A}^{E} \frac{\left(\partial\ \bar{u}\ w_{i,i+1}\right)}{\partial x}}$$

$$N_{TP} \equiv \frac{P_L - P_R}{p_A - p_F}$$

$$N_{TF} = \frac{C}{\sum_{i=A}^{E} c_i} = \frac{\frac{W_{L,R}}{\rho^*_{L,R}}\ W_{L,R}}{\sum_{i=A}^{E} \frac{|w_{i,i+1}|\, w_{i,i+1}}{\rho^*_{i,i+1}}}$$

where ρ^* is the density of fluid at the donor channel for the diversion crossflow. (Refer to Figures 2 and 3 for subscripts A, B, C, D, E and F; L and R).

Appendix A further presents detailed formula for these coefficients in terms of parameters available from multi-channel analysis. In the remainder of thesis, we

a) assess the validity of these formula when analyses are made using the difference forms of the conservation equations used in COBRA IIIC,

b) utilize these formula to present recommended values of the coefficients for the 4 cases of Chapter 1 for a selected range of β and N',

c) assess the errors which still remain in homogenized representation results when these coefficients are employed.

2.3 Problem Solution by Analysis of the Difference (i.e. COBRA IIIC) Form of the Conservation Equations

For reactor analysis which is to be done by lumped channel methods, i.e., COBRA IIIC, difference approximations to the differential form of the conservation equations are employed. Appendix B, formulated with the assistance of Pablo Moreno, presents the conservation equations for both the multi-subchannel case and the homogenized representation in difference form. Unfortunately the complexity of these equations precludes the possibility of employing simple but exact coupling coefficients in the transverse momentum equations. However the simple, albeit approximate, forms of coupling coefficients summarized in the previous section, will

yield satisfactory results for most practical reactor conditions. The most limiting assumptions imposed in using these simple forms of coupling coefficients in the difference equations concern the diversion crossflow terms. Therefore, results utilizing these approximate coefficients for analysis of conditions of severe flow and/or power upset conditions can be in significant error.

Specifically from Appendix C these assumptions are:

a) Use of the following expression for h_C^* in the energy equation:

$$h^* = \frac{H_L + H_R}{2} + \frac{H_L - \frac{H_L + H_R}{2}}{N_H} \quad W_{L,R}>0 \qquad (2.3.1)$$

b) Use of the following expression for u_C^* in the axial momentum equation:

$$u^* = \frac{U_L + U_R}{2} + \frac{U_L - \frac{U_L + U_R}{2}}{N_U} \quad W_{L,R}>0 \qquad (2.3.2)$$

This assumption holds for the condition of symmetric enthalpy profile with respect to the boundary. If not, $\frac{H_L + H_R}{2}$ can not be regarded as the enthalpy at the boundary of two strips, L and R. Appendix C is written to show this asymmetric enthalpy feature around the boundary where diversion crossflow is large.

2.4 Proposed Approach of Utilizing Only One Coupling Coefficient

Study of these five coupling coefficients indicates that N_H is the most important in calculating the changes in enthalpy and axial velocity of the homogenized representation over the axial region of interest. Thus the method of solution can be further simplified by employing only one coupling coefficient, i.e., N_H. However, it is suggested that N_U, N_{TF} and N_{TU} be employed if the diversion crossflow plays an important role in the transverse energy transport between channels. For N less than 23 and flow ratio between assemblies at the inlet less than 1.2, the utilization of only one coupling coefficient (N_H) yields satisfactory results for all cases.

Current approaches for the lumped-parameter calculations either adopt $N_H = 1$ or $N_H = N$ (refer to Reference 5, pg. 276). Further, in these approaches the coupling coefficient is used only in the turbulent mixing component term of the energy equation. With the approach of using $N_H = 1$, the energy transport by the turbulent mixing and the diversion crossflow in the homogenized region calculation is highly exaggerated. Therefore, optimistic results for the axial enthalpy changes in the hot channel are to be expected. On the other hand,

use of $N_H = N$ can excessively suppress the energy transport by the turbulent mixing. Therefore in the case of $N_H = N$, results for axial enthalpy changes of the hot channels in the homogenized region calculation are expected to be conservative but the deviation of the lumped enthalpy change from the averaged values in the multi-subchannel calculation is still rather large with respect to the approach employing $N_H = 1$. However, with the linear enthalpy profile throughout the subchannels, N_H becomes N. (Refer to Appendix D for the derivation)

2.5 Assessment of Errors with the One Coefficient Approach

Since only one coupling coefficient (N_H) is used in our approach, deviations of the results in the homogenized region calculation from that in the multi-subchannel calculation are expected. The major reasons for these deviations are summarized below.

a) due to improper computation of the momentum and the energy carried by the diversion cross-flow through the boundary between homogenized regions, i.e., assumptions of equations (2.3.1) and (2.3.2),

b) due to the lack of a corrective method for

matching the homogenized region axial and transverse momentum to the standard values of the multichannel calculation, i.e., N_U, N_{TU}, N_{TF} and N_{TP} are not employed.

The general expectation for predictions using only N_H in the homogenized region calculation is discussed below under the specific cases of interest since the importance of N_H varies under different conditions, i.e., enthalpy upset, flow upset, power upset and power and flow upset. For the cases of small diversion crossflow, the importance of N_H can be studied by assuming there is no diversion crossflow through the boundary. In Appendix E a relation between the errors of the homogenized region axial enthalpy changes and the operational conditions, i.e., F_R, H_R, P_R, $\bar{q}'$ and β under the no crossflow condition has been derived. A qualitative study for the role of N_H under different conditions has been made in the following sections. It is convenient to study these cases in the order of ENTHALPY UPSET Case, ENTHALPY AND FLOW Case, POWER UPSET Case and POWER AND FLOW UPSET Case.

2.5.1 Unheated Cases

2.5.1.1 Enthalpy Upset Cases

Since there is no flow upset in this case, significant diversion crossflow does not occur. It is expected that good homogenized region enthalpy rise results can be obtained in this case by only employing N_H.

From the derivation in Appendix E, the error for the homogenized region axial enthalpy change using N_H = 1 of the hotter channel can be expressed as:

$$\text{ERROR} = (1 - \bar{N}_H) \qquad (C.9)$$

where $\bar{N}_H$ is the axially averaged N_H computed by our suggested method.

Since $\bar{N}_H$ is slightly proportional to the number of channels, i.e., N, and always larger than 1, the error is always negative and increases slightly as N increases. The negative error means the predicted hot channel exit enthalpies are always less than that in the multi-subchannel calculation.

If N_H = N is employed in the homogenized region calculation, the error for the homogenized region axial enthalpy change can be expressed as:

$$\text{ERROR} = (N - \bar{N}_H) \qquad (2.5.1.1)$$

which is always positive. Since $\bar{N}_H$ is usually less

than one third of N, it is expected that the error in the case of N_H = N is about two times larger than that in the case of N_H = 1.

The effect of β and H_R do not directly come into play. However, the error is expected to increase as β decreases. This is because the axial rise of the homogenized enthalpy decreases as β decreases.

2.5.1.2 Enthalpy and Flow Upset Case

The role of the diversion crossflow in this case is between that in the enthalpy upset case and that in the power and flow upset case. Therefore the error in the axial enthalpy changes is expected to lie between that in the enthalpy upset case and in the power and flow upset case.

Furthermore, the error for the axial enthalpy changes in the hot channel by employing N_H = 1 can be expressed in the same way as that in the enthalpy upset case. Therefore, N_H has the same importance as that in the enthalpy upset case.

2.5.2 Heated Cases

2.5.2.1 Power Upset Case

Axial enthalpy changes are due to three mechanisms: heat added from the rods, energy transport by

the turbulent interchange between channels and energy transport by the diversion crossflow between channels.

From equation E.14 in Appendix E, the error for the enthalpy change in hot channel by using $N_H = 1$ can be expressed as the following:

$$\text{ERROR} = \frac{\frac{1}{N_H} - 1}{\frac{P_R A_S N'}{(P_R - 1)\beta SL} - \frac{1}{N_H}} \qquad \text{(E.20)}$$

Since the axial enthalpy change due to the heat added from the fuel rods is generally larger than that due to the diversion crossflow, the errors in the determination of the lumped energy transport by the diversion crossflow have less effect on the total axial enthalpy change than in the unheated cases. Thus, favorable results in the homogenized region predictions are expected to be obtained for even crude estimates of N_H.

It is interesting to note that the error is not a function of the heat generation rate ($\bar{q}'$). In the meanwhile, the error decreases as N increases and as P_R approaches unity. Thus, the larger the P_R and the smaller the N, the more important the N_H.

2.5.2.2 Power and Flow Upset Condition

For the same reason as stated in 2.2.1, good

results are expected to be obtained even though the diversion crossflow in this case is larger than that in the power upset case. The importance of N_H is also the same as that in the power upset case. However, the error increases as F_R increases.

CHAPTER 3

RECOMMENDED COUPLING COEFFICIENTS FOR UNHEATED BUNDLES

Two cases are discussed in this chapter, i.e., the enthalpy upset case and the enthalpy and flow upset case. Numerical values of N_H of these two cases are obtained for three values of N and three values of β, i.e., N = 5, 11 and 23; β = 0.005, 0.02, and 0.04. Other input data in COBRA IIIC, $\frac{S}{L}$ and K, are kept constant and equal to 0.5.

3.1 Enthalpy Upset Case

The numerical values of N_H are evaluated from the results of multi-channel computation utilizing a step shaped inlet enthalpy upset. It is suggested that two half-sized subchannels C and D always be utilized to obtain the subchannel parameters h_C and h_D. The reason is that the required difference, $h_C - h_D$, in the definition of N_H is generally poorly approximated by the enthalpies of the subchannel B and E (refer to Figure 2 for subscripts B, C, D and E). For instance, if we compute N_H by the following relation

$$N_H = \frac{H_L - H_R}{\frac{h_B - h_E}{4}} \tag{3.1}$$

the error of the enthalpy rise involved in the homogenized region case will be 45% higher than that using N_H evaluated by the parameters of the half-sized subchannels C and D.

It is worthwhile noting that the numeric solution of COBRA IIIC imposes a limitation on β due to enthalpy fluctuation when the energy transport is assumed to occur only by the turbulent interchange which is more restrictive in the half-size channel computation than in the full-sized computation. The maximum allowable value for this case is 0.048 (refer to Appendix F for the derivation). Therefore β=0.04 is picked as the upper bound of β in our approach.

3.1.1 Comparison Between Various Forms of N_H

In this section the results of hot zone enthalpy in the homogenized case using the following expressions for N_H are examined

$N_H(z)$

$\overline{N}_H$

$N_H = 1.0$, all z

$N_H = N$, all z

where

$$\overline{N_H} = \frac{\Delta H_{T.I.}}{\sum_i \frac{\Delta H_{i,T.I.}}{N_{H_i}}} \qquad (3.1.1)$$

$i \equiv$ subscript of elevation node

$\Delta H_{T.I.} \equiv$ enthalpy rise of the "homogenized representation" due to turbulent interchange.

The results are illustrated in Figure 4. As we have seen in this figure, the enthalpy changes of the homogenized case by using $N_H(z)$ and $\overline{N_H}$ coincide with that of the multi-subchannel case. On the other hand, $N_H = 1$ and $N_H = N$ have errors of enthalpy rise equal to -203% and 57.4% respectively compared with the results of the multi-subchannel representation. This example demonstrates the need for utilizing a value of N_H other than 1 for application in ENTHALPY and ENTHALPY AND FLOW UPSET CASES.

3.1.2 N_H Values for ENTHALPY UPSET CASE

In this section N_H values for the enthalpy upset condition with different values of β and N are presented. The method used to compute N_H from the multi-subchannel computation is illustrated in Appendix G. The values of $N_H(z)$ versus axial elevation is shown in Figures 5, 6 and 7. The dips and humps of N_H at low elevation positions for $\beta = 0.04$ are due to enthalpy fluctuation by turbulent interchange as mentioned previously. Note that the fluctuation amplitude of N_H is not going to be damped out

if values of β larger than 0.048 are used.

The validity of these recommended N_H values is determined by comparing the hot zone enthalpy of the homogenized case with that of the multi-subchannel case at each axial node. The results for β = 0.005, 0.02 and 0.04; N = 5, 11 and 23 of the homogenized cases coincide with that calculated in the multi-subchannel case just as we expect. This equivalence is demonstrated in Figures 8, 9 and 10.

The inlet enthalpy shape for this case is a step function, abruptly changing at the center of the strip of the subchannels. For example, the inlet enthalpies of channel A, B and C are taken as a constant value and the inlet enthalpies of subchannel C, D and E are taken as another constant value. In the case of gradual enthalpy change at the center of the strip of subchannels, e.g., the inlet enthalpy at the center subchannel for N odd is taken as the averaged value of the inlet enthalpy of the hot zone and that of the cold zone, the N_H will have a completely different shape versus channel length from that of step inlet enthalpy case. N_H in this case will be infinite at the inlet of the channel and abruptly dips and then gradually increase. The $N_H(z)$ for N = 23 in this case is shown in Figure 11. It is good to see

that even though N_H is changed abruptly versus channel length, the results for homogenized case still coincide with the multi-subchannel results (Figure 11a).

3.1.3 Recommended Values of N_H for Design Use

In this section, two methods are investigated to illustrate the behavior of N_H versus β, N and the axial position of the subchannel. One is curve fitting of our predicted $N_H(z)$ results, the other is the averaging of the $N_H(z)$ over the axial enthalpy increment of the hot zone to give an $\overline{N_H}$. Each of them provides a convenient way to incorporate the N_H concept in design practice.

3.1.3.1 Curve Fits

The $N_H(z)$ predictions can be represented using a continuous function f(z) versus channel position z.

$$f(z) = 1.0 + \frac{bz}{a + z} \qquad (3.1.3.1)$$

The values of "a" and "b" can be evaluated by fitting two values of N_H with smallest deviation from the true value at every elevation node. The values of "a" and "b" for the nine cases we have analyzed are tabulated in Table 1.

3.1.3.2 Averaged Value of $N_H(z)$, i.e. $\overline{N_H}$

From the definition of $\overline{N_H}$ (refer to equation 3.1.1), it is expected that the enthalpy of the hot zone at any axial position z in the homogenized representation predicted using $\overline{N_H}$ will coincide with that in the multi-subchannel case. The $\overline{N_H}$ for β = 0, 0.005, 0.02 and 0.04,; N = 2, 5, 11 and 23, and L = 144 inches are tabulated in Table 2. For β = 0.02, $\overline{N_H}$ for a range of channel lengths and N = 2, 5, 11, 17 and 23 are plotted in Figure 12. It is interesting to notice that $\overline{N_H}$ increases with channel length due to the development of the enthalpy profile along the channel (refer to Figure 13). Further, the $\overline{N_H}$ curve becomes asymptotic as N increases for certain β and N. The phenomenon is due to the average parameters $\bar{h}_L$ and $\bar{h}_R$ which becomes less dependent on the subchannel parameters of the center half-sized subchannels, i.e., h_C and h_D when N is large.

3.2 Enthalpy and Flow Upset Case

For the step inlet flow upset with the higher flow rate in the hot zone, together with the inlet enthalpy upset, N_H will increase as the flow ratio increases. It is convenient to define the ratio between these cases in terms of a multiplier, R where

$$R_H = \frac{\bar{N}_H \text{ (ENTHALPY AND FLOW UPSET)}}{\bar{N}_H \text{ (ENTHALPY UPSET)}} \qquad (3.2)$$

Figure 14 demonstrates that this multiplication factor for $H_R = 1.22$ is roughly directly proportional to F_R, where F_R is defined as:

$$F_R = \frac{F_{HOT}}{F_{COLD}}$$

F_{HOT} = inlet flow of the hot zone in the homogenized representation

F_{COLD} = inlet flow of the cold zone in the homogenized representation

The comparison between the results of the homogenized cases using $N_H(z)$ and $N_H = 1$ and the results of the multi-subchannel case is illustrated in Figure 15. It should be noticed that the result of the homogenized representation, using only one coupling coefficient N_H, is not as good as that in the enthalpy upset case, Figure 4.

The 13% error for the enthalpy rise of the homogenized region case can be explained as follows:

1) Assumption (A.1.10a) made to derive the N'_H in terms of N_H and known parameters becomes invalid

when flow upset goes up, i.e., diversion crossflow becomes significant.

2) Under the large diversion crossflow condition in this case the neglect of N_U, N_{TF}, N_{TP} and N_{TU} effects the results.

3) Error exists due to the difference approximation made in COBRA IIIC computation as assessed in Appendix B.

CHAPTER 4

RECOMMENDED COUPLING COEFFICIENTS FOR HEATED BUNDLES

Two cases are discussed in this chapter, i.e., the POWER UPSET CASE and the POWER AND FLOW UPSET CASE.

4.1 POWER UPSET CASE

The numerical values of N_H are evaluated for three values of N and three values of β, i.e., N = 5, 11 and 23; β = 0.005, 0.02 and 0.04. The maximum β in this case is limited to 0.048 when half-sized subchannels are used to obtain the subchannel parameters required in the evaluation of N_H. Because the exit enthalpy difference between the homogenized representation and the multi-subchannel representation in this case is less sensitive to N_H then that for ENTHALPY UPSET CASE (as mentioned in section 2.5.2.1), N_H can be evaluated by equation (3.1) without the half-sized subchannels in the center region and yields good results of the homogenized representation.

4.1.1 Comparison Between Various Forms of N_H

In this section the results of the hot zone enthalpy in the homogenized representation using the following expressions for N_H are examined:

$N_H(z)$

$\overline{N_H}$

$N_H = 1.0$, all z

$N_H = N$, all z

where $\overline{N_H}$ is defined by equation (3.1.1).

The results are illustrated in Figure 16 for a typical N, β combination. The predicted hot zone enthalpies for the homogenized representation using $N_H(z)$ coincide with that of the multi-subchannel representation. However, result for $N_H = 1$ and $N_H = N$ have errors of enthalpy rise equal to -3.2% and 2.1% respectively. Note that for the POWER UPSET CASE the error in hot side enthalpy for the homogenized representation is not as sensitive to the form of N_H as in the unheated bundle cases. This example demonstrates that the need for computing N_H in the heated bundle is not as crucial as that in the unheated bundle case .

4.1.2 N_H Values for POWER UPSET CASE

In this section N_H values for the power upset condition with different values of β and N are presented. The method used to compute the N_H from the multi-subchannel computation is illustrated in Appendix E. The values of $N_H(z)$ versus axial elevation are shown in Figures 17, 18

and 19. The dips and humps of N_H at low elevation positions which were present in the analogous plots of the ENTHALPY UPSET CASE are not shown in these figures. The reason is that the heat added from the rods overcomes the small axial enthalpy fluctuation due to the turbulent interchange. However, the computational impossibility for the enthalpy fluctuation due to the turbulent interchange still imposes an upper limit on β, i.e. 0.048, in the homogenized calculation with half-sized subchannels in the center region.

The validity of these recommended N_H values is determined by comparing the hot zone enthalpy of the homogenized representation with that of the multi-subchannel representation at each axial elevation. The results are shown in Figs. 20, 21, and 22. As demonstrated in Figure 16, the enthalpies of the homogenized representation employing $N_H(z)$ and $\overline{N_H}$ coincide with that of the multi-subchannel representation.

4.1.3 Recommended Values of N_H for Design Use

In this section, the same methods are employed to illustrate the N_H versus β, N and the axial position of the subchannel as those discussed in 3.1.3. The details for each method are discussed in the following section.

4.1.3.1 Curve Fits

The N_H can be presented by using a continuous function f(z) versus channel position z for β = 0.005, 0.02 and 0.04; N = 5, 11, 23.

$$f(z) = a + \frac{cz}{b+z} \qquad (4.1.4.1)$$

The values of a, b and c can be evaluated by fitting three values of N_H with the smallest error deviating from the true value at every elevation node. The values of a, b and c for the nine cases (three β and three N) are tabulated in Table 3.

4.1.3.2 Average Value of N_H

The $\overline{N_H}$ for β = 0, 0.005, 0.02, and 0.04; N = 2.5, 11 and 23 are tabulated in Table 4. For β = 0.02, $\overline{N_H}$ for a range of channel lengths and N = 2, 5, 11 and 23 are plotted in Figure 23. As we can observe, N_H saturates faster when N increases than it does in the unheated bundle case. This is because the transverse power profile contributes much to the transverse enthalpy profile which determines the $\overline{N_H}$.

4.1.4 Effectiveness of Coupling Coefficients (N_H, N_U, N_{TP}, N_{TF} and N_{TU}) in POWER UPSET CASE

The total enthalpy transport across the boundary between homogenized regions can be broken into three components.

These components listed below are consistent with the COBRA representation of the overall transport process as due to turbulent interchange and diversion crossflow where the enthalpy transport due to crossflow is itself broken into two components:

a) turbulent interchange

b) enthalpy of the diversion crossflow

c) mass flowrate of the diversion crossflow.

In this section three parameters of the homogenized representations are examined to compare with those of the multi-subchannel representation in order to evaluate the effectiveness of using several coupling coefficients simultaneously.

The first component, the enthalpy change in the hot zone due to turbulent interchange only, gives us an idea of the effectiveness of each coupling coefficient for the homogenized representation on the energy transport due to turbulent mixing. The second parameter is the enthalpy increment in the hot zone due to the diversion crossflow transport. This will illustrate the effectiveness of each coupling coefficient on the energy transport by the diversion crossflow. The third parameter is the total diversion crossflow across the boundary in the homogenized representation. In the case we examine here, the diversion crossflows at the boundary always move toward the cold zone for any channel axial position, and therefore it is considered convenient to utilize the total diversion crossflow through the boundary as a para-

meter to illustrate the effectiveness of the coupling coefficients on the transverse momentum transport.

The results are shown in Tables 5, 6 and 7. Table 5 tabulates the parameters which are the enthalpy change with respect to the inlet enthalpy of the hot zone due to the turbulent interchange only. As can be observed in this table, the $N_H(z)$ used in the homogenized computation is most effective in matching the homogenized results to that of the multi-subchannel computation. All the other coupling coefficients show negligible effects on this parameter. Table 6 tabulates the second parameters for the multi-subchannel representation and homogenized representation, i.e., $\Delta h_{D.C.}$ and $\Delta H_{D.C.}$ respectively. It is worth noting that the results of the homogenized representation using all the coupling coefficients have the best agreement with that of the multi-subchannel representation. However, $N_H(z)$ and $N_U(z)$ are most effective compared to the other three coupling coefficients. Table 7 tabulates the integral value of diversion crossflow across the central boundary for both the multi-subchannel representation and the homogenized representation. The conclusion we can draw from this table is similar to that from Table 6. However, if accurate diversion crossflow is desired, it is recommended that N_{TP}, N_{TF}, and N_{TU} be used together with N_H and N_U.

4.2 POWER and FLOW UPSET Case

For the step inlet flow upset, together with the step linear heat generation rate, N_H for the homogenized representation will increase as the flow ratio increases. This phenomenon can be expected from the results of the ENTHALPY and FLOW UPSET Case (Section 3.2). The multiplication factor for this case is defined as

$$R_p = \frac{\overline{N_H}\ \text{(POWER and FLOW UPSET)}}{\overline{N_H}\ \text{(POWER UPSET)}}$$

and is plotted versus F_R in Figure 24.

The validity of $N_H(z)$ and $\overline{N_H}$ is illustrated in Figure 25. In this figure, using $N_H = 1.0$ and $N_H = N$, the hot zone enthalpy results of the homogenized representation are also plotted in comparison to the results using $N_H = N_H(z)$. From our calculation, we are aware that there is a slight difference of 0.1% between the hot zone enthalpy results of the homogenized representation using $N_H = N_H(z)$ and that of the multi-subchannel representation. This small difference is believed to be due to the error caused by the difference computation scheme as we mentioned in Section 2.3 and Appendix B.

CHAPTER 5

SUMMARY OF RESULTS FOR ALL CASES

5.1 Numerical Values of $N_H(z)$ and $\overline{N_H}$

The numerical values for $N_H(z)$ and $\overline{N_H}$ for the two dimensional subchannel layout under different operational conditions considered in this thesis, are summarized in the following summary tables.

$N_H(z)$

	ENTHALPY UPSET	POWER UPSET
No Flow Upset	Figure 5 (N=5) Figure 6 (N=11) Figure 7 (N=23) Table 1 (best fit curves)	Figure 17 (N=5) Figure 18 (N=11) Figure 19 (N=23) Table 3 (best fit curves)

$\overline{N_H}$

	ENTHALPY UPSET	POWER UPSET
No Flow Upset	Table 2 (z=114") Figure 12(β=0.02)	Table 4 (z=144") Figure 23(β=0.02)
Flow Upset	Figure 14 (multiplication factor	Figure 24(multiplication factor

Figures 5, 6 and 7 plot the $N_H(z)$ versus the channel length for β = 0.005, 0.02 and 0.04, N = 5, 11 and N, under the enthalpy upset condition. Figures 17, 18 and 19 plot the $N_H(z)$ versus the channel length for β = 0.005, 0.02 and

0.04, N = 5, 11 and 23, under the power upset condition. Tables 1 and 3 tabulate the parameter values to obtain $N_H(z)$ from the best fitting correlation for $\beta = 0.005$, 0.02 and 0.04, N = 5, 11 and 23, for the ENTHALPY UPSET CASE and the POWER UPSET CASE, respectively. Tables 2 and 4 tabulate the $\overline{N_H}$ values for $\beta = 0.005$, 0.02 and 0.04, N = 5, 11 and 23 with the channel length equal to 12 ft., for the ENTHALPY UPSET CASE and the POWER UPSET CASE, respectively. Figures 12 and 23 plot the $\overline{N_H}$ values versus N and L for $\beta = 0.02$ for channel length less than 12 ft. Figures 14 and 23 give the multiplication factors which are a function of F_R and are needed to evaluate $\overline{N_H}$ from equations (3.2) and (4.2) for the ENTHALPY UPSET CASE and the POWER UPSET CASE, respectively.

For subchannels with axial length less than 12 ft., $N_H(z)$ gives detailed values at each axial position up to the exit, whereas $\overline{N_H}$ has been calculated for only certain specific axial locations (Figs. 12 and 23). However, it is easy to incorporate $\overline{N_H}$ into the computer code. Two empirical correlations for $\overline{N_H}$ for the cases we discussed in this thesis are represented as follows by equations (5.1.1) and (5.1.2) which can be used directly without resorting to the tables and figures listed in the summary tables.

$$\overline{N_H} = \{1+\ln[1+353(\frac{N-2}{N})^{\frac{3.5\beta}{0.015+\beta}} \beta^{1.1}(\frac{L}{144})^{1.5}]\}R_p \qquad \pm 15\% \quad (5.1.1)$$

Equation (5.1.1) determines the value of $\overline{N_H}$ for the POWER

UPSET CASE and the POWER and FLOW UPSET CASE.

$$\overline{N_H} = \{1+\ln[1+4200(\frac{N-2}{N})^{1+100\beta}\beta^{1.43}(\frac{L}{144})^{1.5}]\}\ R_H\}\ \pm 15\% \quad (5.1.2)$$

Equation (5.1.2) determines the value of $\overline{N_H}$ for the ENTHALPY UPSET CASE and the ENTHALPY and FLOW UPSET CASE.

These correlations are valid for $N<23$, $\beta<0.04$ and $L<144$ inches, where

$L \equiv$ channel length in inches

R_H and $R_p \equiv$ multiplication factors for Enthalpy Upset and Power Upset respectively, which can be obtained from Figs. 14 and 24 respectively. Under no flow upset condition, $R_H = 1.0$ and $R_p = 1.0$.

5.2 Suggestions on the N_H Values Under Exceptional Conditions

As we mentioned in Section 5.1, the characteristics of $\overline{N_H}$, together with some understanding of the basics of the coupling coefficient N_H, suggest some reasonable values for $\overline{N_H}$ under exceptional conditions. They are as follows:

1) Since $\overline{N_H}$ approaches a saturated value as N increases, $\overline{N_H}$ for $N>23$ has the same value as $N = 23$.

2) For the homogenized representation with two homogenized strips of subchannels with uneven subchannel numbers, $\overline{N_H}$ can be obtained by the following formula:

$$\overline{N_H} = \frac{\overline{N_{H_L}} + \overline{N_{H_R}}}{2}$$

under the criteria

$$\frac{N_L - N_R}{\min(N_L, N_R)} < 0.3$$

where

$\overline{N_{H_L}} \equiv \overline{N_H}$ value for $N = 2N_L$

$\overline{N_{H_R}} \equiv \overline{N_H}$ value for $N = 2N_R$

(refer to Appendix H for the derivation).

3) Since $\overline{N_H}$ is not a function of power level and P_R, $\overline{N_H}$ can be taken as a constant value through the period of power transient (power excursion or shut down transient) when $\overline{N_H}$ is used in the transient computation.

CHAPTER 6

CONCLUSIONS AND RECOMMENDATIONS FOR FUTURE WORK

6.1 Characteristics of Coupling Coefficients

Listed below are several conclusions relating to the characteristics of the coupling coefficients.

6.1.1 Overall Characteristics

6.1.1.1 Use of a single coupling coefficient $N_H(z)$ can lead to favorable results in the homogenized representation as long as the diversion crossflow does not play a major role in the energy transport between channels.

6.1.1.2 $N_H(z)$ and $N_U(z)$ are most effective in getting good results for cases with diversion crossflow in the homogenized representation.

6.1.2 Thermal Entry Development Characteristics

6.1.2.1 $N_H(z)$ is strongly dependent on the transverse enthalpy profile among subchannels at channel elevation z.

6.1.2.2 $\overline{N_H}$ approaches a saturated value as the number of subchannels, N, increases.

6.1.3 Basic Characteristics

6.1.3.1 $\overline{N_H}$ is not a function of $\overline{q}'$, H_R OR P_R. (Refer to Figs. 26, 27, and 28). This was demonstrated analytically by P. Moreno and confirmed here for the case of numerical determination of coupling coefficients.

6.1.3.2 The effectiveness of $N_H(z)$ is not a function of heat generation rate ($\bar{q}'$). This characteristic can be illustrated by equation (E.20) and Figure 26 which show that the error of hot channel enthalpy rise between multi-subchannel case and homogenized case is independent of $\bar{q}'$.

6.2 Effectiveness of $N_H(z)$ Under Different N and β Combinations

In this section, the effectiveness of $N_H(z)$ is explored under POWER UPSET CASE which is encountered in the practical application with different N and β combinations. The effectiveness of N_H on the homogenized case can be numerically indicated by the error of exit enthalpy rise between the multi-subchannel case and the homogenized case. A conservative scheme to estimate this error has been derived in Appendix E (equation E.20) and quoted in Section 2.5.2.1. With the aid of the correlation 5.1.1, we can evaluate the errors with different N and β combinations. The results are tabulated in Table 8. As can be observed, the maximum error of 14.4% happens at large β and intermediate N, i.e. $\beta = 0.06$, $N = 4$. In other words, $N_H(z)$ is relatively important at this specific combination of N and β.

6.3 Recommendations for Future Work

In response to the problems presented in this thesis, several recommendations for future work are listed below.

1) The characteristics of coupling coefficients N_U, N_{TF}, N_{TP} and N_{TU} need further investigation in order to deal with the homogenized representation with very large diversion crossflows.

2) Two dimensional (planar) linkage of the homogenized representation (with the aid of coupling coefficients) or the 3D problem should be studied in order to analyze the corewide thermal behavior in a more detailed way than that done by the cascade method[5] for the PWR.

3) Corewide study (with the aid of coupling coefficients) on MDNBR under power excursion transient case is recommended. Under this condition, large amount of diversion crossflow is expelled from the hot zone which can cause misleading MDNBR results provided there are no coupling coefficients incorporated.

REFERENCES

1. Rowe, D.S., "COBRA III: A Digital Computer Program for Steady State and Transient Thermal Hydraulic Analysis of Rod Bundle Nuclear Fuel Elements," BNWL-B-82, Pacific Northwest Laboratory (1972).

2. H. Chelemer, J. Weisman and L.S. Tong, Nucl. Eng. and Design 21, 3 (1972).

3. France, D.M. and Ginsberg, T.,"Evaluation of lumped parameter heat transfer techniques for nuclear reactor applications," Nucl. Sci. Eng. 51, 41-51 (1973).

4. Ramm, H., Johannsen, K., and Todreas, N.E., "Single phase transrport within bare rod arrays at laminar, transition and turbulent flow conditions," Nucl. Eng. and Design 30, 186-204 (1974).

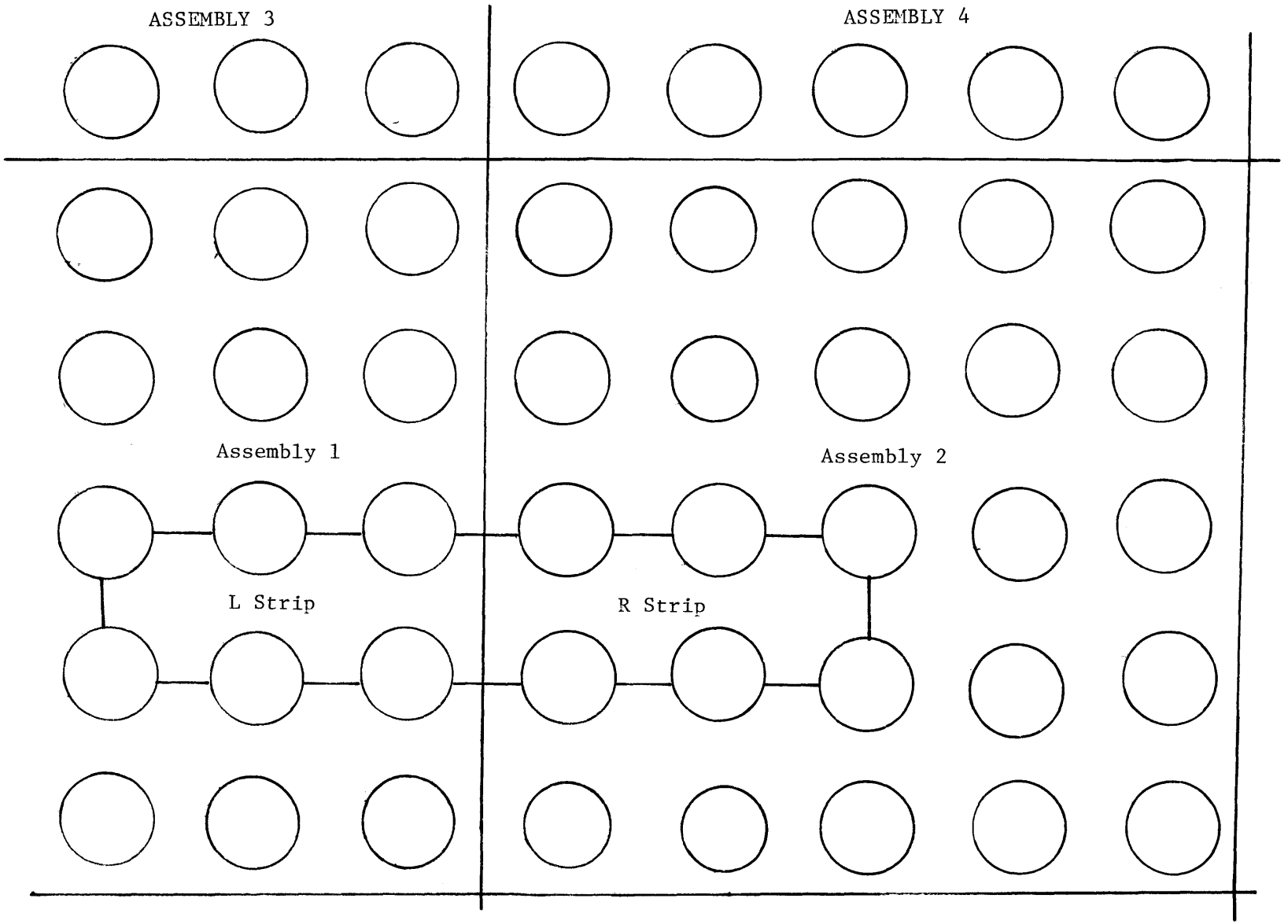

Figure 1. NxN Rod Assemblies in Square Array, N=5

Letters - Channel Subscripts

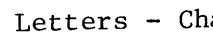 = Adiabatic Boundary

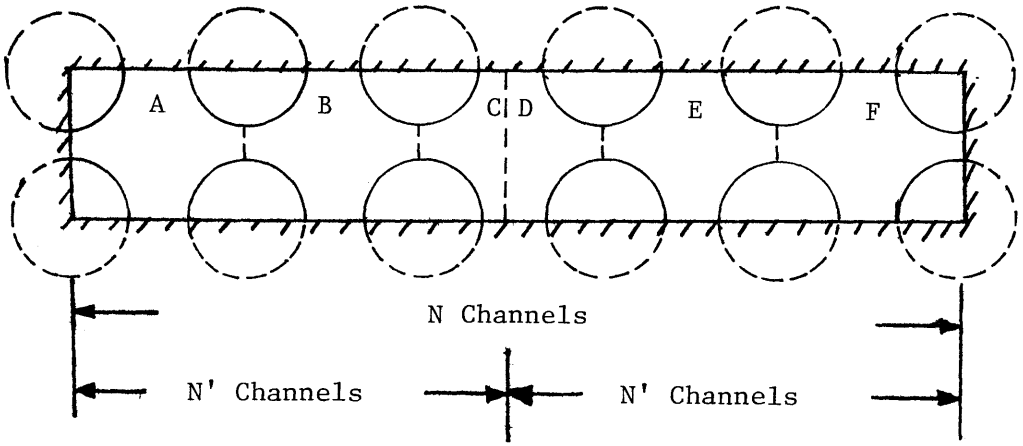

Figure 2. Strips of Adjacent N' Channels

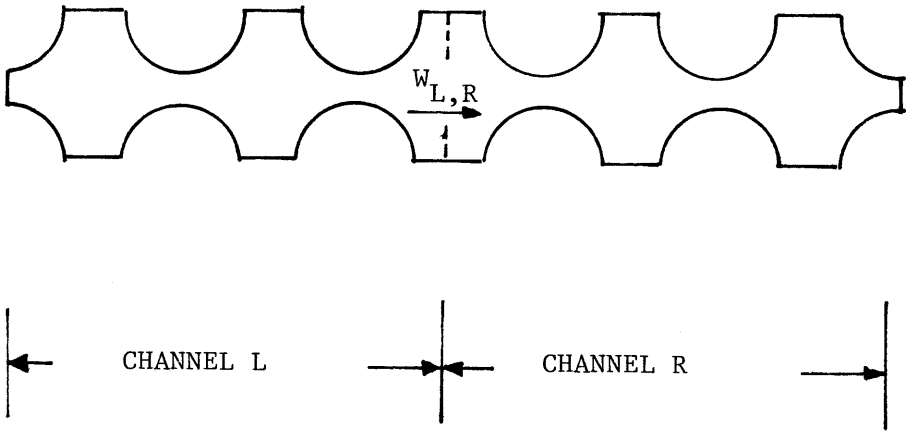

Figure 3. Homogenized Representation of Strips of N' Subchannels

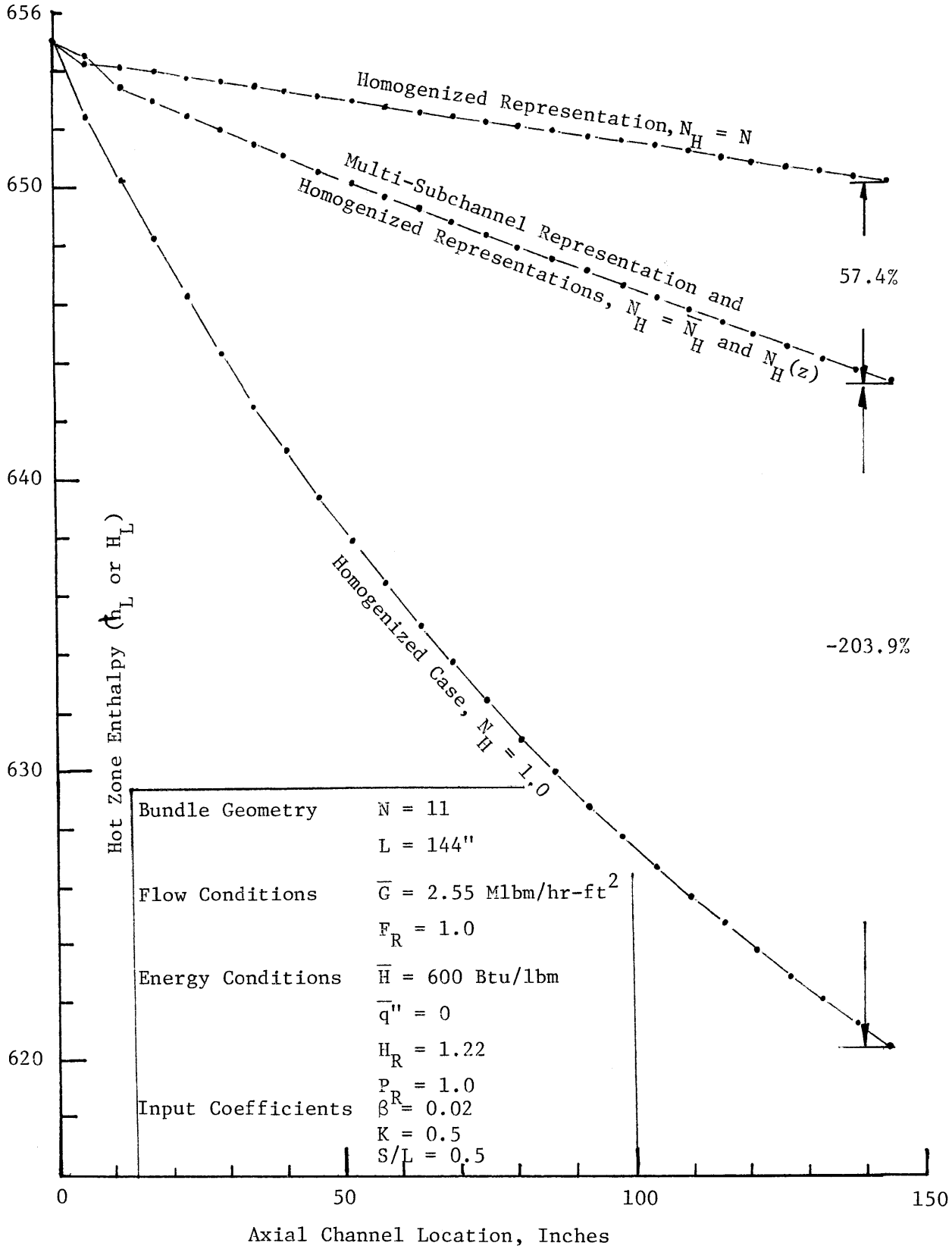

Figure 4. Comparison between results of multi-subchannel representations and homogenized representations

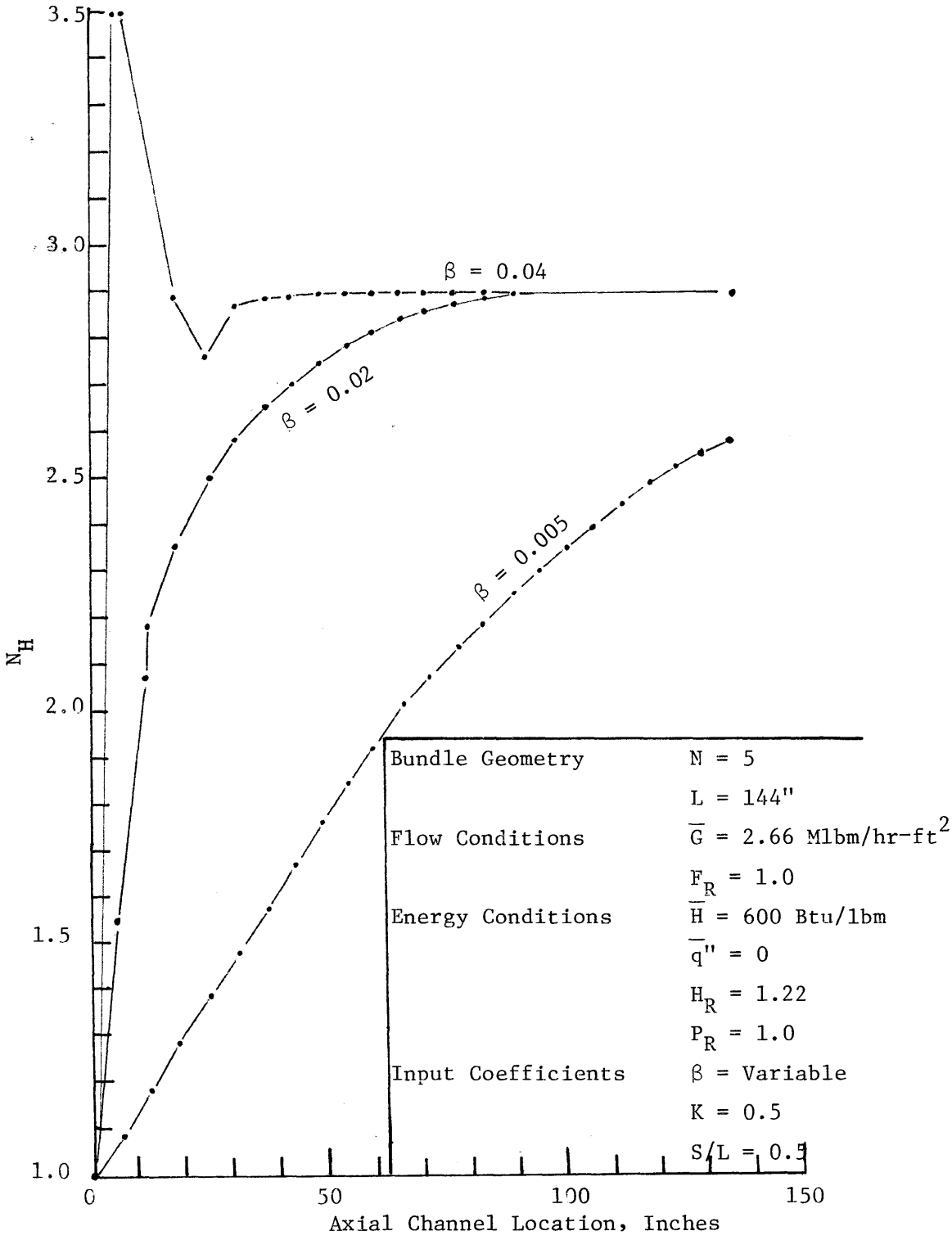

Figure 5. $N_H(z)$ versus channel length for ENTHALPY UPSET CASE
N = 5

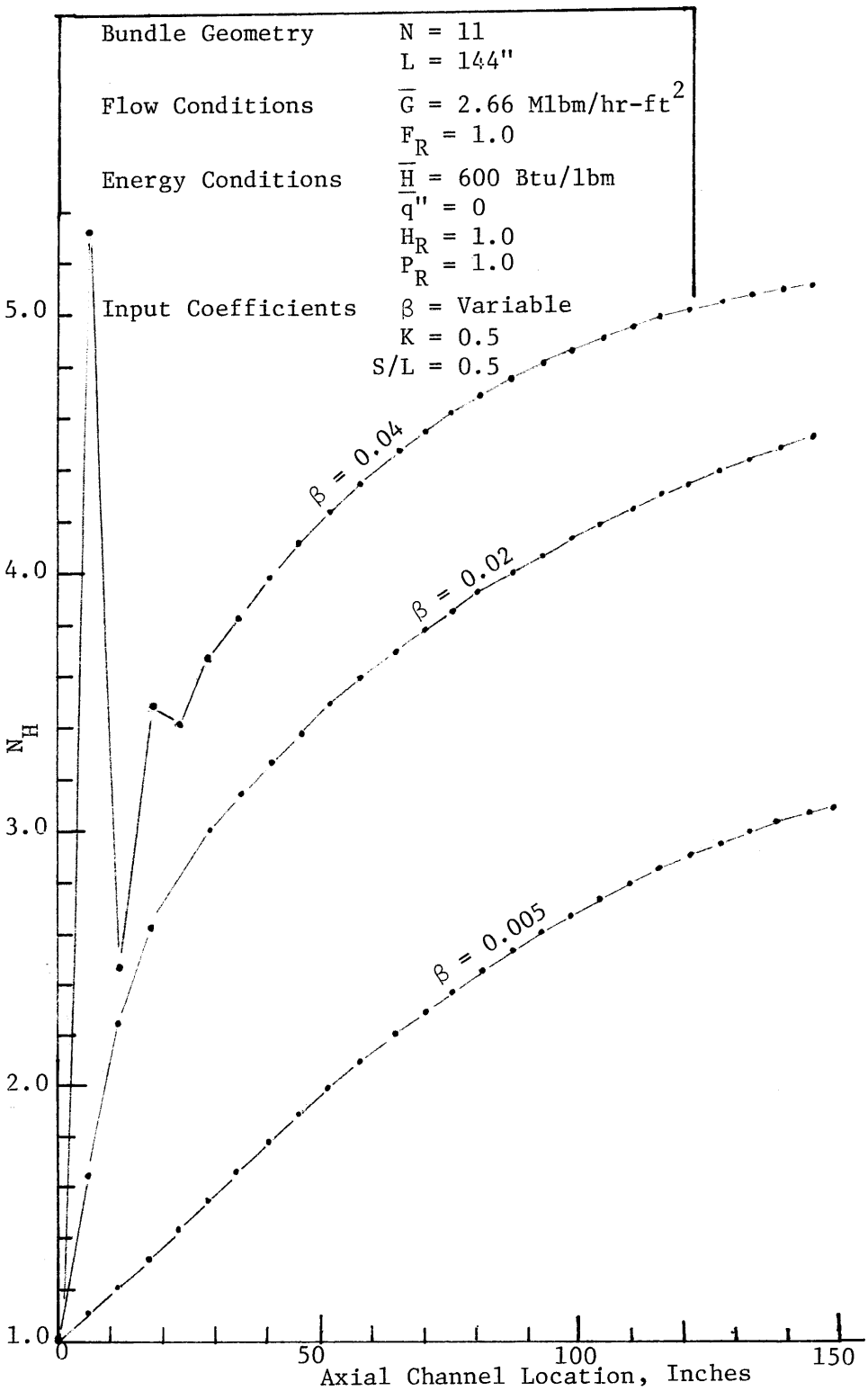

Figure 6. $N_H(z)$ versus channel length for ENTHALPY UPSET CASE
N = 11

Bundle Geometry	N = 23
	L = 144"
Flow Conditions	$\overline{G}$ = 2.66 Mlbm/hr-ft^2
	F_R = 1.00
Energy Conditions	$\overline{H}$ = 600 Btu/lbm
	$\overline{q}$" = 0
	H_R = 1.22
	P_R = 1.0
Input Coefficients	β = Variable
	K = 0.5
	S/L = 0.5

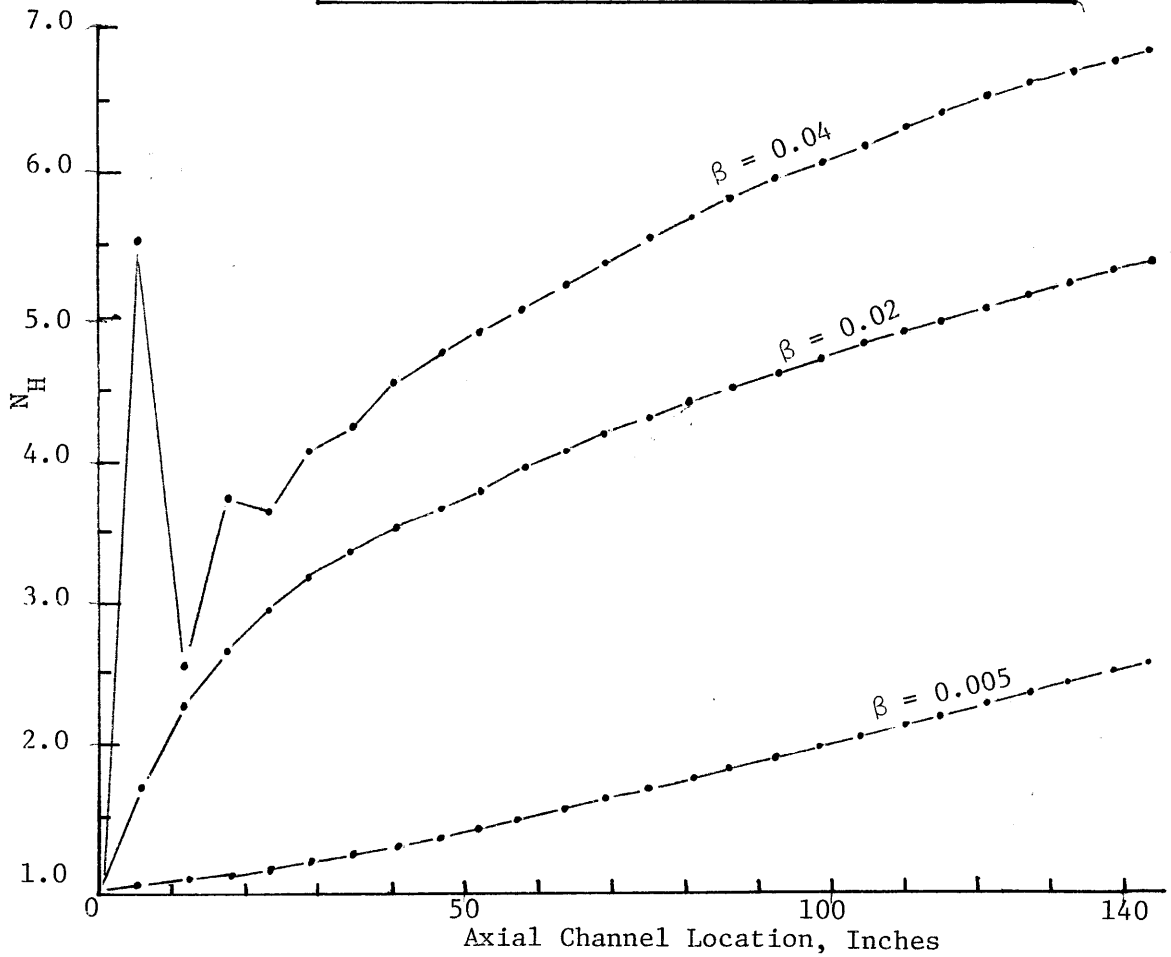

Figure 7. $N_H(z)$ versus channel length for ENTHALPY UPSET CASE N = 23

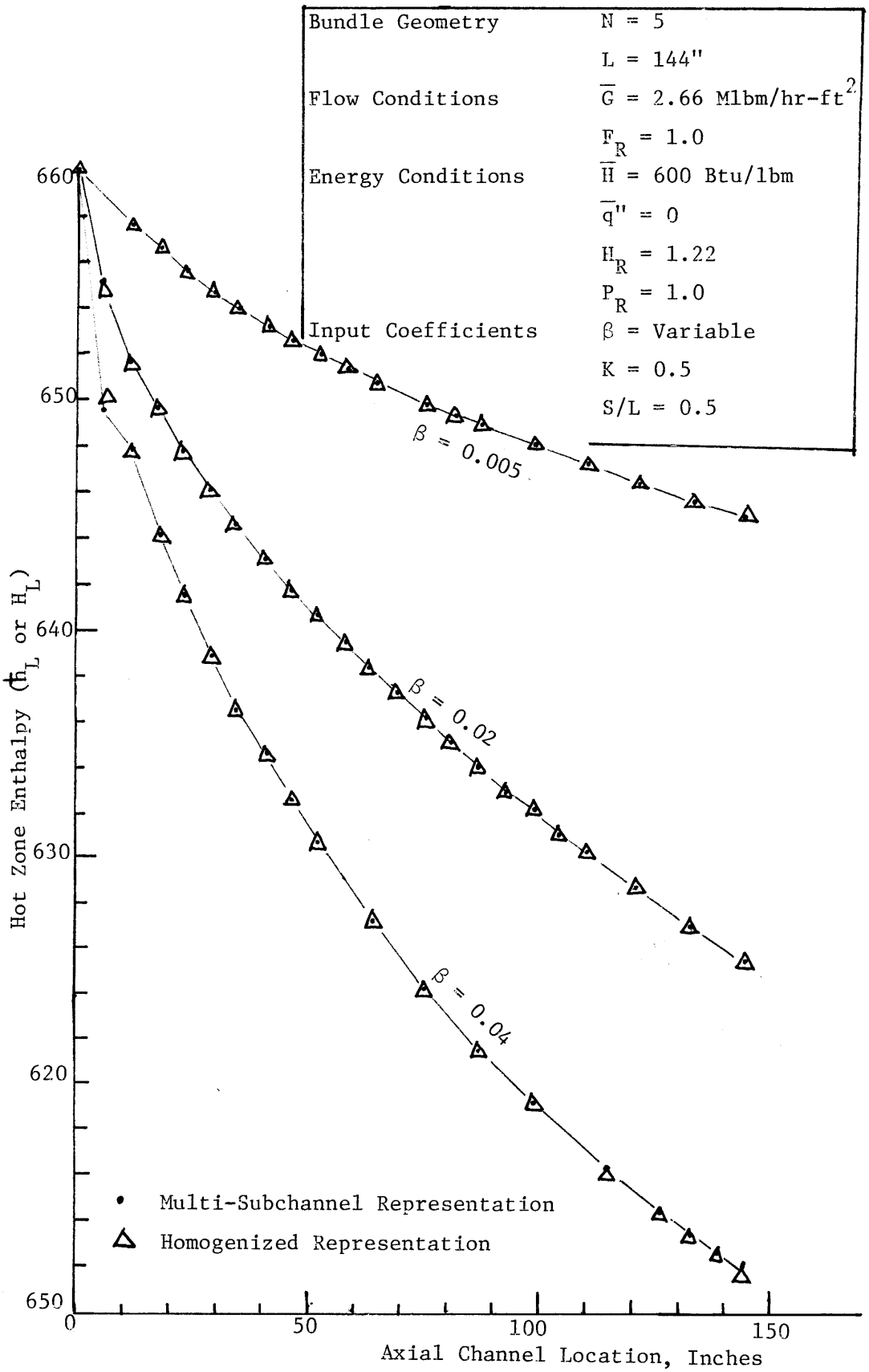

Figure 8. Validity of $N_H(z)$ for ENTHALPY UPSET CASE
N = 5

Figure 9. Validity of $N_H(z)$ for ENTHALPY UPSET CASE, N=11

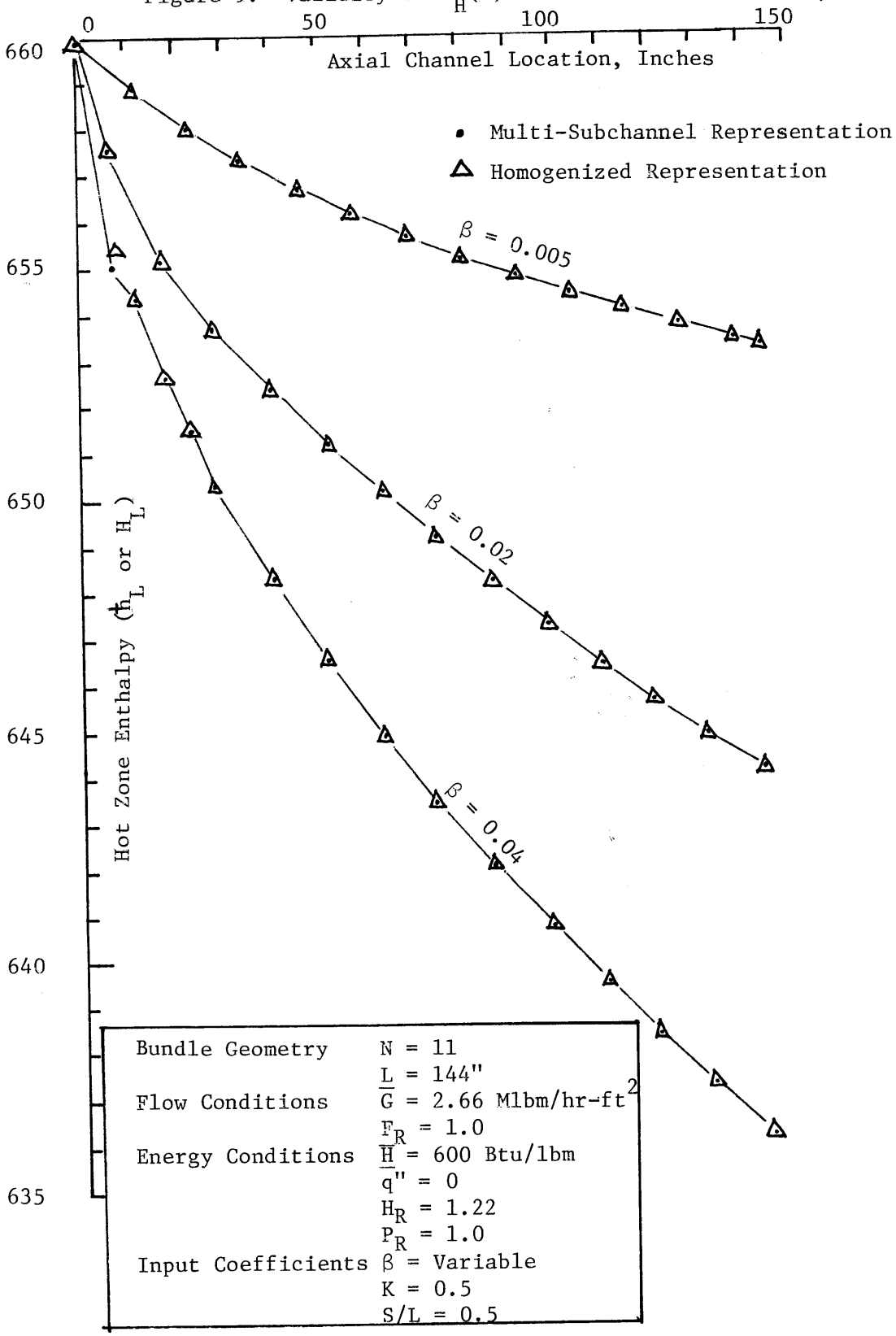

Bundle Geometry	N = 23
	L = 144"
Flow Conditions	$\overline{G}$ = 2.55 Mlbm/hr-ft^2
	F_R = 1.0
Energy Conditions	$\overline{H}$ = 600 Btu/lbm
	$\overline{q}$" = 0
	H_R = 1.22
	P_R = 1.0
Input Coefficients	β = Variable
	K = 0.5
	S/L = 0.5

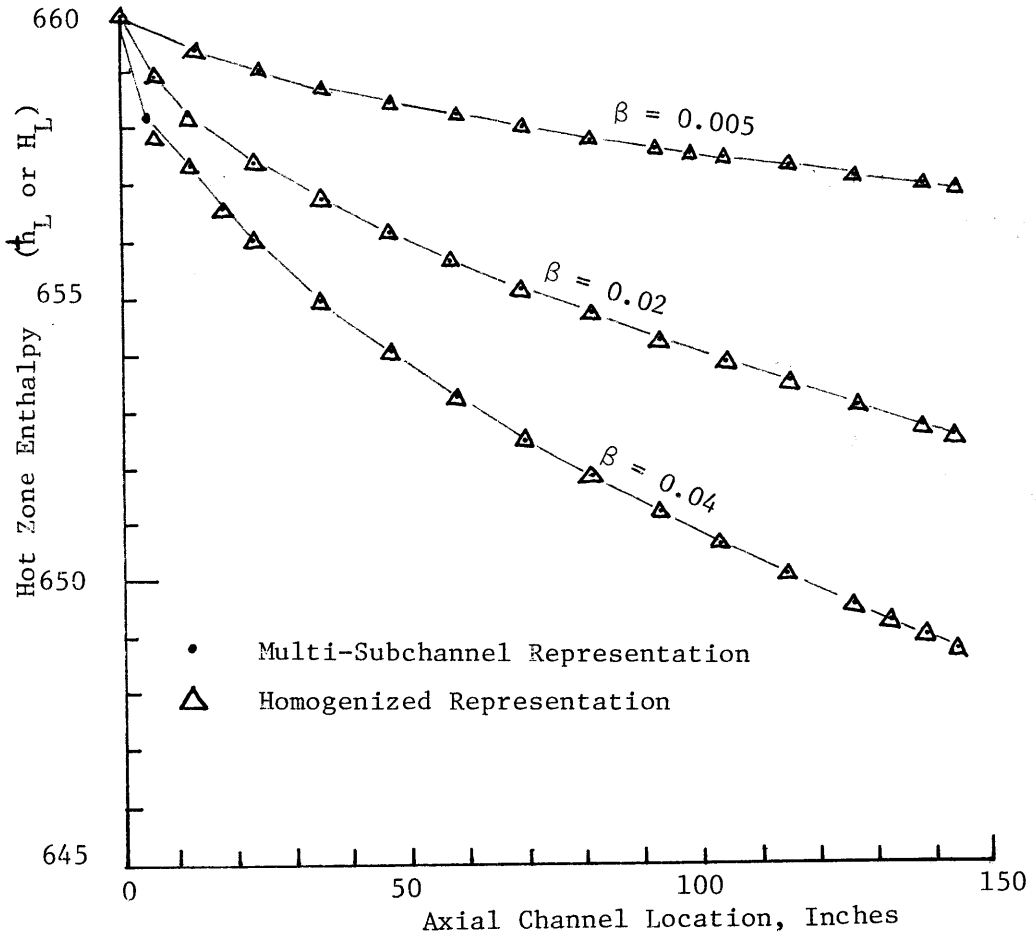

Figure 10. Validity of $N_H(z)$ for ENTHALPY UPSET CASE
N = 23

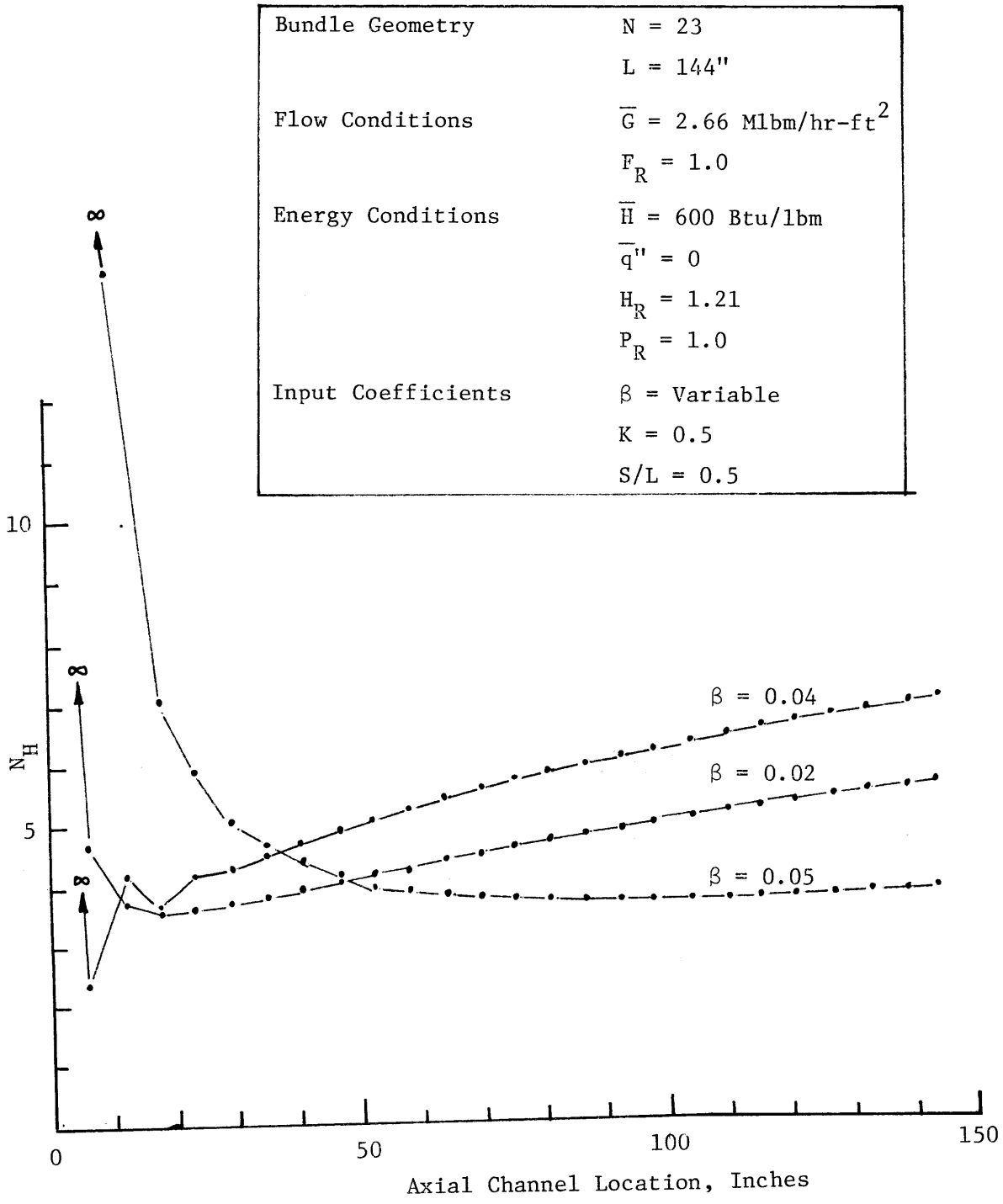

Figure 11. N_H for ENTHALPY UPSET CASE with the gradually changed inlet enthalpy

Bundle Geometry	N = 23
	L = 144"
Flow Conditions	$\bar{G}$ = 2.66 Mlbm/hr-ft^2
	P_R = 1.0
Energy Conditions	$\bar{H}$ = 600 Btu/lbm
	$\bar{q}''$ = 0
	H_R = 1.21
	P_R = 1.0
Input Coefficients	β = Variable
	K = 0.5
	S/L = 0.5

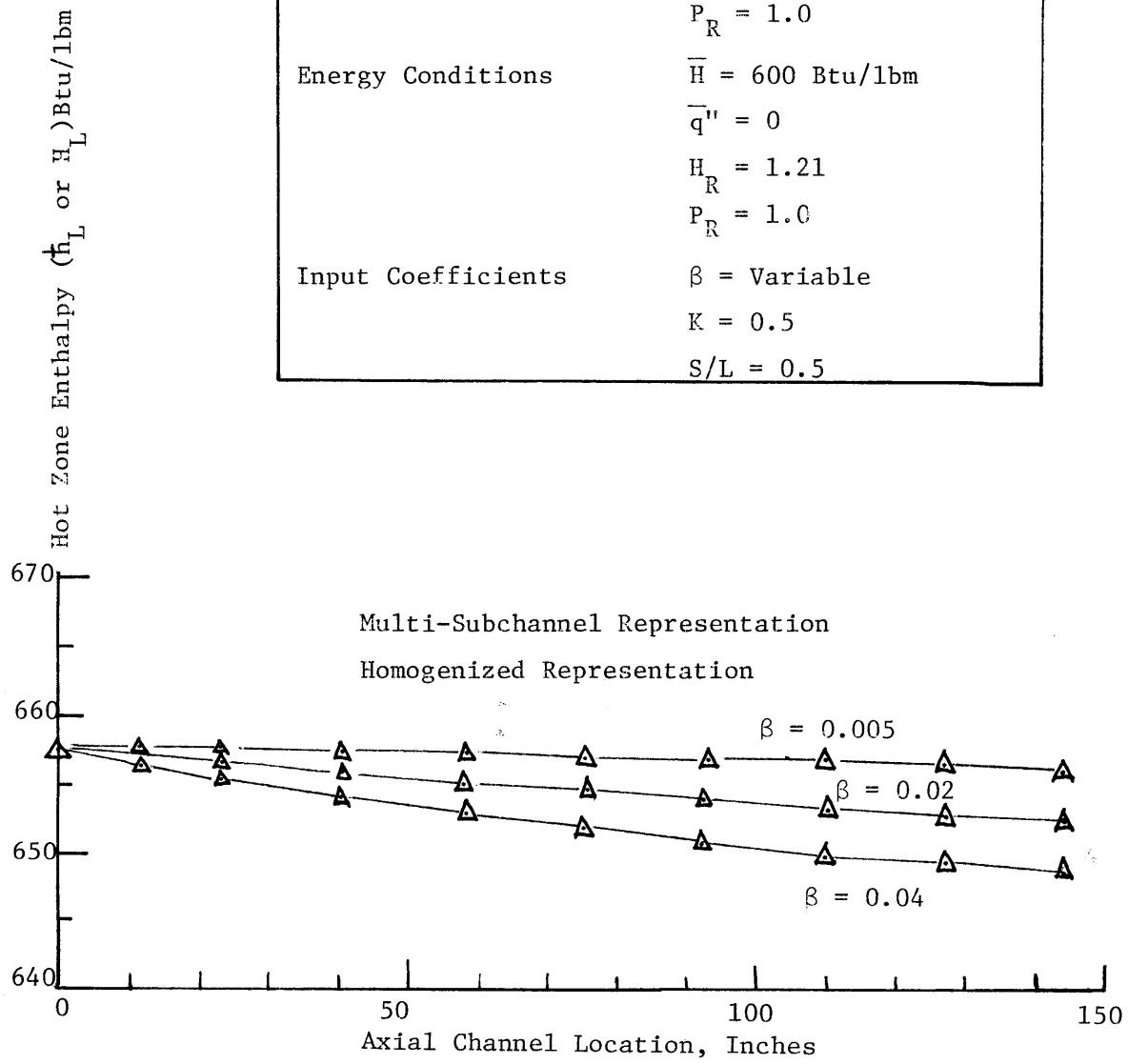

Figure 11a. Validity of N_H for ENTHALPY UPSET CASE

Bundle Geometry	N = Variable
	L = Variable
Flow Conditions	$\overline{G}$ = 2.66 x 10^6 lbm/hr
	F_R = 1.0
Energy Conditions	$\overline{H}$ = 600 Btu/lbm
	$\overline{q}$" = 0
	H_R = 1.22
	P_R = 1.0
Input Coefficients	β = 0.02
	K = 0.5
	S/L = 0.5

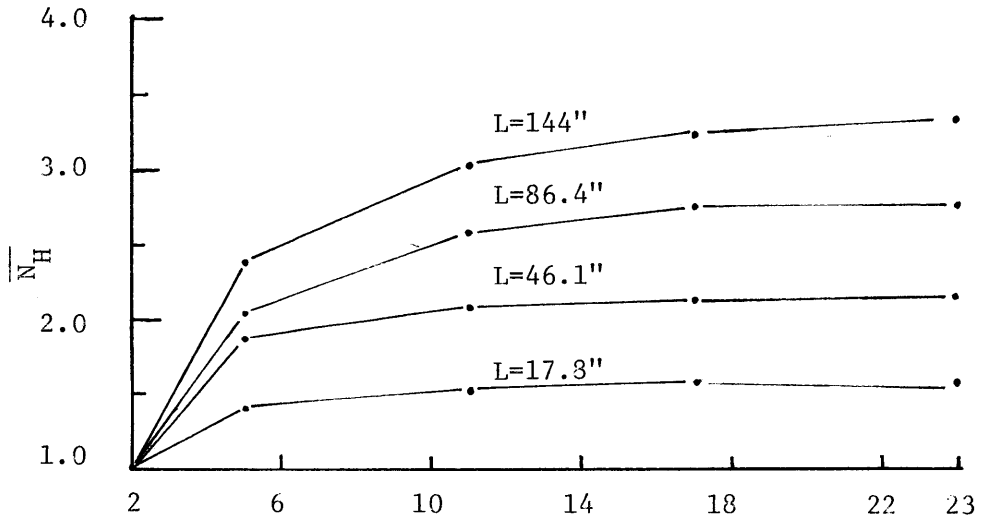

Figure 12. $\overline{N_H}$ versus N

Bundle Geometry	N = 11
	L = Variable
Flow Conditions	$\overline{G}$ = 2.66 Mlbm/ft^2-hr
	F_R = 1.0
Energy Conditions	$\overline{H}$ = 600 Btu/lbm
	$\overline{q}''$ = 0
	H_R = 1.22
	P_R = 1.0
Input Coefficients	β = 0.02
	K = 0.5
	S/L = 0.5

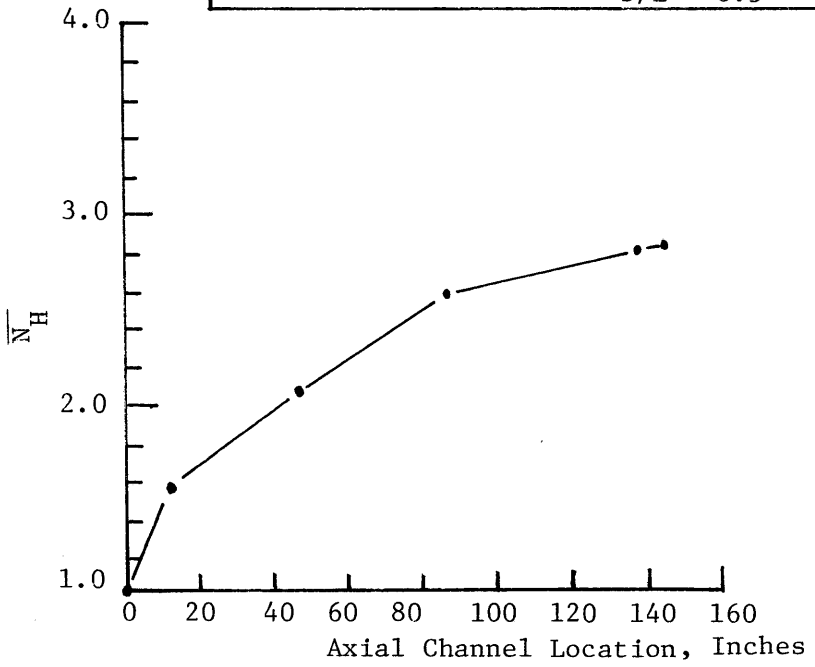

Figure 13. Development of $\overline{N}_H$ through channel length

Bundle Geometry	N = 11
	L = 144"
Flow Conditions	$\overline{G}$ = 2.66 Mlbm/hr-ft^2
	F_R = Variable
Energy Conditions	$\overline{H}$ = 600 Btu/lbm
	$\overline{q}''$ = 0
	H_R = 1.22
	P_R = 1.0
Input Coefficients	β = 0.02
	K = 0.5
	S/L = 0.5

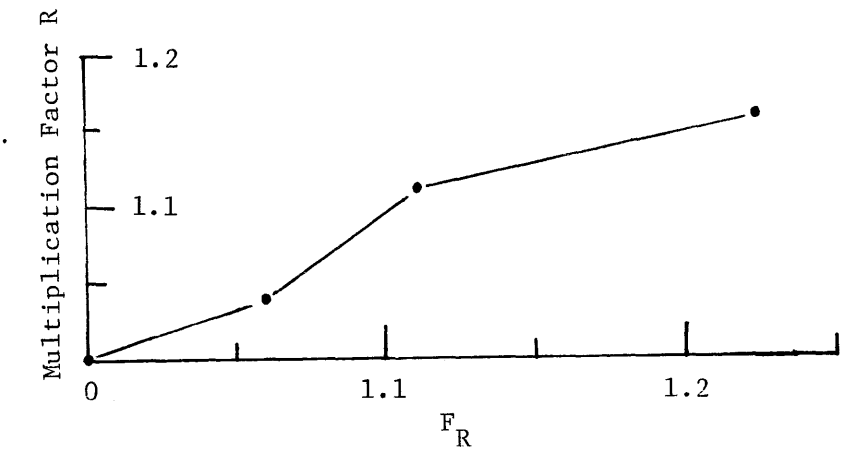

Figure 14. Multiplication factor versus F_R for ENTHALPY and FLOW UPSET CASE

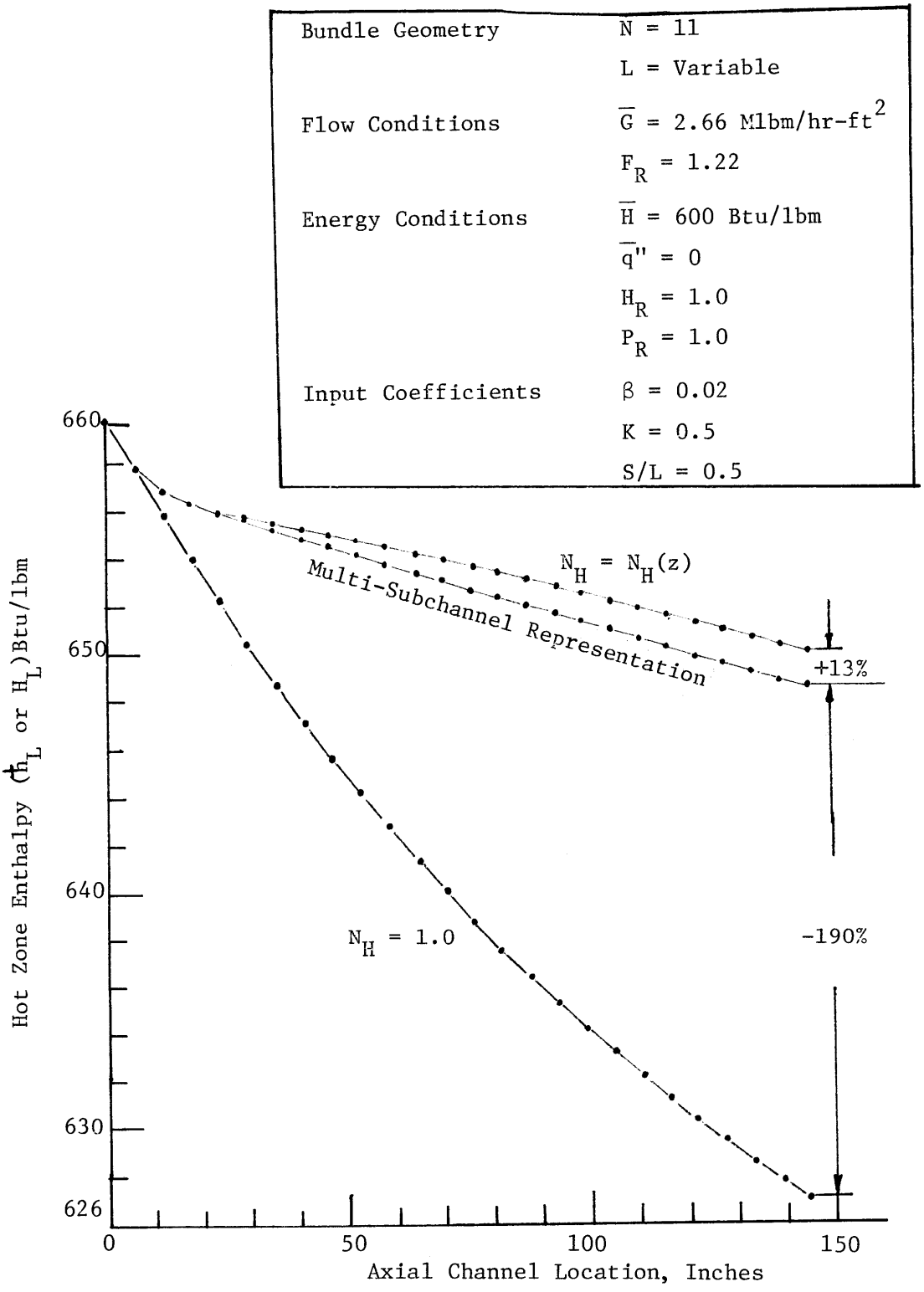

Figure 15. Comparison of multi-subchannel representation and homogenized representations with Enthalpy and Flow Upset

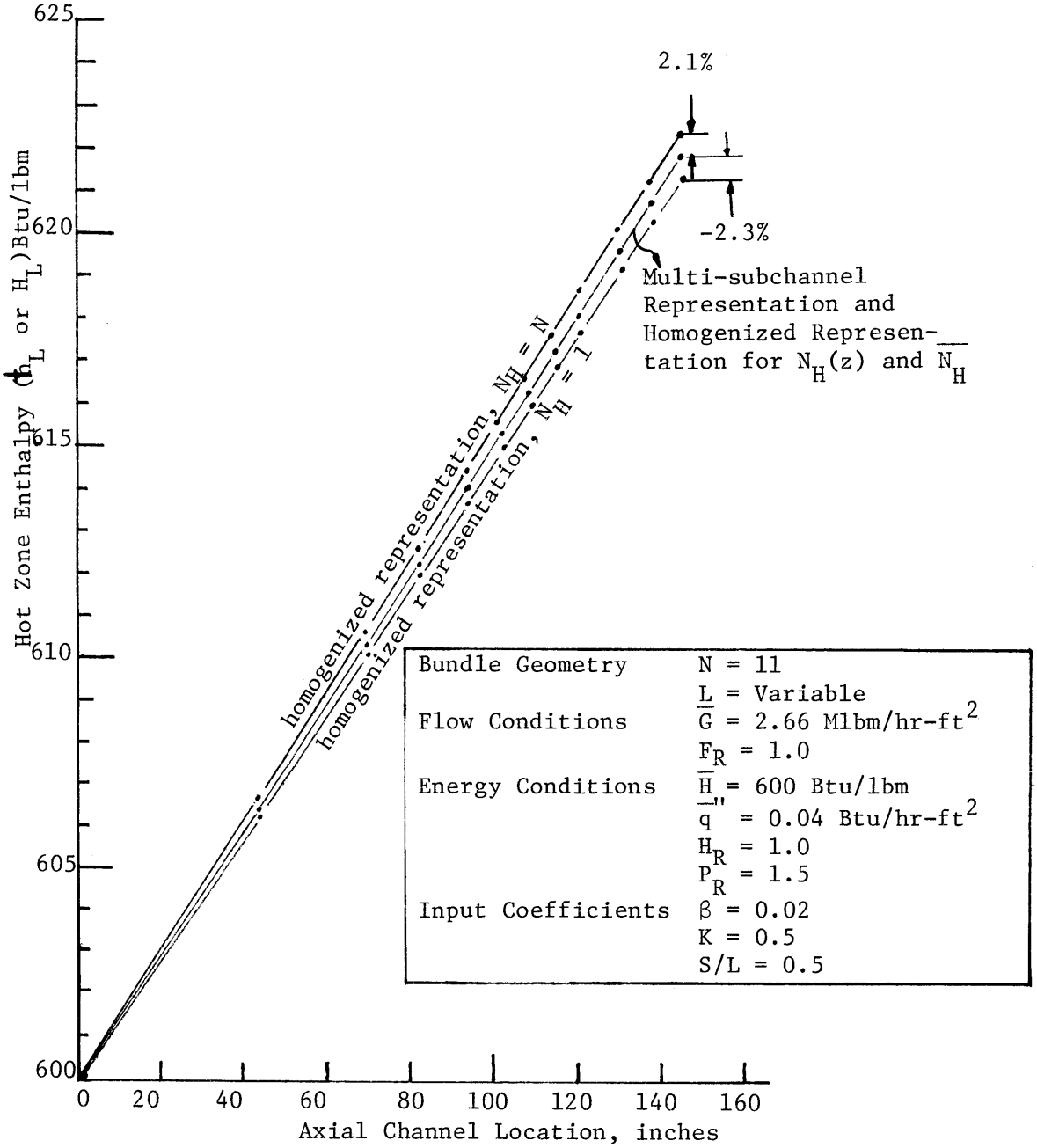

Figure 16. Comparison between results of homogenized representations and multi-subchannel representation for Power Upset Case

Bundle Geometry	N = 5
	L = Variable
Flow Conditions	$\overline{G}$ = 2.66 Mlbm/hr-ft^2
	F_R = 1.0
Energy Conditions	$\overline{H}$ = 600 Btu/lbm
	$\overline{q''}$ = 0.04 MBtu/hr-ft^2
	H_R = 1.0
	P_R = 1.5
Input Coefficients	β = Variable
	K = 0.5
	S/L = 0.5

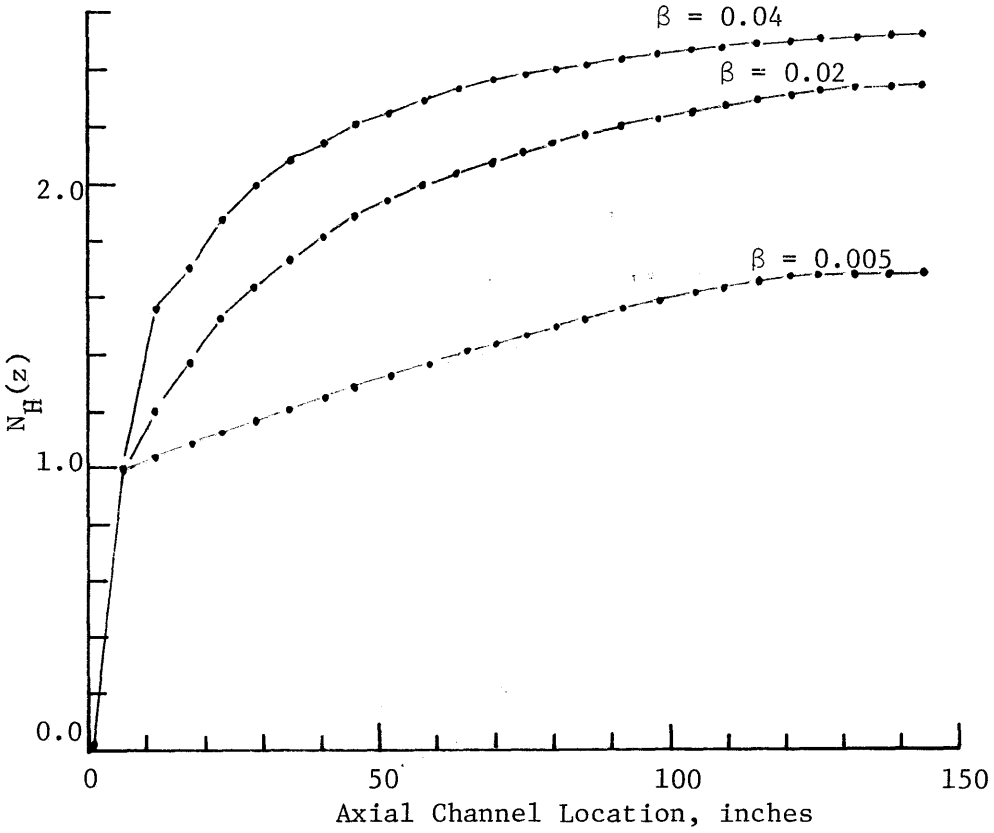

Figure 17. $N_H(z)$ versus channel length for POWER UPSET CASE, N=5

Bundle Geometry	N = 11
	L = Variable
Flow Conditions	$\overline{G}$ = 2.66 Mlbm/hr-ft^2
	F_R = 1.0
Energy Conditions	$\overline{H}$ = 600 Btu/lbm
	$\overline{q''}$ = 0.04 MBtu/hr-ft^2
	H_R = 1.0
	P_R = 1.5
Input Coefficients	β = Variable
	K = 0.5
	S/L = 0.5

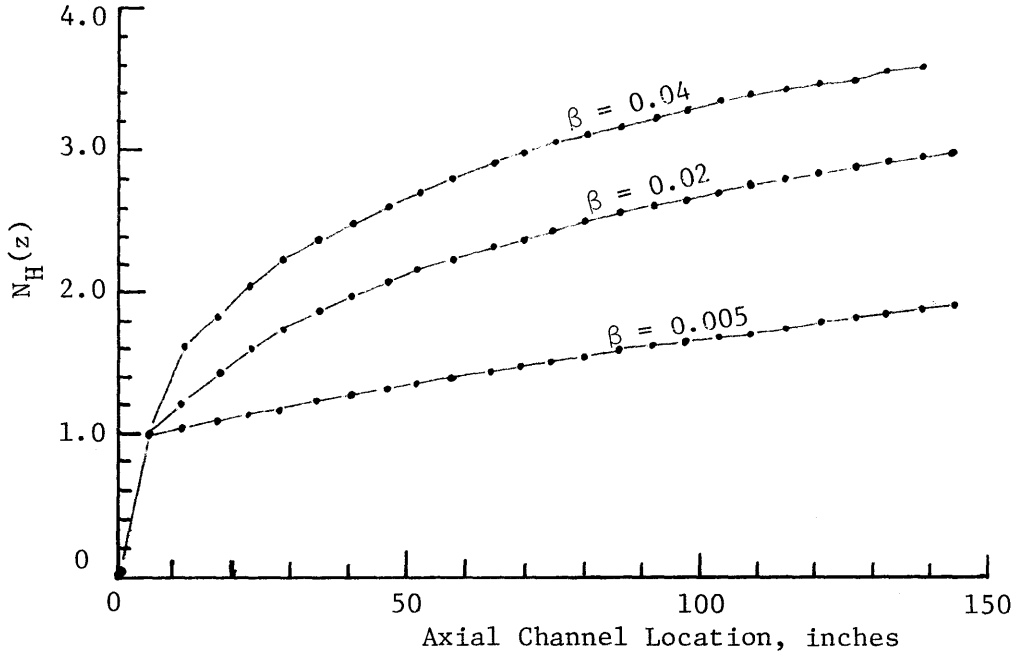

Figure 18. $N_H(z)$ versus channel length for POWER UPSET CASE, N=11

Bundle Geometry	N = 23
	L = Variable
Flow Conditions	$\overline{G}$ = 2.66 Mlbm/hr-ft^2
	F_R = 1.0
Energy Conditions	$\overline{H}$ = 600 Btu/lbm
	$\overline{q}''$ = 0.04 MBtu/hr-ft^2
	H_R = 1.0
	P_R = 1.5
Input Coefficients	β = Variable
	K = 0.5
	S/L = 0.5

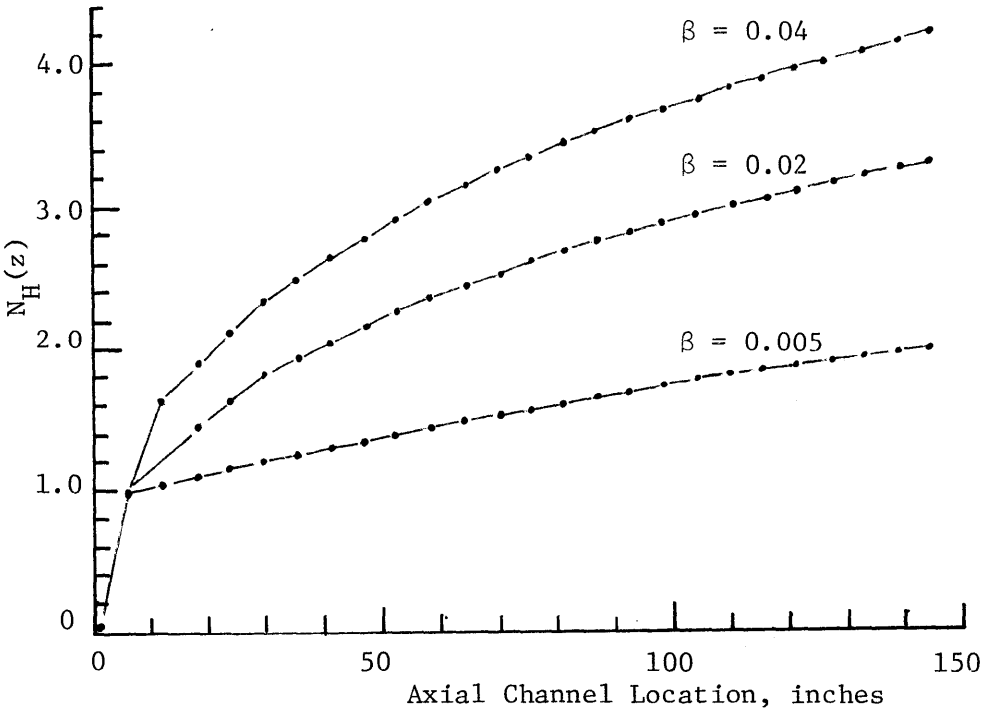

Figure 19. $N_H(z)$ versus channel length for POWER UPSET CASE, N=23

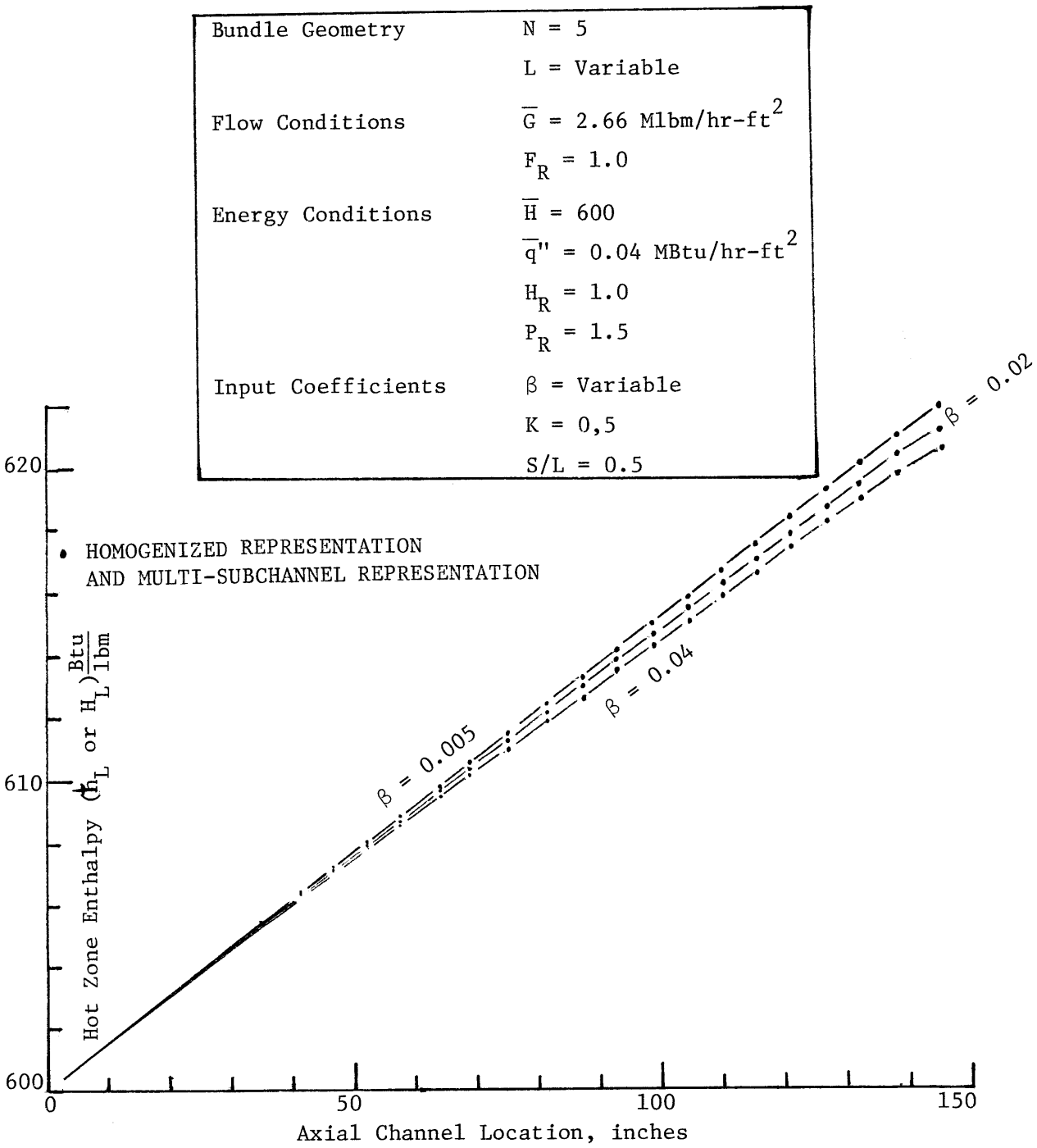

Figure 20. Validity of $N_H(z)$ for POWER UPSET CASE, N=5

Bundle Geometry	N = 11
	L = Variable
Flow Conditions	$\bar{G}$ = 2.66 Mlbm/hr-ft^2
	F_R = 1.0
Energy Conditions	$\bar{H}$ = 600 Btu/lbm
	$\bar{q}''$ = 0.04 x 10^6 Btu/hr-ft^2
	H_R = 1.0
	P_R = 1.5
Input Coefficients	β = Variable
	K = 0.5
	S/L = 0.5

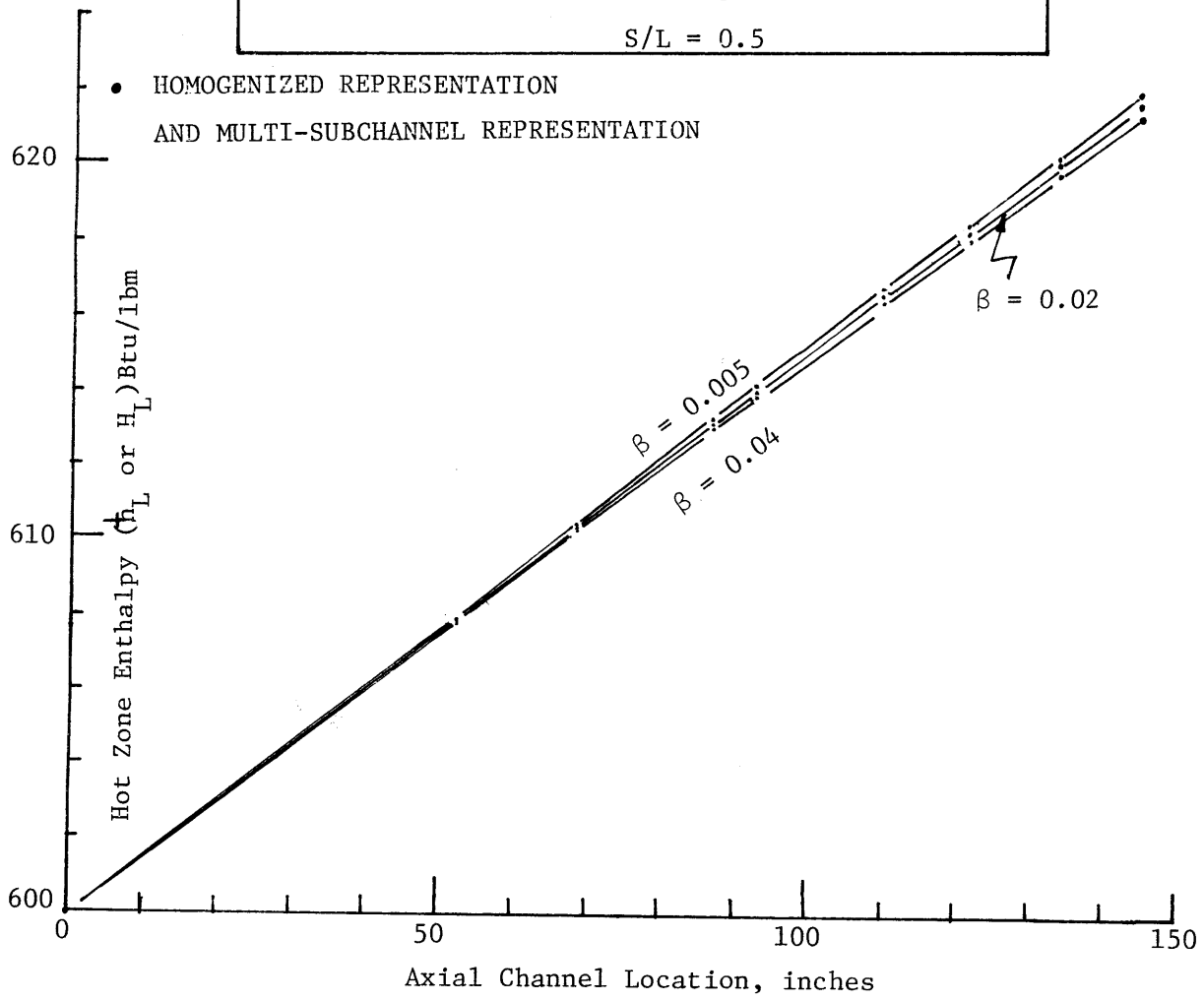

Figure 21. Validity of $N_H(z)$ for POWER UPSET CASE
N = 11

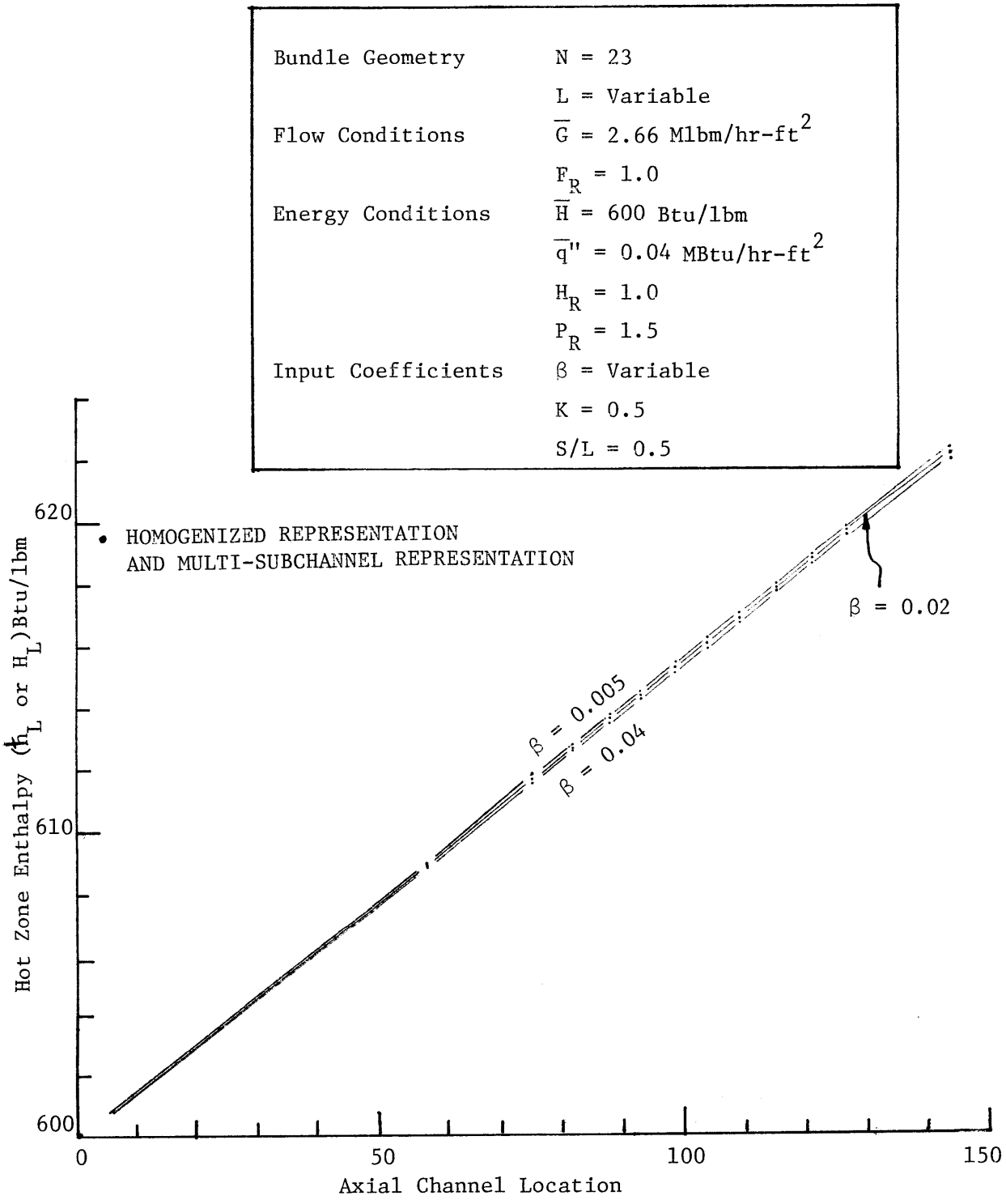

Figure 22. Validity of $N_H(z)$ for POWER UPSET CASE, N=23

Bundle Geometry	N = Variable
	L = Variable
Flow Conditions	$\overline{G}$ = 2.66 Mlbm/ft^2-hr
	F_R = 1.0
Energy Conditions	$\overline{H}$ = 600 Btu/lbm
	$\overline{q}$" = 0.04 MBtu/ft^2-hr
	H_R = 1.0
	P_R = 1.5
Input Coefficients	β = 0.02
	K = 0.5
	S/L = 0.5

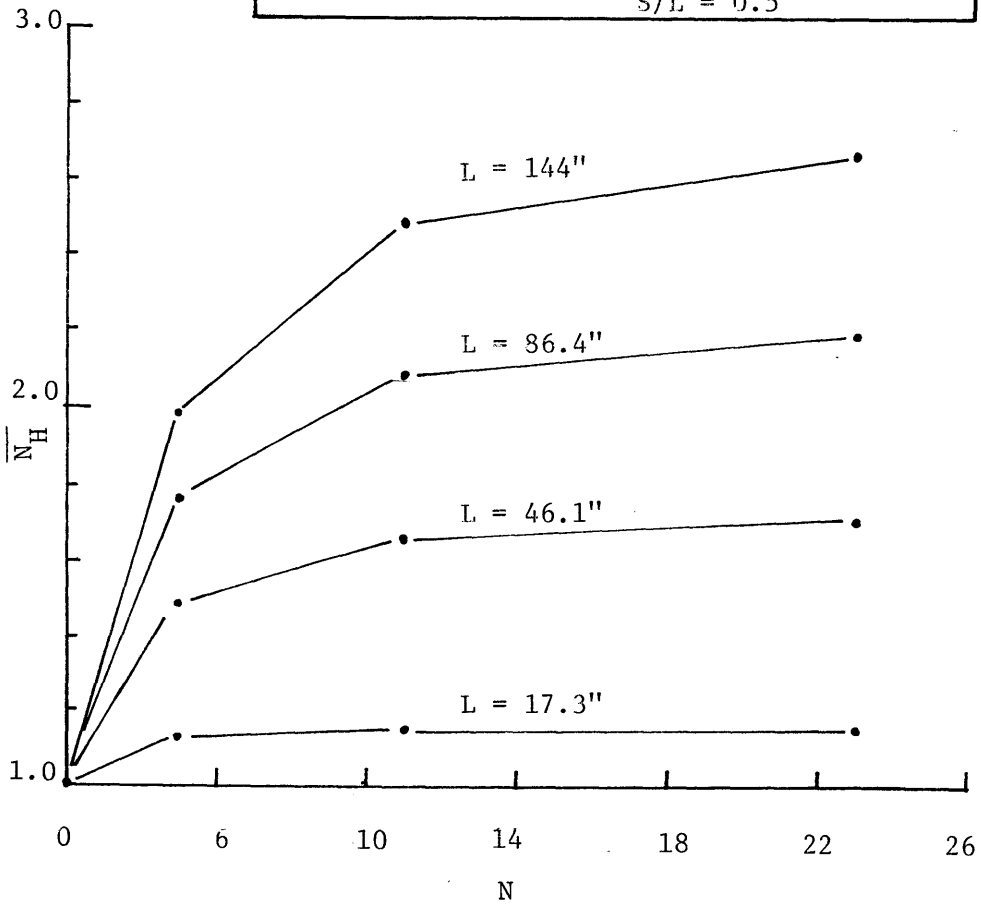

Figure 23. $\overline{N_H}$ versus N and L

Bundle Geometry	N = 11
	L = 144"
Flow Conditions	$\overline{G}$ = 2.66 Mlbm/hr-ft^2
	F_R = Variable
Energy Conditions	$\overline{H}$ = 600 Btu/lbm
	$\overline{q}$"= 0.04 MBtu/hr-ft^2
	H_R = 1.0
	P_R = 1.0
Input Coefficients	β = 0.02
	K = 0.5
	S/L = 0.5

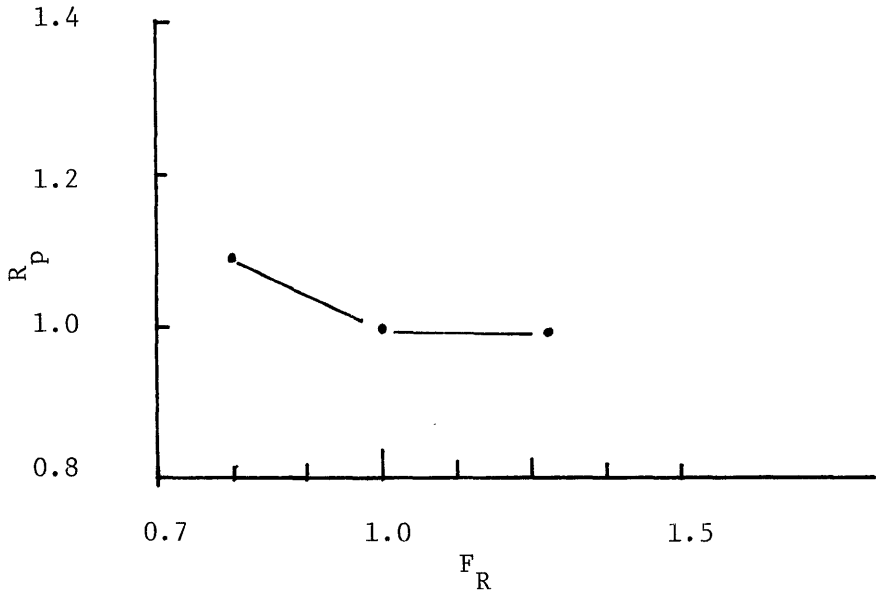

Figure 24. R_p versus F_R

Bundle Geometry	N = 11
	$\underline{L}$ = 144"
Flow Conditions	$\underline{G}$ = 2.66 Mlbm/hr-ft^2
	F_R = 1.22
Energy Conditions	$\underline{H}$ = 600 Btu/lbm
	$\underline{q}''$ = 0.04 MBtu/hr-ft^2
	H_R = 1.0
	P_R = 1.0
Input Coefficients	β = 0.02
	K = 0.5
	S/L = 0.5

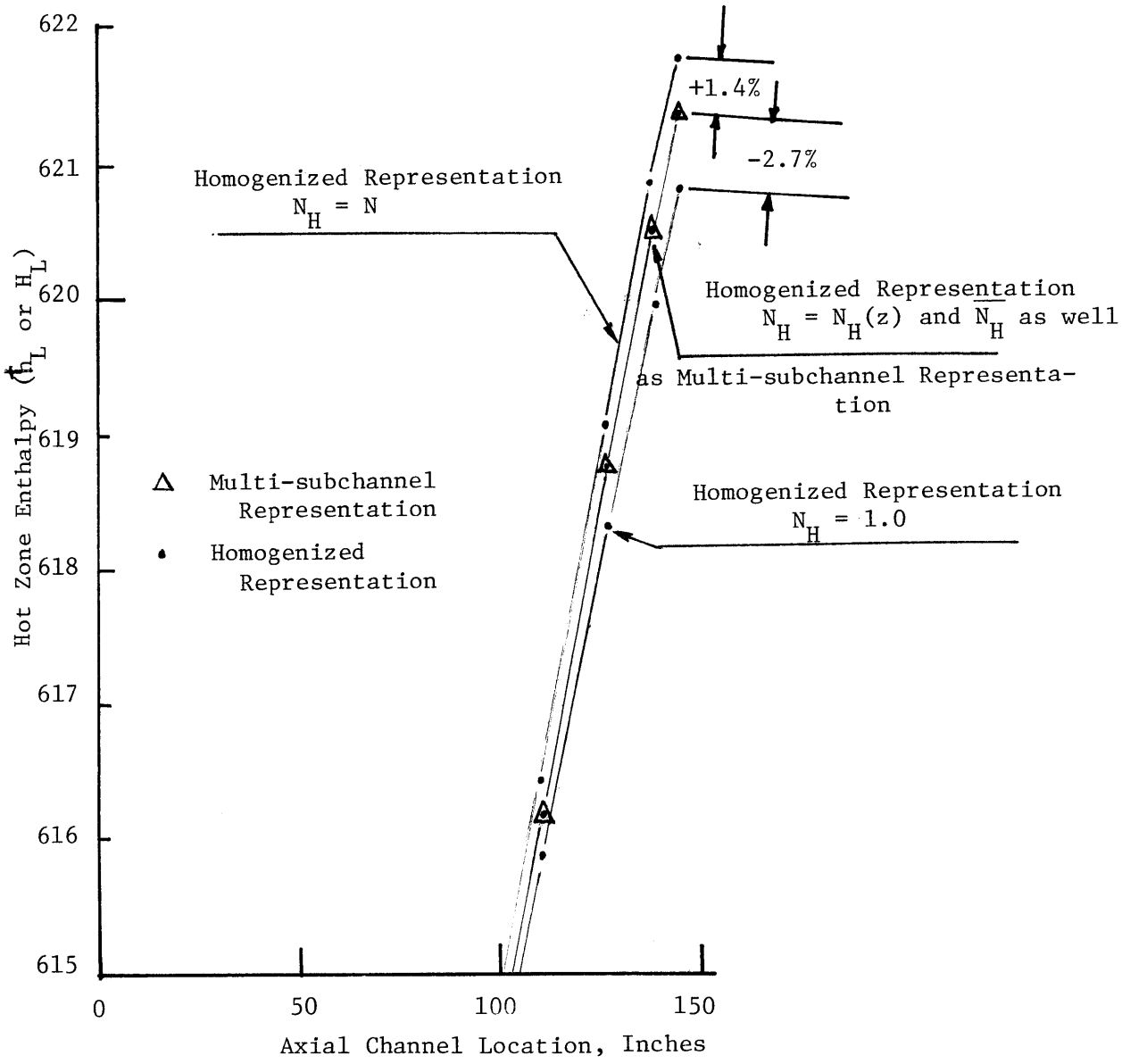

Figure 25. Validity of $N_H(z)$ for POWER and FLOW UPSET CASE in the subchannel exit region

Bundle Geometry	N = 11
	L = 144"
Flow Conditions	$\overline{G}$ = 2.66 Mlbm/ft^2-hr
	F_R = 1.0
Energy Conditions	$\overline{H}$ = 600
	$\overline{q}$" = Variable
	H_R = 1.0
	P_R = 1.5
Input Coefficients	β = 0.02
	K = 0.5
	S/L = 0.5

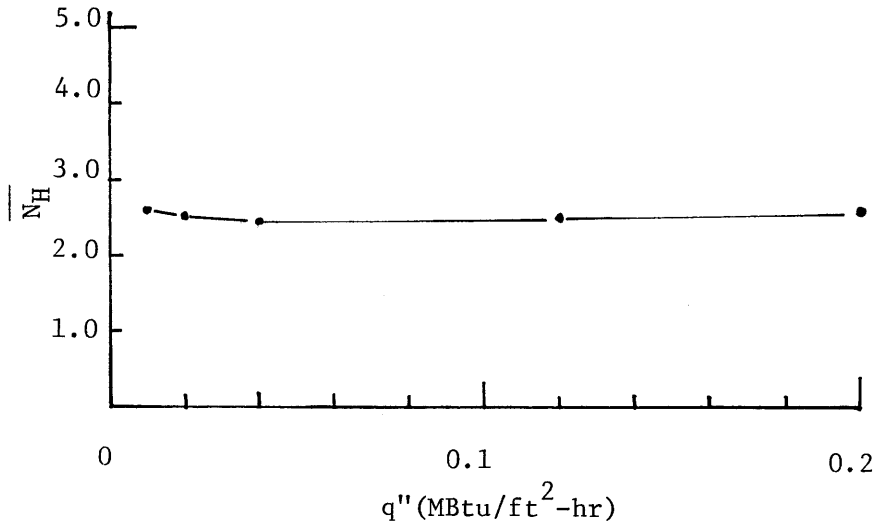

Figure 26. $\overline{N_H}$ versus q"

Bundle Geometry	N = 11
	L = 144"
Flow Conditions	$\overline{G}$ = 2.66 Mlbm/hr-ft^2
	F_R = 1.0
Energy Conditions	$\overline{H}$ = 600 Btu/lbm
	$\overline{q}$" = 0.0
	H_R = Variable
	P_R = 1.0
Input Coefficients	β = 0.02
	K = 0.5
	S/L = 0.5

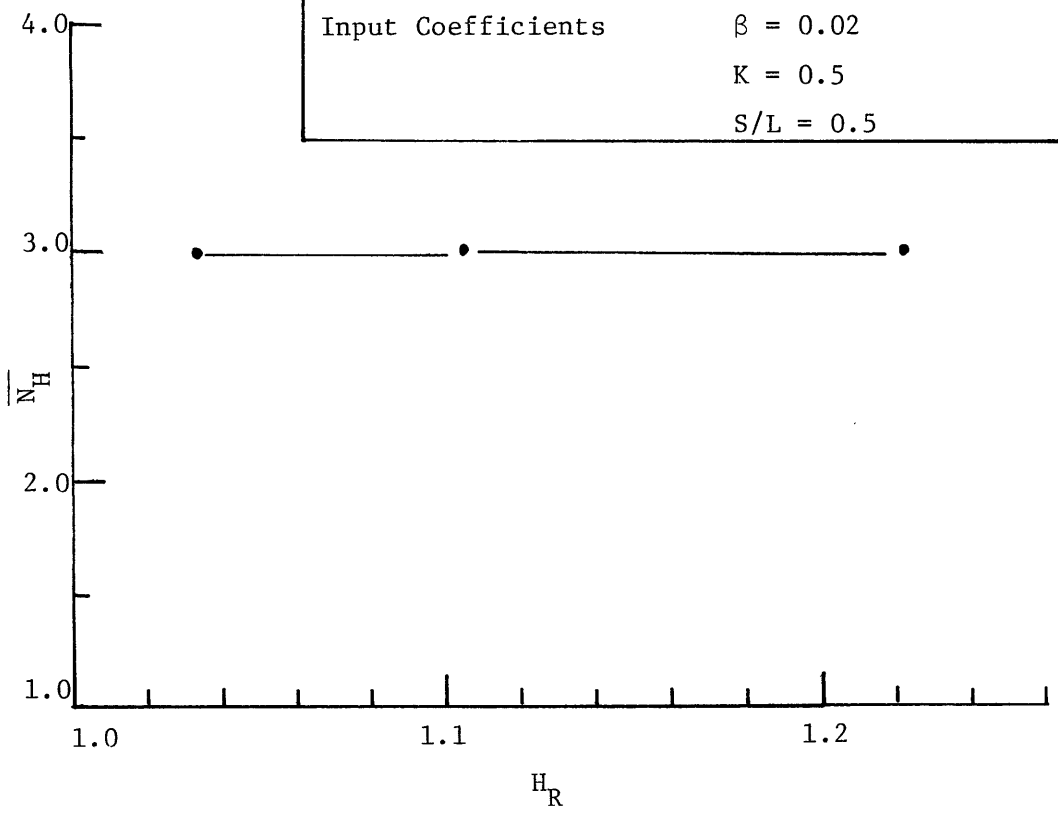

Figure 27. $\overline{N_H}$ versus H_R

Bundle Geometry	N = 11
	L = 144"
Flow Conditions	$\overline{G}$ = 2.66 Mlbm/hr-ft^2
	F_R = 1.0
Energy Conditions	$\overline{H}$ = 600 Btu/lbm
	$\overline{q}$" = 0.2 MBtu/hr-ft^2
	H_R = 1.0
	P_R = Variable
Input Coefficients	β = 0.02
	K = 0.5
	S/L = 0.5

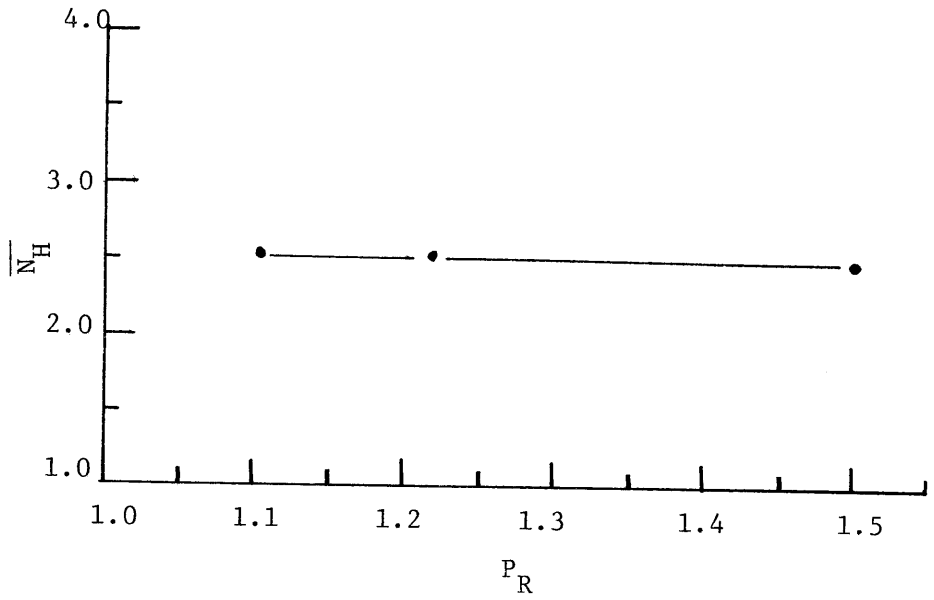

Figure 28. $\overline{N_H}$ versus P_R

Bundle Geometry	N = Variable
	L = 144"
Flow Conditions	$\overline{G}$ = 2.66 Mlbm/hr-ft^2
	F_R = 1.0
Energy Conditions	$\overline{H}$ = 600 Btu/lbm
	$\overline{q}$" = 0
	H_R = 1.22
	P_R = 1.0
Input Coefficients	β = Variable
	K = 0.5
	S/L = 0.5

β \ N	2	5	11	23
0.005	a = 1.0	a = 3.66 b = 183	a = 6.11 b = 275	a = 6.75 b = 269
0.02	a = 1.0	a = 2.04 b = 9.22	a = 4.36 b = 34.0	a = 5.96 b = 52.4
0.04	a = 1.0	a = 1.93 b = 0.31	a = 4.79 b = 22.7	a = 8.09 b = 54.8

TABLE 1

Coefficients for $N_H(z) = 1.0 + \frac{bz}{a+z}$

Under Enthalpy Upset Condition

Bundle Geometry	N = Variable
	L = 144"
Flow Conditions	$\overline{G}$ = 2.66 Mlbm/hr-ft^2
	F_R = 1.0
Energy Conditions	$\overline{H}$ = 600 Btu/lbm
	$\overline{q}$" = 0
	H_R = 1.22
	P_R = 1.0
Input Coefficients	β = Variable
	K = 0.5
	S/L = 0.5

$\overline{N}_H$

β \ N	2	5	11	23
0	1.00	∿1.00	∿1.00	∿1.00
0.005	1.00	1.77	1.93	2.03
0.02	1.00	2.40	3.03	3.32
0.04	1.00	2.57	3.65	4.23

TABLE 2

$\overline{N}_H$ for Different β and Different N over Z = 0 to 144"
Under Enthalpy Upset Condition

Bundle Geometry	N = Variable
	L = 144"
Flow Conditions	$\overline{G}$ = 2.66 Mlbm/hr-ft^2
	F_R = 1.0
Energy Conditions	$\overline{H}$ = 600 Btu/lbm
	$\overline{q}$" = 0.04 MBtu/hr-ft^2
	H_R = 1.0
	P_R = 1.5
Input Coefficients	β = Variable
	K = 0.5
	S/L = 0.5

β \ N		2	5	11	23
0.005	a	1.0	0.96	0.95	0.94
	b	1.0	314	383	384
	c	0.0	2.60	3.6	3.9
0.02	a	1.0	0.82	0.75	0.73
	b	-	48.5	70.6	81.1
	c	0.0	1.94	3.4	4.0
0.04	a	1.0	0.096	0.47	1.2
	b	1.0	10.8	38.8	124
	c	0.0	2.60	4.00	5.00

TABLE 3

Coefficients for $N_H(z) = a + \frac{cz}{b+z}$ Under Power Upset Condition, Where z is the Channel Location

Bundle Geometry	N = Variable
	L = 144"
Flow Conditions	$\overline{G}$ = 2.66 Mlbm/hr-ft^2
	F_R = 1.0
Energy Conditions	$\overline{H}$ = 600 Btu/lbm
	$\overline{q}$" = 0.04 MBtu/hr-ft^2
	H_R = 1.0
	P_R = 1.5
Input Coefficients	β = Variable
	K = 0.5
	S/L = 0.5

β \ N	2	5	11	23
0	1	∿1	∿1	∿1
0.005	1	1.51	1.61	1.66
0.02	1	2.0	2.49	2.67
0.04	1	2.33	3.05	3.20

TABLE 4

$\overline{N}_H$ For Different N and β Under The Power Upset Condition

z = 144"

Bundle Geometry	N = 11
	L = 144"
Flow Conditions	$\bar{G}$ = 2.66 Mlbm/hr-ft^2
	F_R = 1.0
Energy Conditions	$\bar{H}$ = 600 Btu/lbm
	$\bar{q}"$ = 0.2 MBtu/hr-ft^2
	H_R = 1.0
	P_R = 1.5
Input Coefficients	β = 0.02
	K = 0.5
	S/L = 0.5

	$\Delta\dot{h}_{T.I.}$ (Btu/lbm)
Multi-Subchannel Representation	-3.096

Homogenized Representation	$\Delta H_{T.I.}$ (Btu/lbm)	ERROR %
$N_H(z)$, $N_U(z)$, $N_{TU}(z)$, N_{TF} and N_{TP}	-3.012	-2.7%
$N_H(z)$, $N_U(z)$	-3.012	-2.7%
$N_H(z)$	-3.012	-2.7%
N_H = 1.0	-7.07	+128.4%

$$\text{ERROR} \equiv \frac{\Delta H_{T.I.} - \Delta\dot{h}_{T.I.}}{\Delta\dot{h}_{T.I.}}$$

TABLE 5

Comparison of the hot zone enthalpy increments due to turbulent interchange only between the multi-subchannel representation and the homogenized representations with different combination of coupling coefficients for Power Upset Case

Bundle Geometry	N = 11
	L = 144"
Flow Conditions	$\bar{G}$ = 2.66 Mlbm/hr-ft^2
	F_R = 1.0
Energy Conditions	$\bar{H}$ = 600 Btu/lbm
	$\bar{q}"$ = 0.2 MBtu/hr-ft^2
	H_R = 1.0
	P_R = 1.5
Input Coefficients	β = 0.02
	K = 0.5
	S/L = 0.5

	$\Delta\dot{h}_{D.C.}$ (Btu/lbm)
Multi-Subchannel Representation	0.244

Homogenized Representation	$\Delta H_{D.C.}$ (Btu/lbm)	ERROR %
$N_H(z)$, $N_U(z)$, $N_{TU}(z)$, N_{TF} and N_{TP}	0.251	3.0%
$N_H(z)$, $N_U(z)$	0.253	3.8%
$N_H(z)$	0.261	7.1%
N_H = 1.0	0.001	-99.6%

$$\text{ERROR} \equiv \frac{\Delta\dot{h}_{D.C.} - \Delta H_{D.C.}}{\Delta\dot{h}}$$

TABLE 6

Comparison of the hot zone enthalpy increments due to diversion crossflow only between the multi-subchannel representation and the homogenized representations with different combination of coupling coefficients for Power Upset Case

Bundle Geometry	N = 11
	L = 144"
Flow Conditions	$\bar{G}$ = 2.66 Mlbm/hr-ft^2
	F_R = 1.0
Energy Conditions	$\bar{H}$ = 600 Btu/lbm
	$\bar{q}"$ = 0.2 MBtu/hr-ft^2
	H_R = 1.0
	P_R = 1.5
Input Coefficients	β = 0.02
	K = 0.5
	S/L = 0.5

	$\int w_{C,D}(z)dz$ (Btu/hr)
Multi-Subchannel Representation	0.1758

Homogenized Representation	$\int W_{L,R}(z)dz$(Btu/hr)	ERROR %
$N_H(z)$, $N_U(z)$, $N_{TU}(z)$, N_{TP} and N_{TF}	0.1776	2.2%
$N_H(z)$, $N_U(z)$	0.1798	2.3%
$N_H(z)$	0.1825	3.8%
N_H = 1.0	0.1120	-36.3%

$$\text{ERROR} \equiv \frac{\int W_{L,R}dz - \int w_{C,D}dz}{\int w_{C,D}dz}$$

TABLE 7

Comparison of the total diversion crossflow only across the boundary between the multi-subchannel representation and the homogenized representations with different combination of coupling coefficients for Power Upset Case

TABLE 8

EXPECTED ERRORS IN 2D HOMOGENIZED REGION ENTHALPY FOR POWER UPSET CASE

β \ N	2	3	4	5	7	9	11	15	23
0.0	0	0	0	0	0	0	0	0	0
0.005	0	-0.66	-0.61	-0.53	-0.40	-0.33	-0.27	-0.206	-0.135
0.02	0	-3.4	-3.6	-3.2	-2.3	-2.0	-1.72	-1.3	-0.86
0.04	0	-7.83	-8.5	-7.56	-5.31	-4.63	-3.9	-2.83	-1.83
0.06	0	-13.3	-14.4	-12.3	-9.34	-7.4	-6.12	-4.53	-2.36

NOTE: This table is built by using

$$\text{ERROR\%} = \frac{1 - \frac{1}{\overline{N_H}}}{\frac{P_R N A_s}{(P_r - 1) L \beta S} - \frac{1}{\overline{N_H}}}$$ Equation E.20

where $L = 12'$
$A_s = 0.00519\ ft^2$
$P_r = 1.5$
$S = 0.22"$

$$\overline{N_H} = 1 + \ln\{1 + [353(\frac{N-2}{N})^{\frac{3.5\beta}{0.015+\beta}} \beta^{1.1}]\} \pm 5\%$$ Equation 5.1.1

APPENDIX A

DERIVATIONS OF THE COUPLING COEFFICIENTS

In this appendix, the coupling coefficients, N_H, N_U, N_{TP}, N_{TF} and N_{TU} are derived in (A.1), (A.2) and (A.3). The multi-subchannel layout and homogenized representation layout can be seen in Figures 2 and 3 respectively. For N odd, subchannels C and D can be regarded as half channels. For N even, subchannels C and D can be regarded as full channels. The derivations presented here for these coupling coefficients are valid for N either even or odd.

A.1 Derivation of N_H

The steady state energy equation for adjacent subchannels i and j following (1, equation A-6) can be written as:

$$\frac{\partial m_i h_i}{\partial x} = q_i - \sum_{j=1}^{N} (t_i - t_j) c_{i,j} - \sum_{j=1}^{N} (h_i - h_j) w'_{i,j} - \sum_{j=1}^{N} w_{i,j} h^* \qquad \text{(A.1.1)}$$

where
$$\begin{cases} w_{i,j} h^* = w_{i,j} h_i & \text{if } w_{i,j} > 0 \qquad \text{(A.1.2a)} \\ w_{i,j} h^* = w_{i,j} h_j & \text{if } w_{i,j} < 0 \qquad \text{(A.1.2b)} \end{cases}$$

Note that $w_{i,j} > 0$ means the direction of diversion cross-flow is from channel i to channel j, and $w_{i,j} < 0$ means

the direction of diversion crossflow is from channel j to channel i.

We consider a multi-subchannel layout shown in Figure 2 and write the energy equation for each subchannel.

$$\frac{\partial m_A h_A}{\partial x} = q_A' - (t_A - t_B)c_{A,B} - (h_A - h_B)w_{A,B}' - w_{A,B}h^* \qquad \text{(A.1.3a)}$$

$$\frac{\partial m_B h_B}{\partial x} = q_B' - (t_B - t_C)c_{B,A} - (t_B - t_A)c_{B,A} - (h_B - h_C)w_{B,C}' - (h_B - h_A)w_{B,A}' - w_{B,C}h^* - w_{B,A}h^* \qquad \text{(A.1.3b)}$$

$$\frac{\partial m_C h_C}{\partial x} = q_C' - (t_C - t_D)c_{C,D} - (t_C - t_B)c_{C,B} - (h_C - h_D)w_{C,D}' - (h_C - h_B)w_{C,B}' - w_{C,D}h^* - w_{C,B}h^* \qquad \text{(A.1.3c)}$$

$$\frac{\partial m_D h_D}{\partial x} = q_D' - (t_D - t_E)c_{D,E} - (t_D - t_C)c_{D,C} - (h_D - h_E)w_{D,E}' - (h_D - h_C)w_{D,C}' - w_{D,E}h^* - w_{D,C}h^* \qquad \text{(A.1.3d)}$$

$$\frac{\partial m_E h_E}{\partial x} = q_E' - (t_E - t_F)c_{E,F} - (t_E - t_D)c_{E,D} - (h_E - h_F)w_{E,F}' - (h_E - h_D)w_{E,D}' - w_{E,F}h^* - w_{E,D}h^* \qquad \text{(A.1.3e)}$$

$$\frac{\partial m_F h_F}{\partial x} = q_F' - (t_F - t_F)c_{F,E} - (h_F - h_E)w_{F,E}' - w_{F,E}h^* \qquad \text{(A.1.3f)}$$

Some relationships exist for each pair of channels between the energy carried by diversion flows, conductivity factors $c_{i,j}$ and energy carried by turbulent interchanges. For example for the channel pair A,B, the following relationships hold:

$$c_{A,B} = c_{B,A} \tag{A.1.4a}$$

$$w'_{A,B} = w'_{B,A} \tag{A.1.4b}$$

$$w_{A,B} = -w_{B,A} \tag{A.1.4c}$$

$$\begin{cases} w_{A,B}{}^{h^*} = w_{A,B}{}^{h_A} \\ \\ w_{B,A}{}^{h^*} = w_{B,A}{}^{h_A} \end{cases} \quad \text{if } w_{A,B} > 0 \text{ (i.e. } w_{B,A} < 0) \tag{A.1.4d}$$

$$\begin{cases} w_{A,B}{}^{h^*} = w_{A,B}{}^{h_B} \\ \\ w_{B,A}{}^{h^*} = w_{B,A}{}^{h_B} \end{cases} \quad \text{if } w_{A,B} < 0 \text{ (i.e. } w_{B,A} > 0) \tag{A.1.4e}$$

Therefore, a simple relationship between $w_{A,B}{}^{h^*}$ and $w_{B,A}{}^{h^*}$ can be derived from equations (A.1.4c), (A.1.4d) and (A.1.4e).

$$w_{A,B}{}^{h^*} = -w_{B,A}{}^{h^*} \quad \text{for} \quad w_{A,B} \gtrless 0 \tag{A.1.5}$$

We define the region composed of subchannels A, B, and C as region L, and similarly, D, E, and F as region R. Now adding the energy equations for region L and region R and utilizing the relations of equations (A.1.4a, A.1.4b) and (A.1.5) we obtain the following two energy equations:

$$\sum_{i=A}^{C} \frac{\partial h_i m_i}{\partial x} = \sum_{i=A}^{C} q_i' - (t_C - t_D)c_{C,D} - (h_C - h_D)w'_{C,D} - h^* w_{C,D} \qquad \text{(A.1.6a)}$$

$$\sum_{i=D}^{F} \frac{\partial h_i m_i}{\partial x} = \sum_{i=D}^{E} q_i' - (t_D - t_C)c_{D,C} - (h_D - h_C)w'_{D,C} - h^* w_{D,C} \qquad \text{(A.1.6b)}$$

On the other hand, we can express the energy equation for the homogenized regions of Figure 3 directly as

$$\frac{\partial H_L M_L}{\partial x} = Q_L' - \left(\frac{T_L - T_R}{N_H''}\right) C_{L,R} - \left(\frac{H_L - H_R}{N_H}\right) W'_{L,R} - \frac{H^*}{N_H'} W_{L,R} \qquad \text{(A.1.7a)}$$

$$\frac{\partial H_R M_R}{\partial x} = Q_R' - \left(\frac{T_R - T_L}{N_H''}\right) C_{R,L} - \left(\frac{H_R - H_L}{N_H}\right) W'_{R,L} - \frac{H^*}{N_H'} W_{R,L} \qquad \text{(A.1.7b)}$$

If we assume

$$\sum_{i=A}^{C} \frac{\partial h_i m_i}{\partial x} = \frac{\partial H_L M_L}{\partial x} \qquad \text{(A.1.8a)}$$

$$\sum_{i=D}^{F} \frac{\partial h_i m_i}{\partial x} = \frac{\partial H_R M_R}{\partial x} \qquad \text{(A.1.8b)}$$

$$Q_L' \equiv \sum_{i=A}^{C} q_i' \qquad \text{(A.1.8c)}$$

$$Q'_R \equiv \sum_{i=D}^{F} q'_i \qquad \text{(A.1.8d)}$$

and

$$W'_{L,R} = w'_{C,D} \qquad \text{(A.1.8e)}$$

$$W_{L,R} = w_{C,D} \qquad \text{(A.1.8f)}$$

then N_H, N'_H, and N''_H can be defined as follows:

$$N''_H \equiv \frac{T_L - T_R}{t_C - t_D} \qquad \text{(A.1.9a)}$$

$$N_H \equiv \frac{H_L - H_R}{h_C - h_D} \qquad \text{(A.1.9b)}$$

$$N'_H \equiv \frac{H^*}{h^*} \quad \text{where} \quad \frac{H^*}{h^*} = \frac{H_L}{h_C} \text{ if } W_{L,R} > 0 \qquad \text{(A.1.9c)}$$

$$\frac{H^*}{h^*} = \frac{H_R}{h_D} \text{ if } W_{R,L} < 0$$

If we assume the specific heat at each elevation is constant, then

$$N''_H = N_H \quad . \qquad \text{(A.1.10)}$$

Also the subchannel enthalpy h^* can be expressed as a function of N_H in the following manner by virtue of the definitions of H_L, H_R and N_H (eqn. A.1.9b) and the assumption of a symmetric enthalpy profile with respect to the central boundary (see Appendix C for derivation of the following relations).

$$\frac{h_C + h_D}{2} = \frac{H_L + H_R}{2} \qquad \text{(A.1.11)}$$

$$h^* = \frac{H_L+H_R}{2} + \frac{H_L - \frac{H_L+H_R}{2}}{N_H} \quad \text{if } w_{C,D} > 0 \qquad \text{(2.3.1)}$$

and $$h^* = \frac{H_L+H_R}{2} - \frac{H_R - \frac{H_L+H_R}{2}}{N_H} \quad \text{if } w_{C,D} < 0 \qquad \text{(2.3.1a)}$$

Therefore, we can obtain N_H' in terms of N_H and other known quantities.

$$N_H' = \frac{H^*}{h^*} = \frac{H_L}{\frac{H_L+H_R}{2} + \frac{H_L - \frac{H_L+H_R}{2}}{N_H}} \quad \text{if } w_{C,D} > 0 \qquad \text{(A.1.12a)}$$

and $$N_H' = \frac{H^*}{h^*} = \frac{H_R}{\frac{H_L+H_R}{2} - \frac{H_R - \frac{H_L+H_R}{2}}{N_H}} \quad \text{if } w_{C,D} < 0 \qquad \text{(A.1.12b)}$$

From the above derivation we have determined the coupling coefficients required in the energy equations (A.1.7a) and (A.1.7b). By virtue of equations (A.1.10) and (A.1.12a and b) these coefficients are all expressable in terms of the single coefficient N_H.

A.2 Derivation of N_U

The steady state axial momentum equation for channel i and adjacent channels j following (1, equation A-11) can be written as:

$$-F_i - gA_i\rho_i\cos\theta - A_i \frac{\partial p_i}{\partial x} = \frac{\partial}{\partial x} \; m_i u_i + (u_i - u_j) w'_{i,j} + u^* w_{i,j} \qquad (A.2.1)$$

where

$$F = \text{friction factor} = \left[\frac{A\nu f\phi}{2D} + \frac{ak\nu'}{2\Delta x} \right] \left[\frac{m}{A} \right]^2$$

where the parameters in the definition are per Cobra, BNWL-

$$u^* w_{i,j} = u_i w_{i,j} \quad \text{if } w_{i,j} > 0$$

$$u^* w_{i,j} = u_j w_{i,j} \quad \text{if } w_{i,j} < 0$$

Consider a multi-subchannel layout shown in Figure 2 and write the axial momentum equation for each channel. In the steady state condition, obtain:

$$A_A \frac{\partial p_A}{\partial x} = \frac{\partial}{\partial x}(m_A u_A) - (F+\rho g A \cos\theta)_A - w'_{A,B}(u_A - u_B) + u^* w_{A,B} \quad \text{(A.1.2a)}$$

$$A_B \frac{\partial p_B}{\partial x} = \frac{\partial}{\partial x}(m_B u_B) - (F+\rho g A \cos\theta)_B - w'_{B,C}(u_B - u_C) - w'_{B,A}(u_B - u_A) + u^* w_{B,C} + u^* w_{B,A} \quad \text{(A.2.2b)}$$

$$A_C \frac{\partial p_C}{\partial x} = \frac{\partial}{\partial x}(m_C u_C) - (F+\rho g A \cos\theta)_C - w'_{C,D}(u_C - u_D) - w'_{C,B}(u_C - u_B) + u^* w_{C,D} + u^* w_{C,B} \quad \text{(A.2.2c)}$$

$$A_D \frac{\partial p_D}{\partial x} = \frac{\partial}{\partial x}(m_D u_D) - (F+\rho g A \cos\theta)_D - w'_{D,E}(u_D - u_E) - w'_{D,C}(u_D - u_C) + u^* w_{D,E} + u^* w_{D,C} \quad \text{(A.2.2d)}$$

$$A_E \frac{\partial p_E}{\partial x} = \frac{\partial}{\partial x}(m_E u_E) - (F+\rho g A \cos\theta)_E - w'_{E,F}(u_E - u_F) - w'_{E,D}(u_E - u_D) + u^* w_{E,F} + u^* w_{E,D} \quad \text{(A.2.2e)}$$

$$A_F \frac{\partial p_F}{\partial x} = \frac{\partial}{\partial x}(m_F u_F) - (F+\rho g A \cos\theta)_F - w'_{F,E}(u_F - u_E) + u^* w_{F,E} \quad \text{(A.2.2f)}$$

where $w'_{i,j} = w'_{j,i}$ (A.2.3a)

$$w_{i,j} = -w_{j,i} \quad \text{(A.2.3b)}$$

$$u^* w_{i,j} = u_i w_{i,j} \quad \text{if} \quad w_{i,j} > 0 \quad \text{(A.2.3c)}$$

$$= u_j w_{i,j} \quad \text{if} \quad w_{i,j} < 0 \quad \text{(A.2.3d)}$$

We define the region composed of three channels A, B, and C are region L, and similarly channels D, E, and F as region R. Now, adding all the axial momentum equations for region L and R, we obtain:

$$\sum_{i=A}^{C} \frac{\partial A_i p_i}{\partial x} = \sum_{i=A}^{C} (m_i u_i) - \sum_{i=A}^{C} [(F+gA\cos\theta)_i] - w'_{C,D} (u_C - u_D) - u^* w_{C,D} \qquad \text{(A.2.4a)}$$

$$\sum_{i=D}^{F} \frac{\partial A_i p_i}{\partial x} = \sum_{i=D}^{F} (m_i u_i) - \sum_{i=D}^{F} [(F+gA\cos\theta)_i] - w'_{D,C} (u_D - u_C) - u^* w_{D,C} \qquad \text{(A.2.4b)}$$

We now write the two axial momentum equations for regions L and R in the two channel representation obtained:

$$\frac{\partial A_L P_L}{\partial x} = M_L U_L - [(F+gA\cos\theta)_L] - W'_{L,R} \left(\frac{U_L - U_R}{N_U}\right) - \frac{U^* W_{L,R}}{N_U'} \qquad \text{(A.2.5a)}$$

$$\frac{\partial A_R P_R}{\partial x} = M_R U_R - [(F+gA\cos\theta)_R] - W'_{R,L} \left(\frac{U_R - U_L}{N_U}\right) - \frac{U^* W_{R,L}}{N_U'} \qquad \text{(A.2.5b)}$$

The N_U and N_U' can be defined as follows:

$$N_U \equiv \frac{U_L - U_R}{u_C - u_D} \qquad \text{(A.2.7a)}$$

$$N_U' \equiv \frac{U^*}{u^*} \qquad \text{(A.2.7b)}$$

where $$N_U' = \frac{U_L}{u_C} \quad \text{if} \quad w_{C,D} > 0 \qquad \text{(A.2.8a)}$$

$$N_U' = \frac{U_R}{u_D} \quad \text{if} \quad w_{C,D} < 0 \qquad \text{(A.2.8b)}$$

The subchannel velocity u^* can be expressed as a function of N_U in the following manner by virtue of the previous specified definition of N_U (equation A.2.7a) and the assumption of a symmetric axial velocity profile with respect to the central boundary

$$\frac{u_C + u_D}{2} = \frac{U_L + U_R}{2} \qquad \text{(A.2.9)}$$

$$u^* = \frac{U_L + U_R}{2} + \frac{U_L - \frac{U_L + U_R}{2}}{N_U} \quad \text{if } w_{L,R} > 0 \qquad \text{(2.3.2)}$$

$$u^* = \frac{U_L + U_R}{2} + \frac{U_R - \frac{U_L + U_R}{2}}{N_U} \quad \text{if } w_{L,R} < 0 \qquad \text{(2.3.2a)}$$

Therefore we get:

$$N_U' = \frac{U_L}{\frac{U_L+U_R}{2} + \frac{U_L - \frac{U_L+U_R}{2}}{N_U}} \quad \text{if } w_{L,R} > 0 \qquad \text{(A.2.10a)}$$

$$N_U' = \frac{U_R}{\frac{U_L+U_R}{2} + \frac{U_R - \frac{U_L+U_R}{2}}{N_U}} \quad \text{if } w_{L,R} < 0 \qquad \text{(A.2.10b)}$$

From the above derivation we have determined the coupling coefficients required in the axial momentum equations (A.1.7a) and (A.1.7b). By virtue of equations (A.2.7b) and (A.2.10a and b), these coupling coefficients are all expressible in terms of the single coefficient N_U.

A.3 Derivation of N_{TP}, N_{TU} and N_{TF}

The steady state transverse momentum equation for adjacent channels i and j following (1, equation A-17) can be written as:

$$\frac{\partial(\bar{u}w_{i,j})}{\partial x} = \frac{s}{\ell}(p_i - p_j) - c_i \qquad \text{(A.3.1)}$$

where

$$\overline{uw}_{i,j} = \frac{1}{2} (u_i + u_j) w_{i,j} \qquad (A.3.2a)$$

$$c_i = \frac{s}{\ell} \left(\frac{k|w_{i,j}|}{2s^2 \rho^*_{i,j}} \right) w_{i,j} \qquad (A.3.2b)$$

$$\rho^*_{i,j} = \rho_i \quad \text{if} \quad w_{i,j} > 0 \qquad (A.3.2c)$$

$$\rho_j \quad \text{if} \quad w_{i,j} < 0 \qquad (A.3.2d)$$

where subscripts i and j denote adjacent channels.

Consider a multichannel layout shown in Figure 2 and write the transverse momentum equations associated with each boundary we obtain:

$$\frac{\partial(\overline{uw}_{A,B})}{\partial x} = \frac{s}{\ell} (p_A - p_B) - c_A \qquad (A.3.3a)$$

$$\frac{\partial(\overline{uw}_{B,C})}{\partial x} = \frac{s}{\ell} (p_B - p_C) - c_B \qquad (A.3.3b)$$

$$\frac{\partial(\overline{uw}_{C,D})}{\partial x} = \frac{s}{\ell} (p_C - p_D) - c_C \qquad (A.3.3c)$$

$$\frac{\partial(\bar{u}w_{D,E})}{\partial x} = \frac{s}{\ell}(p_D - p_E) - c \qquad (A.3.3d)$$

$$\frac{\partial(\bar{u}w_{E,F})}{\partial x} = \frac{s}{\ell}(p_E - p_F) - c_E \qquad (A.3.3e)$$

We can derive a combined transverse momentum for all these channels.

$$\sum_{i=A}^{E} \frac{\partial(\bar{u}w_{i,i+1})}{\partial x} = \frac{s}{\ell}(p_A - p_E) - \sum_{i=A}^{E} c_i \qquad (A.3.4)$$

If we consider these N channels as two channels, i.e., we combine channel A, B, and C as channel L and channel D, E and F as channel R, we can write the two channel transverse momentum equations as follows:

$$\frac{\partial(\bar{U}W_{L,R})}{N_{TU}\partial x} = \frac{s}{\ell}\left(\frac{P_L - P_R}{N_{TP}}\right) - \frac{C}{N_{TF}} \qquad (A.3.5)$$

where $$\bar{U} = \frac{U_L + U_R}{2} \qquad (A.3.6)$$

and N_{TU}, N_{TP}, N_{TF} are coupling coefficients introduced to match equation (A.3.4) with equation (A.3.5).

Therefore N_{TU}, N_{TP} and N_{TF} can be defined as follows:

$$N_{TU} \equiv \frac{\frac{\partial(\bar{U}W_{L,R})}{\partial x}}{\sum_{i=A}^{E}\left(\frac{\partial\ \bar{u}\ \ w_{i,i+1}}{\partial x}\right)} \qquad \text{(A.3.7a)}$$

$$N_{TP} \equiv \frac{P_L - P_R}{p_A - p_F} \qquad \text{(A.3.7b)}$$

$$N_{TF} = \frac{C}{\sum_{i=A}^{E} c_i} = \frac{\frac{W_{L,R}}{\rho^*_{L,R}}\ W_{L,R}}{\sum_{i=A}^{E}\frac{|w_{i,i+1}|\,w_{i,i+1}}{\rho^*_{i,i+1}}} \qquad \text{(A.3.7c)}$$

From the above derivation we have determined the coupling coefficients required in the transverse momentum equation (A.3.5).

APPENDIX B

ANALYSIS OF COUPLING COEFFICIENTS IN COBRA IIIC

Introduction

The general coupling coefficients N_H, N_H', N_H'', N_U, N_U', N_{TF}, N_{TP} and N_{TU} are derived from the differential conservation equations in Appendix A. However, it is questionable whether these derivations are applicable to the difference conservation equations which are always employed in the code computation.

The purpose of this appendix is first to show the difference between H_L and $\bar{h}_L$ resulting from introduction of the coefficients N_H, N_H' and N_H'' from Appendix A into the COBRA IIIC computation, and second, to investigate a general way to derive the coupling coefficients from the difference conservation equations.

B.1 Error Between H_L and $\bar{h}_L$ Employing N_H, N_H' and N_H'' in the Homogenized Computation

If the equations used in COBRA IIIC were those described in Appendix A, both values ($\bar{h}_L$ and H_L) should be identical in cases where either the diversion crossflow is negligible or is the same for the boundary that separates the left and right hand sides. But from the results presented in this thesis (figures 8, 9,10) we can observe the existence of slight differences between these values.

These differences, as will be shown below, are due to the fact that the difference equations used in COBRA IIIC are not exactly those of Appendix A.

Let us take the following example:

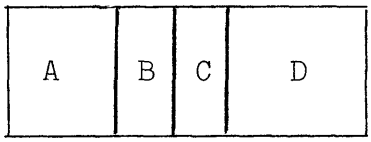

multi-subchannel layout

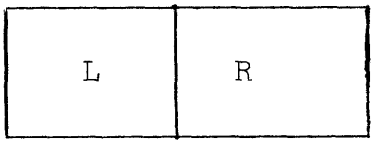

homogenized channel layout

In the COBRA IIIC formulation, the energy equations for each channel are written as:

$$h_A(J) = h_A(J-1) + \frac{q'_A(J-\frac{1}{2})}{m_A(J-1)} \cdot \Delta x - \frac{(t_A(J-1)-t_B(J-1)C_{A,B}\cdot\Delta x}{m_A(J-1)}$$

$$- \frac{(h_A(J-1)-h_B(J-1))w'_{A,B}(J-1)\cdot\Delta x}{m_A(J-1)}$$

$$- \frac{(h_A(J-1)-h^*(J-1))w_{A,B}(J-1)\cdot\Delta x}{m_A(J-1)} \quad \text{(B.1.1)}$$

$$h_B(J) = h_B(J-1) + \frac{q'_B(J-\frac{1}{2})}{m_B(J-1)} \cdot \Delta x - \frac{(t_B(J-1)-t_C(J-1))C_{B,C}\cdot\Delta x}{m_B(J-1)}$$

$$- \frac{(t_B(J-1)-t_A(J-1))C_{A,B}\Delta x}{m_B(J-1)}$$

$$- \frac{(h_B(J-1)-h_C(J-1))}{m_B(J-1)} w'_{B,C}(J-1)\Delta x$$

$$- \frac{(h_B(J-1)-h_A(J-1))}{m_B(J-1)} w'_{B,A}(J-1)\Delta x$$

$$- \frac{(h_B(J-1)-h^*(J-1)w_{B,C}(J-1)\Delta x}{m_B(J-1)}$$

$$- \frac{(h_B(J-1)-h^*(J-1))w_{B,A}(J-1)\Delta x}{m_B(J-1)} \qquad \text{(B.1.2)}$$

The multi-subchannel averaged enthalpy for the left hand side strip can be calculated from the following equation:

$$\bar{h}_L(J) = \frac{h_A(J)m_A(J) + h_B(J)m_B(J)}{m_A(J) + m_B(J)} \qquad \text{(B.1.3)}$$

Inserting equations (B.1.1) and (B.1.2) into equation (B.1.3) with the assumption $C_{i,j} = 0$, we obtain

$$\bar{h}_L(J) = \frac{h_A(J-1)m_A(J) + h_B(J-1)m_B(J)}{m_A(J) + m_B(J)}$$

$$+ \frac{\left(q'_A(J-\tfrac{1}{2}) \frac{m_A(J)}{m_A(J-1)} + q'_B(J-\tfrac{1}{2}) \frac{m_B(J)}{m_B(J-1)}\right)\Delta x}{m_A(J) + m_B(J)}$$

$$- \frac{\Delta x \left[\frac{h_A(J-1)-h_B(J-1))w'_{A,B}(J-1)m_A(J)}{m_A(J-1)} + \frac{(h_B(J-1)-h_A(J-1)w'_{B,A}m_B(J)}{m_B(J-1)} \right]}{m_A(J) + m_B(J)}$$

$$+ \frac{\left[\frac{(h_B(J-1)-h_C(J-1)w'_{B,C}(J-1)\cdot m_B(J)}{m_B(J-1)} \right] \Delta x}{m_A(J) + m_B(J)}$$

$$- \left[\frac{(h_A(J-1)-h^*(J-1))w_{A,B}(J-1)m_A(J)}{m_A(J-1)} + \frac{(h_B(J-1)-h^*(J-1)w_{B,A}(J-1)m_B(J)}{m_B(J-1)} \right.$$

$$\left. + \frac{(h_B(J-1)-h^*(J-1))w_{B,C}(J-1)m_B(J)}{m_B(J-1)} \right] \frac{\Delta x}{m_A(J) + m_B(J)} \qquad \text{(B.1.4)}$$

In the COBRA IIIC formulation, the energy equation for the homogenized strip L incorporating the coupling coefficients can be written as follows:

$$H_L(J) = H_L(J-1) + \frac{Q'_L(J-\frac{1}{2})}{M_L(J-1)} \Delta x - \frac{(H_L(J-1)-H_R(J-1))W'_{L,R}(J-1)\Delta x}{M_L(J-1)N_H(J-1)}$$

$$- \frac{(H_L(J-1)-\frac{H^*(J)}{N'_H(J-1)}) W_{L,R}(J-1)\Delta x}{M_L(J-1)} \qquad \text{(B.1.5)}$$

where $N_H(J-1)$ and $N'_H(J-1)$ are the coupling coefficients for the turbulent and crossflow interchange, and are defined following equations (A.1.9a), (A.1.9b) and (A.1.9c) as:

$$N_H(J-1) \equiv \frac{H_L(J-1) - H_R(J-1)}{h_B(J-1) - h_C(J-1)} \qquad \text{(B.1.6a)}$$

$$N_H' \equiv \frac{H^*(J-1)}{h^*(J-1)} \quad \text{where} \quad \frac{H^*}{h^*} = \frac{H_L(J-1)}{h_B(J-1)} \quad \text{if } W_{L,R} > 0$$

$$\frac{H^*}{h^*} = \frac{H_R(J-1)}{h_D(J-1)} \quad \text{if } W_{R,L} < 0 \qquad \text{(B.1.6b)}$$

and $H_L(J-1)$ is defined as

$$H_L(J-1) = \frac{h_A(J-1)m_A(J-1) - h_B(J-1)m_B(J-1)}{m_A(J-1) + m_B(J-1)} \qquad \text{(B.1.6c)}$$

Inserting equations (B.1.6a), (B.1.6b) and (B.1.6c) into (B.1.5) we obtain

$$H_L(J) = H_L(J-1) + \frac{Q_L'(J-\frac{1}{2})}{[m_A(J-1)-m_B(J-1)]}\Delta x - \frac{(h_B(J-1)-h_C(J-1))W_{L,R}(J-1)\Delta x}{[m_A(J-1)+m_B(J-1)]}$$

$$- \frac{(H_L(J-1)-h^*(J-1))W_{L,R}(J-1)\Delta x}{[m_A(J-1)+m_B(J-1)]} \qquad \text{(B.1.7)}$$

Therefore, forming the desired difference from equations (B.1.4) and (B.1.7), we obtain

$$\bar{h}_L(J) - H_L(J) = \left\{ \frac{h_A(J-1)m_A(J) + h_B(J-1)m_B(J)}{m_A(J) + m_B(J)} - H_L(J-1) \right\}$$

$$+ \quad \Delta x \left\{ \frac{q'_A(J-\frac{1}{2}) \frac{m_A(J)}{m_A(J-1)} + q'_B(J-\frac{1}{2}) \frac{m_B(J)}{m_B(J-1)}}{m_A(J) + m_B(J)} - \frac{Q_L(J-\frac{1}{2})}{m_A(J-1) + m_B(J-1)} \right\}$$

$$+ \left\{ \frac{(h_A(J-1)-h_B(J-1))w'_{A,B}(J-1)m_A(J)}{[m_A(J) + m_B(J)]m_A(J-1)} + \frac{(h_B(J-1)-h_A(J-1)w'_{B,A}(J-1)m_B(J)}{[m_A(J) + m_B(J)]m_B(J-1)} \right.$$

$$\left. + \frac{(h_B(J-1)-h_C(J-1))w'_{B,C}(J-1)m_B(J)}{[m_A(J) + m_B(J)]m_B(J-1)} - \frac{(h_B(J-1)-h_C(J-1))W'_{L,R}(J-1)}{[m_A(J-1) + m_B(J-1)]} \right\} \Delta x$$

$$+ \left\{ \frac{(h_A(J-1)-h^*(J-1))w_{A,B}(J-1)m_A(J)}{m_A(J-1)} + \frac{(h_B(J-1)-h^*(J-1))w_{B,A}(J-1)m_B(J)}{m_B(J-1)} \right.$$

$$+ \left[\frac{h_B(J-1)-h^*(J-1)w_{B,C}(J-1)m_B(J)}{m_B(J-1)} \right] \frac{1}{m_B(J) + m_A(J)}$$

$$\left. - \frac{(H_L(J-1)-h^{**}J-1))W_{L,R}(J-1)}{m_A(J-1) + m_B(J-1)} \right\} \quad \Delta x$$

$$= \text{ERROR 1} + \text{ERROR 2} + \text{ERROR 3} + \text{ERROR 4} \qquad \text{(B.1.8)}$$

From the above formulation, we find that the error between $\bar{h}_L(J)$ and $H_L(J)$ is composed of four terms, i.e., the four terms in parentheses ({}) in equation (B.1.8). Now, we examine equation (B.1.8) term by term to highlight the

factors causing the error between $\bar{h}_L$ and $H_L(J)$.

B.1.1 Error on the Averaged Enthalpy at (J-1)

From the first term of equation (B.1.8), the error due to the averaged enthalpy at (J-1) can be rewritten as:

$$\text{ERROR1}(J) = \frac{h_A(J-1)m_A(J)+h_B(J-1)m_B(J)}{m_A(J) + m_B(J)} - \frac{h_A(J-1)m_A(J-1)+h_B(J-1)m_B(J-1)}{m_A(J-1) + m_B(J-1)} \qquad \text{(B.1.1.1)}$$

From equation (B.1.1.1) we observe that ERROR1(J) increases as the diversion crossflow and subchannel enthalpy increase.

B.1.2 Error on the Heat Added from Rods

The second term of equation (B.1.8) is

$$\text{ERROR2}(J) = \left\{ \frac{\left[q_A'(J-\tfrac{1}{2}) \frac{m_A(J)}{m_A(J-1)} + q_B'(J-\tfrac{1}{2}) \frac{m_B(J)}{m_B(J-1)} \right]}{m_A(J) + m_B(J)} - \frac{Q_L'(J-\tfrac{1}{2})}{m_A(J-1)+m_B(J-1)} \right\} \Delta x \qquad \text{(B.1.2.1)}$$

Now

$$Q_L'(J-\tfrac{1}{2}) = q_A'(J-\tfrac{1}{2}) + q_B'(J-\tfrac{1}{2}) \qquad \text{(B.1.2.2)}$$

Inserting equation (B.1.2.2) into (B.1.2.1) we obtain

$$\text{ERROR2}(J) = \left\{ \frac{\left[q'_A(J-\tfrac{1}{2}) \frac{m_A(J)}{m_A(J-1)} + q'_B(J-\tfrac{1}{2}) \frac{m_B(J)}{m_B(J-1)} \right]}{m_A(J) + m_B(J)} - \frac{q'_A(J-\tfrac{1}{2}) + q'_B(J-\tfrac{1}{2})}{m_A(J-1) + m_B(J-1)} \right\} \Delta x \qquad \text{(B.1.2.3)}$$

From the above equation, we observe ERROR2 increases as diversion crossflow increases and the rod linear power generation rate increases. For low power generation, this term is much smaller than the other terms.

B.1.3 Error on the Energy Carried by the Turbulent Interchange

From equation (B.1.8), the error on the energy transported by the turbulent interchange between $\bar{h}_L(J)$ and $H_L(J)$ can be written as:

$$\text{ERROR3}(J) = \frac{(h_A(J-1)-h_B(J-1))w'_{A,B}(J-1)m_A(J)\,\Delta x}{[m_A(J) + m_B(J)]m_A(J-1)}$$

$$+ \frac{(h_B(J-1)-h_A(J-1))w'_{B,A}(J-1)m_B(J)\,\Delta x}{[m_A(J) + m_B(J)]m_B(J-1)}$$

$$+ \frac{(h_B(J-1)-h_C(J-1))w'_{B,C}(J-1)m_B(J)\,\Delta x}{[m_A(J) + m_B(J)]m_B(J-1)}$$

$$- \frac{(h_B(J-1)-h_C(J-1)W'_{L,R}(J-1)\ \Delta x}{m_A(J-1) + m_B(J-1)} \qquad \text{(B.1.3.1)}$$

From the above equation, we observe ERROR3 increases as the diversion crossflow and the difference between $W'_{L,R}(J-1)$ and $w'_{B,C}(J-1)$ increases. Usually, the difference between $W'_{L,R}$ and $w'_{B,C}$ is small and does not contribute too much to the ERROR3.

B.1.4 Error on the Energy Carried by the Diversion Crossflow

From equation (B.1.8), the error on the energy transported by the diversion crossflow between $\bar{h}_L(J)$ and $H_L(J)$ can be written as

$$\begin{aligned} \text{ERROR4}(J) = \Bigg\{ & \frac{[h_A(J-1)-h^*(J-1)]w_{A,B}(J-1)m_A(J)\ \Delta x}{m_A(J-1)[m_B(J) + m_A(J)]} \\ & + \frac{[h_B(J-1)-h^*(J-1)w_{B,A}(J-1)m_B(J)\ \Delta x}{m_B(J-1)[m_B(J) + m_A(J)]} \\ & + \frac{[h_B(J-1)-h^*(J-1)]w_{B,C}(J-1)m_B(J)\ \Delta x}{m_B(J-1)[m_B(J) + m_A(J)]} \\ & - \frac{[H_L(J-1)-h^*(J-1)]W_{L,R}(J-1)\ \Delta x}{m_A(J-1) + m_B(J-1)} \Bigg\} \end{aligned} \qquad \text{(B.1.4.1)}$$

$$\text{where} \quad H_L(J-1) = \frac{h_A(J-1)m_A(J-1)+h_B(J-1)m_B(J-1)}{m_A(J-1) + m_B(J-1)} \qquad \text{(B.1.4.2)}$$

For simplicity, we assume $w_{A,B}$, $w_{B,C}$, $W_{L,R}$ are less than zero. Then

$$h^*(J-1)w_{A,B}(J-1) = h_B(J-1)w_{A,B}(J-1) \qquad \text{(B.1.4.3a)}$$

$$h^*(J-1)w_{A,B}(J-1) = h_B(J-1)w_{B,A}(J-1) \qquad \text{(B.1.4.3b)}$$

$$h^*(J-1)w_{B,C}(J-1) = h_C(J-1)w_{B,C}(J-1) \qquad \text{(B.1.4.3c)}$$

Inserting equations (B.1.4.2), (B.1.4.3a), (B.1.4.3b), (B.1.4.3c) and (B.1.4.3d) into equation (B.1.4.1) we obtain,

$$\text{ERROR4}(J) = \left\{ \frac{[h_A(J-1)-h_B(J-1)]w_{A,B}(J-1)m_A(J)\,\Delta x}{m_A(J-1)[m_B(J)+m_A(J)]} + \frac{[h_B(J-1)-h_C(J-1)]w_{B,C}(J-1)m_B(J)\,\Delta x}{m_B(J-1)[m_B(J)+m_A(J)]} - \frac{\left[\frac{h_A(J-1)m_A(J-1)+h_B(J-1)m_B(J-1)}{m_A(J-1)+m_B(J-1)} - h_C(J-1)\right]}{m_A(J-1)+m_B(J-1)} \right\} W_{L,R}(J-1)\,\Delta x$$

(B.1.4.4)

ERROR4(J) can be rearranged as follows:

$$\text{ERROR4}(J) = \left[\frac{W_{L,R}(J-1)\,\Delta x}{m_A(J-1)+m_B(J-1)} - \frac{w_{B,C}(J-1)m_B(J)\,\Delta x}{[m_B(J)+m_A(J)]m_B(J-1)} \right] h_C(J-1)$$

$$+\left|\frac{w_{A,B}(J-1)m_A(J)\ \Delta x}{m_A(J-1)[m_B(J)+m_A(J)]}-\frac{m_A(J-1)W_{L,R}(J-1)\ \Delta x}{[m_A(J-1)+m_B(J-1)]^2}\right| h_A(J-1)$$

$$+\left|\frac{w_{B,C}(J-1)m_B(J)\ \Delta x}{m_B(J-1)[m_B(J)+m_A(J)]}-\frac{w_{A,B}(J-1)m_A(J)\ \Delta x}{m_A(J-1)[m_B(J)+m_A(J)]}\right.$$

$$\left.-\frac{m_B(J-1)W_{L,R}(J-1)\ \Delta x}{[m_A(J-1)+m_B(J-1)]^2}\right| h_B(J-1) \qquad \text{(B.1.4.5)}$$

Equation (B.1.4.5) is a general expression for the error on the diversion crossflow. This error increases as diversion crossflow and subchannel enthalpies increase.

B.1.5 Numerical Values of Errors Between $\overline{h_L}$ and H_L

From the above derivation, we conclude that all these four errors vanish as the diversion crossflow goes to zero. This gives us strong confidence to neglect the error introduced by using the coefficients N_H, N_H' and N_H'' from Appendix A into the COBRA computation scheme which employs a forward differenced form for the conservation equations. However, this error may not be negligible when the diversion crossflow between subchannels is large.

Let us now evaluate the ERROR1, ERROR2, ERROR3 and ERROR4 in order to see their relative importance under two extreme conditions, i.e., low diversion corssflow condition (ENTHALPY UPSET CONDITION) and high diversion crossflow condition (POWER AND FLOW UPSET

CONDITION).

The input energy and flow conditions together with input coefficients for the cases considered in this section are listed in Table B.1.

TABLE B.1

ENTHALPY UPSET		FLOW AND POWER UPSET	
Bundle Geometry	N = 5	Bundle Geometry	N = 5
	L = 144"		L = 144"
Flow Conditions	$\overline{G}$ = 2.66 $\frac{\text{Mlbm}}{\text{hr-ft}^2}$	Flow Conditions	$\overline{G}$ = 2.66 $\frac{\text{Mlbm}}{\text{hr-ft}^2}$
	F_R = 1.0		F_R = 1.22
Energy Conditions	$\overline{H}$ = 600 Btu/lbm	Energy Conditions	$\overline{H}$ = 600 Btu/lbm
	$\overline{q}''$ = 0 $\frac{\text{MBtu}}{\text{hr-ft}^2}$		$\overline{q}''$ = 0.04 $\frac{\text{MBtu}}{\text{hr-ft}^2}$
	H_R = 1.22		H_R = 1.0
	P_R = 1.0		P_R = 1.5
Input Coefficients	β = 0.02	Input Coefficients	β = 0.02
	K = 0.5		K = 0.5
	S/L = 0.5		S/L = 0.5

The total errors between $\bar{h}_{EXIT}$ and $H_{L_{EXIT}}$ can be evaluated by using equations similar to (B.1.1.1), (B.1.2.1), (B.1.3.1) and (B.1.4.1) but reformulated to deal with five subchannels. The results are tabulated in the following table (Table B.2).

TABLE B.2

	ENTHALPY UPSET	POWER AND FLOW UPSET
ΔH	-34.4 BTU/lbm	21.5 BTU/lbm
$\sum_{J=1}^{EXIT}$ ERROR1(J)	0.097 $\frac{Btu}{lbm}$	0.058 $\frac{Btu}{lbm}$
$\sum_{J=1}^{EXIT}$ ERROR2(J)	0.0004 $\frac{Btu}{lbm}$	0.0004 $\frac{Btu}{lbm}$
$\sum_{J=1}^{EXIT}$ ERROR3(J)	0.147 $\frac{Btu}{lbm}$	0.127 $\frac{Btu}{lbm}$
$\sum_{J=1}^{EXIT}$ ERROR4(J)	-0.233 $\frac{Btu}{lbm}$	-0.130 $\frac{Btu}{lbm}$
TOTAL	0.011 $\frac{Btu}{lbm}$	0.055 $\frac{Btu}{lbm}$

B.1.6 Conclusions

The coupling coefficient derived in the differential form conservation euqations can be used in the difference form conservation equations with some practical tolerable

error. However, if the subchannel enthalpies become abnormally high (under channel blockage condition) or the diversion crossflows between subchannels becomes very large (under severe boiling condition or channel blockage), the errors between $H_{L_{EXIT}}$ and $\bar{h}_{L_{EXIT}}$ will become substantial from the practical point of view.

B.2 General Approach to Derive Coupling Coefficients From the Different Conservation Equations

Coupling coefficients derived from the differential conservation equations are applicable to the code application only if the subchannel enthalpies and diversion crossflows are within the range of normal operation, as we discussed in Section B.1.6. One way to eliminate this constraint to handle abnormal operational conditions is to derive the coupling coefficients directly from the difference conservation equations. For instance, we derive coupling coefficients in the difference conservation equations by first letting

$$\bar{h}_L(J) \equiv \bar{H}_L(J) \tag{B.2.1}$$

and then define the coupling coefficients in each term of $H_L(J)$ to make $H_L(J)$ equal $\bar{h}_L(J)$ term by term. Using the same

procedures, we can derive the coupling coefficients for the axial velocity and axial pressure drop. However, it is worthwhile noting that the complexity of the coupling coefficients resulting from this kind of derivation generally will make them undesirable for practical application.

APPENDIX C

VALIDITY OF EQUATION (2.3.1)

Equation (2.3.1) is written under the assumption that the enthalpy profile is symmetrical with respect to the central boundary. Under this assumption and from the definition of N_H,

$$N_H \equiv \frac{H_L - H_R}{h_C - h_D} \qquad \text{(A.1.9b)}$$

we get

$$h_C - h_D = \frac{H_L - H_R}{N_H} \qquad \text{(C.1)}$$

$$\frac{h_C - h_D}{2} = \frac{H_L - H_R}{2N_H} \qquad \text{(C.2)}$$

$$\frac{h_C + h_D}{2} = \frac{H_L + H_R}{2} \quad \text{(under the assumption of the symmetrical enthalpy profile)} \qquad \text{(C.3)}$$

Adding equations (C.3) and (C.2) we obtain

$$h^* = h_C = \frac{h_C - h_D}{2} + \frac{h_C + h_D}{2} = \frac{H_L - H_R}{2N_H} - \frac{H_L + H_R}{2}$$

$$= \frac{H_L - \frac{H_L - H_R}{2}}{N_H} + \frac{H_L + H_R}{2} \quad \text{if } W_{L,R} > 0 \qquad \text{(C.4)}$$

(C.4) is stated in Appendix A (A.1.11a) without any comments on it. However, the assumption of symmetrical enthalpy profile used in the derivation of (C.4) is not valid when the diversion crossflow and flow upset exist. This point is verified in detail in the following section (C.1).

C.1 Verification of validity of (C.4) only under the condition of no diversion crossflow and no flow upset

If there are no diversion crossflows and no flow upset between subchannels, equation (C.3) is valid. This can be proven by using equations (A.1.7a) and (A.1.7b) with $W_{L,R} = W_{R,L} = 0$,

$$\frac{\partial H_L M_L}{\partial x} = Q_L' - \left(\frac{H_L - H_R}{N_H}\right) W_{L,R}' \qquad (C.7)$$

$$\frac{\partial H_R M_R}{\partial x} = Q_R' - \left(\frac{H_R - H_L}{N_H}\right) W_{R,L}' \qquad (C.8)$$

Since there are no diversion crossflows

$$M_L = \text{constant} \qquad (C.9a)$$

$$M_R = \text{constant} \qquad (C.9b)$$

and from (A.1.8c), (A.1.8d) and (A.1.9b)

$$Q_L' \equiv \sum_{i=A}^{C} q_i' \qquad \text{(A.1.8c)}$$

$$Q_R' \equiv \sum_{i=D}^{F} q_i' \qquad \text{(A.1.8d)}$$

$$N_H \equiv \frac{H_L - H_R}{h_C - h_D} \qquad \text{(A.1.9b)}$$

Equations (C.7) and (C.8) become

$$\Delta H_L = \sum_i \frac{Q_L'}{M_L} \Delta x_i - \sum_i (h_C - h_D) W_{L,R}' \Delta x_i \qquad \text{(C.10a)}$$

$$\Delta H_R = \sum_i \frac{Q_R'}{M_R} \Delta x_i - \sum_i (h_D - h_C) W_{R,L}' \Delta x_i \qquad \text{(C.10b)}$$

Therefore

$$\frac{\Delta H_L + \Delta H_R}{2} \equiv \frac{H_L(z) + H_R(z)}{2} - \frac{H_L(o) + H_R(0)}{2}$$

$$= \frac{\sum_i \frac{Q_L'}{M_L} \Delta x_i + \sum_i \frac{Q_R'}{M_R} \Delta x_i}{2} \qquad \text{(C.11)}$$

and

$$\frac{H_L(z) + H_R(z)}{2} = \frac{H_L(o) + H_R(o)}{2} + \frac{\sum_i \frac{Q_L'}{M_L} \Delta x_i + \sum_i \frac{Q_R'}{M_R} \Delta x_i}{2} \qquad \text{(C.12)}$$

This evaluates the RHS of Eq. (C.3). Next we evaluate $\frac{h_C + h_D}{2}$, the LHS of Eq. (C.3) to show the equality of RHS and LHS.

To obtain the expression for $\frac{h_C(z) + h_D(z)}{2}$, we use a different derivation philosophy which is stated below.

From equations (A.1.3c) and (A.1.3d), we get

$$\frac{\partial m_C h_C}{\partial x} = q_C' - (h_C - h_D)w_{C,D}' - (h_C - h_B)w_{C,B}' \qquad \text{(A.1.3c)}$$

$$\frac{\partial m_D h_D}{\partial x} = q_C' - (h_D - h_C)w_{D,C}' - (h_D - h_E)w_{D,E}' \qquad \text{(A.1.3d)}$$

In order to proceed with the derivation, we have to recognize the following statement as true:

"If the enthalpy profile at axial node j is transversely symmetrical, we can prove the enthalpy profile at axial node j+1 is also transversely symmetrical as long as the transverse linear heat generation profile is symmetric."

This statement needs an involved proof and we can heuristically prove this by observing equations (A.1.3c) and (A.1.3d) in the difference scheme:

$$m_C \frac{h_C(J+1) - h_C(J)}{\Delta x} = q_C' - (h_C(J) - h_D(J))w_{C,D}' - (h_c(J) - h_B(J))w_{C,B}' \qquad \text{(C.13)}$$

$$m_D \frac{h_D(J+1) - h_D(J)}{\Delta x} = q_D' - (h_D(J) - h_C(J))w_{C,D}' - (h_D(J) - h_E(J))w_{D,E}' \qquad \text{(C.14)}$$

Because of symmetry at the axial node J, we have

$$(h_C(J) - h_B(J)) = (h_D(J) - h_E(J)) \qquad (C.15)$$

and

$$w'_{D,C} = w'_{C,D} \qquad (C.16)$$

$$w'_{C,B} = w'_{C,E} \qquad (C.17)$$

Thus we know is $q'_C = q'_D = 0$, the enthalpy increment in subchannel C equals the enthalpy decrease in subchannel D. Also because the transverse linear heat generation rate is symmetrical, then $h_C(J+1)$ and $h_D(J+1)$ must be symmetrical with respect to

$$\frac{\frac{q'_C(J)}{m_C} + \frac{q'_D(J)}{m_D}}{2} + \frac{h_C(J) + h_D(J)}{2} .$$

Now we can obtain $\frac{h_C(z) + h_D(z)}{2}$ from equations (A.13c) and (A.13d) by recognizing that $(h_C - h_B) = (h_D - h_E)$.

The result is

$$\frac{h_C(z) + h_D(z)}{2} = \frac{\sum_i \frac{q'_C}{m_C} \Delta x_i + \sum_i \frac{q'_D}{m_D} \Delta x_i}{2} + \frac{h_C(o) + h_D(o)}{2} \qquad (C.18)$$

Since

$$h_C(o) = H_L(o) \tag{C.19a}$$

$$h_D(o) = H_R(o) \tag{C.19b}$$

$$\frac{q'_C}{m_C} = \frac{Q'_L}{M_C} = \frac{\sum_{i=A}^{C} q'_i}{\sum_{i=A}^{C} m_i} \tag{C.19c}$$

$$\frac{q'_D}{m_D} = \frac{Q'_R}{M_R} = \frac{\sum_{i=D}^{F} q'_i}{\sum_{i=D}^{F} m_i} \tag{C.19d}$$

under the condition $q'_A = q'_B = q'_C$, $m_A = m_B = m_C$, $q'_D = q'_E = q'_F$ and $m_D = m_E = m_F$.

Therefore, from equations (C.18) and (C.12) we get

$$\frac{h_C(z) + h_D(z)}{2} = \frac{H_L(z) + H_R(z)}{2} \tag{C.20}$$

However, under large inter-subchannel diversion crossflow or flow upset conditions, equations (C.15), (C.17), (C.19c) and (C.19d) will not hold and hence equations (C.20) and (C.4) become inequalities.

C.2 Suggestions on h* in terms of known parameters

A suggestion is made below regarding h* (stated in

equation (A.1.11a) and (A.1.11b) under the assumptions of no diversion crossflow and no flow upset) in order to cope with the conditions of large diversion crossflow and flow upset.

$$h^* = \frac{H_L(M_{L_{EXIT}} + M_L(o)) + H_R(M_{R_{EXIT}} + M_R(o))}{2(M_L + M_R)} + \frac{H_L - \frac{H_L + H_R}{2}}{N_H} \quad \text{if } W_{L,R} > 0 \quad (C.21)$$

$$h^* = \frac{H_L(M_{L_{EXIT}} + M_L(o)) + H_R(M_{R_{EXIT}} + M_R(o))}{2(M_L + M_R)} + \frac{H_R - \frac{H_L + H_R}{2}}{N_H} \quad \text{if } W_{L,R} < 0 \quad (C.22)$$

These two equations also hold under the conditions of low diversion crossflow and no flow upset, hence it can be used under any conditions we require in this thesis.

APPENDIX D

DERIVATION OF N_H, N_U AND N_{TP} FOR LINEAR GRADIENTS OF ENTHALPY, VELOCITY AND PRESSURE

From Equations (A.1.1.6), (A.2.1.6a) and (A.3.1.6) we define N_H, N_U, N_{TP} in the following way:

$$N_H = \frac{H_L - H_R}{h_C - h_D}$$

$$N_U = \frac{U_L - U_R}{U_C - U_D}$$

$$N_{TP} = \frac{P_L - P_R}{P_A - P_E}$$

If we assume the transverse enthalpy profile through channels is linear with slope S_h, N_H becomes:

$$N_H = \frac{\left(\frac{H_L+H_R}{2} + S_h \cdot \frac{N'}{2} \cdot S_{ij}\right) - \left(\frac{H_L+H_R}{2} - S_h \cdot \frac{N'}{2} \cdot S_{ij}\right)}{\left(\frac{H_L+H_R}{2} + S_h \cdot \frac{S_{ij}}{4}\right) - \left(\frac{H_L+H_R}{2} - S_h \cdot \frac{S_{ij}}{4}\right)}$$

$$= \frac{\frac{N'}{2} + \frac{N'}{2}}{\frac{1}{4} + \frac{1}{4}} = 2N' = N \qquad \text{for N odd} \qquad (D.1)$$

$$N_H = \frac{\left(\frac{H_L+H_R}{2} + S_n \cdot \frac{N'}{2} \cdot S_{ij}\right) - \left(\frac{H_L+H_R}{2} - S_h \cdot \frac{N'}{2} \cdot S_{ij}\right)}{\left(\frac{H_L+H_R}{2} + S_h \cdot \frac{S_{ij}}{2}\right) - \left(\frac{H_L+H_R}{2} - S_h \cdot \frac{S_{ij}}{2}\right)}$$

$$= \frac{\frac{N'}{2} + \frac{N'}{2}}{\frac{1}{2} + \frac{1}{2}} = N' \qquad \text{for N even} \qquad (D.2)$$

For the same reason for N_U, N_{TP}, we obtain:

$$N_U = \frac{\left(\frac{U_L+U_R}{2} + S_u \cdot \frac{N'}{2} \cdot S_{ij}\right) - \left(\frac{U_L+U_R}{2} - S_u \cdot \frac{N'}{2} \cdot S_{ij}\right)}{\left(\frac{H_L+H_R}{2} + S_u \cdot \frac{S_{ij}}{4}\right) - \left(\frac{H_L+H_R}{2} - S_u \cdot \frac{S_{ij}}{4}\right)}$$

$$= 2N' = N \qquad \text{for N odd} \qquad (D.3)$$

$$N_U = \frac{\left(\frac{U_L+U_R}{2} + S_u \cdot \frac{N'}{2} \cdot S_{ij}\right) - \left(\frac{U_L+U_R}{2} - S_u \cdot \frac{N'}{2} \cdot S_{ij}\right)}{\left(\frac{H_L+H_R}{2} + S_u \cdot \frac{S_{ij}}{2}\right) - \left(\frac{H_L+H_R}{2} - S_u \cdot \frac{S_{ij}}{2}\right)} = N'$$

$$\text{for N even} \qquad (D.4)$$

$$N_{TP} = \frac{\left(\frac{P_L+P_R}{2} + S_p \cdot \frac{N'}{2} \cdot S_{ij}\right) - \left(\frac{P_L+P_R}{2} - S_p \cdot \frac{N'}{2} \cdot S_{ij}\right)}{\left(\frac{P_L+P_R}{2} + S_p \cdot S_{ij} \cdot (N'-\frac{1}{2})\right) - \left(\frac{P_L+P_R}{2} - S_p \cdot S_{ij} \cdot (N'-\frac{1}{2})\right)}$$

$$= \frac{\frac{N'}{2} + \frac{N'}{2}}{N'+N'-1} = \frac{N'}{2N'-1} \qquad \text{for N odd or even} \qquad (D.5)$$

where S_h, S_p and S_u = transverse slopes of enthalpy, pressure and velocity.

APPENDIX E

PREDICTION OF ENTHALPY RISE IN THE HOT ZONE FOR MULTIREGION AND HOMOGENIZED REPRESENTATIONS

Define the difference between the enthalpy rises in the hot zone for the multi-subchannel and homogenized representations as the enthalpy rise deviation. The purpose of the factor $N_H(z)$ is to reduce this deviation to zero. In this section we derive relations for this deviation in the absence of application of this correction factor, i.e., taking $N_H = 1$, for the ENTHALPY UPSET CASE, ENTHALPY AND FLOW CASE, POWER UPSET CASE and the POWER AND FLOW UPSET CASE.

The defining equation for the enthalpy deviation is

$$\text{Enthalpy deviation for hot zone} \equiv \left.\frac{h_{EXIT}(\text{homogenized}) - h_{EXIT}(\text{multi-subchannel})}{h_{EXIT}(\text{multi-subchannel}) - h_{INLET}}\right|_{\text{hot zone}} \qquad \text{(E.1.a)}$$

Now

$$h_{EXIT}(\text{multi-subchannel}) \equiv \sum_{\text{hot side subchannels}} h_i / \text{no. of hot side subchannels} \equiv \bar{h}$$

$$h_{EXIT}(\text{homogenized}) \equiv H$$

$$\Delta H \equiv H - h_{IN}$$

$$\Delta \bar{h} \equiv \bar{h} - h_{IN}$$

Hence equation (E.1.a) becomes

$$\text{Enthalpy deviation for hot zone} = \frac{\Delta H - \Delta \overset{+}{h}}{\Delta h} \qquad \text{(E.1.b)}$$

In the evaluation of equation (E.1.b) in terms of bundle parameters that follows, we assume that the amount of enthalpy interchange between channels due to turbulent mixing is much more than that due to diversion crossflow. Therefore

$$\Delta \overset{+}{h} = \Delta \overset{+}{h}_{q'} - \Delta \overset{+}{h}_{T.I} \qquad \text{(E.2.a)}$$

$$\text{and} \quad \Delta H = \Delta H_{Q'} - \Delta H_{T.I} \qquad \text{(E.2.b)}$$

where the minus sign is introduced for the hot zone and

$$\Delta H_{T.I.} = \int_{\text{INLET}}^{\text{EXIT}} Q'_{T.I} dz \qquad \text{(E.3)}$$

Since per Appendix A for either side L or R

$$Q' = \sum_i q'_i \qquad \text{(E.4.a)}$$

and

$$M = \sum_i m_i \qquad \text{(E.4.b)}$$

then

$$\Delta H_{Q'} = \Delta \dot{h}_{q'} \qquad \text{(E.4.c)}$$

From (E.2.a), (E.2.b) and (E.4.c), the following equation can be derived:

$$\Delta H - \Delta \dot{h} = \Delta h_{T.I.} - \Delta H_{T.I.} \qquad \text{(E.5)}$$

Hence we can rewrite equation (E.1.b) as

$$\text{Enthalpy deviation for hot zone} = \frac{\Delta \dot{h}_{T.I.} - \Delta H_{T.I.}}{\Delta \dot{h}_{q'} - \Delta \dot{h}_{T.I.}} \qquad \text{(E.6)}$$

Now from equations (A.1.6a and A.1.7a) for an axial step

$$\sum_{i=A}^{C} (\delta h_i m_i)_{T.I} = -(h_C - h_D) w'_{CD} \Delta X$$

and

$$(\delta H_L M_L)_{T.I} = - \frac{H_L - H_R}{N_H(x)} W'_{L,R} \Delta X$$

Since N_H is established so that the LHS of both equations are equal,

$$N_H(x) = \frac{(H_L-H_R)\Delta X}{(h_C-h_D)\Delta X} \left[\frac{W'_{L,R}}{W'_{C,D}}\right] \qquad (E.7)$$

Now since

$$\delta H_{T.I} \equiv (H_L-H_R) \left[W'_{L,R}/M_L\right] \qquad (E.8a)$$

$$\delta h_{T.I} \equiv (h_C-h_D) \left[W'_{C,D}/\Sigma m_i\right] \qquad (E.8b)$$

$$M_L = \sum_i m_i \qquad (E.4b)$$

then

$$N_H(x) = \frac{\delta H_{T.I}}{\delta h_{T.I}} \qquad (E.9a)$$

or when summed over the axial length of the fuel pin

$$\bar{N}_H = \frac{\Delta H_{T.I}}{\Delta h_{T.I}} \qquad (E.9b)$$

Also per equation (C.4b)

$$\Delta h_{q'} = \Delta H_{Q'} \tag{E.4b}$$

Insertion of equations (E.9b) and (E.4b) into (E.6) yields:

$$\text{Enthalpy deviation for hot zone} = \frac{\frac{1}{\bar{N}_H} - 1}{\frac{\Delta H_{Q'}}{\Delta H_{T.I}} - \frac{1}{\bar{N}_H}} \tag{E.11}$$

Now to evaluate equation (E.11) we express the ratio $\frac{\Delta H_{Q'}}{\Delta H_{T.I}}$ in terms as follows.

First we introduce power, flow and enthalpy ratio definitions

$$\text{Power Ratio} \equiv P_R \equiv \frac{Q_{HOT}}{Q_{COLD}} \tag{E.12a}$$

$$\text{Flow Ratio} \equiv F_R \equiv \frac{G_{HOT}}{G_{COLD}} \tag{E.12b}$$

$$\text{Inlet Enthalpy Ratio} \equiv H_R = \frac{H_{HOT}(z=0)}{H_{COLD}(z=0)} \tag{E.12c}$$

and we recall the definition of β

$$w' \equiv \beta s \frac{G_i + G_j}{2} \qquad \text{(E.13)}$$

then

$$\frac{\Delta H_{Q'}}{\Delta H_{T.I}} = \frac{[H' q'_{hot} L] / N' G_{hot} A_s}{\int_{Inlet}^{Exit} \frac{[H_{hot}(z) - H_{cold}(z)]\, \beta S\, \bar{G}\, dz}{N' A_s\, G_{hot}}}$$

$$= \frac{[N' q'_{hot}] / (\bar{G} \beta S)}{\left[\frac{q'_{hot} N' L}{N' G_{hot} A_s} - \frac{q'_{cold} N' L}{N' G_{cold} A_s} - H_{cold}(0) + H_{hot}(0) \right]}$$

$$= \frac{[N' q'_{hot}]\ N' A_s / (\bar{G} \beta S)}{\left[\frac{q'_{hot} N' L}{G_{hot}} - \frac{q'_{cold} N' L}{G_{cold}} \right] + \left[\frac{H_{hot}(0)}{\frac{1}{N' A_s}} - \frac{H_{cold}(0)}{\frac{1}{N' A_s}} \right]}$$

$$= \frac{[N' P_r]\ N' A_s / (\bar{G} \beta S)}{\left[\frac{P_R N' L}{G_{hot}} - \frac{N' L}{G_{cold}} \right] + \left[\frac{H_{hot}(0)}{\frac{q'_{cold}}{N' A_s}} - \frac{H_{cold}(0)}{\frac{q'_{cold}}{N' A_s}} \right]}$$

$$= \frac{[N' P_R]\, N' A_s/(\beta S)}{\left[\frac{P_R N' L\bar{G}}{G_{hot}} - \frac{N' L\bar{G}}{G_{cold}}\right] + \left[\frac{H_{hot}(0)}{\frac{q'_{cold}}{N'A_s}} - \frac{H_{cold}(0)}{\frac{q'_{cold}}{N'A_s}}\right]}$$

$$= \frac{[N' P_R]\, N' A_s/(\beta S)}{\left[\frac{P_R N' L\bar{G}}{G_{hot}} - \frac{N' L\bar{G}}{G_{cold}}\right] + \left[H_{hot}(0) - H_{cold}(0)\right]\frac{GN' A_s}{q'_{cold}}}$$

$$= \frac{[N' P_R]\, N' A_s/(\beta S)}{\frac{1}{2}\left[P_R\ N'\ (1+\frac{1}{F_R}) - N'\ (1+\frac{1}{F_R})\right] L + \left[\frac{H_{hot}(0)}{\bar{H}_{in}} - \frac{H_{cold}(0)}{\bar{H}_{in}}\right]\frac{\bar{H}\bar{G}N' A_s}{q'_{cold}}}$$

$$= \frac{[N' P_R]\, \bar{q}'\, N' A_s/(\beta S)}{\bar{q}'\,\frac{1}{2}\left[P_R\ N'\ (1+\frac{1}{F_R}) - N'\ (1+F_R)\right] L + \left[\frac{2}{1+\frac{1}{H_R}} - \frac{2}{1+H_R}\right]\frac{\bar{H}\bar{G}N' A_S \bar{q}'}{q'_{cold}}}$$

$$= \frac{P_R\ \bar{q}'\ N' A_s/(\beta S)}{\frac{1}{2} L \bar{q}'\left[P_R(1+\frac{1}{F_R}) - (1+F_R)\right] + \left[\frac{H_R-1}{1-H_R}\right]\bar{H}\bar{G}\ A_s\ (1+P_R)}$$

(E.14)

For ENTHALPY UPSET CASE, since $F_R = 1$, $P_R = 1$ and $q' = 0$, equation (E.14) can be reduced to:

$$\frac{\Delta H_{Q'}}{\Delta H_{T.I}} = \frac{q'}{\left[\frac{H_R - 1}{H_R + 1}\right] \overline{HG}\ \beta S} = 0 \qquad \text{(E.15)}$$

then equation (E.11) for this case becomes:

$$\frac{\frac{1}{\overline{N_H}} - 1}{\frac{1}{\overline{N}_H}} = -\overline{N_H} \qquad \text{(E.16)}$$

For ENTHALPY and FLOW UPSET CASE, since $q' = 0$, equation (E.14) can be reduced to:

$$\frac{\Delta H_{Q'}}{\Delta H_{T.I}} = 0 \qquad \text{(E.17)}$$

then equation (E.11) for this case becomes:

$$\frac{\frac{1}{\overline{N_H}} - 1}{\frac{1}{\overline{N}_H}} = (1 - \overline{N}_H) \qquad \text{(E.18)}$$

For POWER UPSET CASE, since $H_R = 1$, $F_R = 1$, equation (E.14) can be reduced to:

$$\frac{\Delta H_Q'}{\Delta H_{T.I}} = \frac{P_R N' A_s}{(P_R-1)L\beta S} \tag{E.19}$$

then equation (E.11) for this case becomes:

$$\frac{(1 - \frac{1}{N_H})}{\frac{P_R N' A_s}{(P_R-1)L\beta S} - \frac{1}{N_H}} \tag{E.20}$$

For FLOW and POWER UPSET CASE since $H_R = 1$, equation (E.14) can be reduced to:

$$\frac{\Delta H_Q'}{\Delta H_{T.I}} = \frac{N' A_s}{\frac{1}{2}\beta S\, L \left[P_R(1+\frac{1}{F_R}) - (1+F_R)\right]} \tag{E.21}$$

then the equation (E.11) for this case becomes:

$$\frac{\frac{1}{\overline{N_H}} - 1}{\frac{P_R N' A_s}{\frac{1}{2} \beta S L \left[P_R(1+\frac{1}{F_R}) - (1+F_R)\right]} - \frac{1}{\overline{N_H}}} \qquad \text{(E.22)}$$

From equations (E.18) and (E.20) we know that the difference of enthalpy for the hot channel at the exit between the homogenized case with $N_H = 1$ and multi-subchannel case for the power upset case and the power and flow upset case is a strong function of β, H_R, F_R, P_R, N' and $\overline{N}_H$.

APPENDIX F

LIMITATIONS ON THE NUMERICAL VALUE OF β USED IN CALCULATIONS WITH COBRA IIIC

The mixing coefficient, β, is an input in COBRA IIIC. It is used to calculate the turbulent interchange per unit length between channels in the lumped subchannel approach. Since it is physically impossible to have the axial enthalpy rise in the flow channel fluctuate for each axial step just due to the energy transport by the turbulent interchange between the channels, a limitation is imposed on the input value of β. Derivation of the limiting values for β under different operating conditions are presented in the following sections.

F.1 Derivation of General Expressions

F.1.1 Unheated Bundles

The limiting condition on β is that the enthalpy rise for each axial step k in any channel i by the energy transport with the adjacent channel j should be less than one half of the transverse enthalpy difference between channels i and j. This statement can be formulated by the following expression:

$$\left|\frac{w_{i,j}(h_i-h_j)\Delta x}{m_i}\right|_k < \frac{\left|h_i-h_j\right|_k}{2} \qquad \text{(F.1.1)}$$

where w_{im}, h_i, h_j are evaluated for any axial node k.

Since

$$w_{i,j} = \beta s \left(\frac{g_i+g_j}{2}\right)_k$$

$$m_i = g_i A_i$$

equation (F.1.1) also can be expressed in a general way:

$$\Delta x \beta s \left(\frac{g_i+g_j}{2(g_i A_i)}\right) \left|(h_i-h_j)\right| < \left|\frac{h_i-h_j}{2}\right| \qquad \text{(F.1.2)}$$

Therefore

$$\beta < \frac{g_i A_i}{s(g_i+g_j)\Delta x} \qquad \text{(F.1.3)}$$

F.1.2 Heated Bundles

Because the limitation set on β has nothing to do with the heat added from heated rods, the expression (E.1.3) is also true for heated bundles.

F.2 Evaluation of Numerical Values for β_{max}

F.2.1 Enthalpy Upset Case

In this case, the diversion crossflow is very small. Therefore, $\frac{g_i}{g_i+g_j}$ is closed to one half throughout the entire length of the channels. For typical PWR geometry, equation (F.1.3) thus can be evaluated by letting:

$$s = 0.122 \text{ inch}$$
$$A_i = 0.0098 \text{ ft}^2$$
$$\Delta x = 5.76 \text{ inch}$$

then

$$\beta_{max} = \frac{0.5 \times 0.00094}{\frac{0.122}{12} \times \frac{5.76}{12}} = 0.096 \qquad \text{(F.2.1.1)}$$

In particular, it should be noted that β_{max} in the half-sized channel calculation becomes one half of its nominal value in the full sized channel calculation. Therefore, as long as a half sized channel is used, β_{max} for half-sized channels becomes a limiting value for β provided a constant β is used for every channel in the calculation. The β_{max} in the half-sized channel calculation can be established as follows:

$$\beta_{max}(\text{half-sized channel}) = \frac{g_i A_i}{2s(g_i+g_j)\Delta x}$$

$$= 0.5\beta_{max}$$

$$= 0.048 \qquad \text{(F.2.1.2)}$$

F.2.2 Enthalpy and Flow Upset Case

In this case, the limiting value of β occurs in the region where the ratio $\frac{g_i}{g_i+g_j}$ has the smallest value provided a constant β is used throughout the channels.

There are three important features of the maximum β under the flow upset condition; i.e.,

(1) β_{max} under the flow upset condition is always less than that under the enthalpy upset of the power upset condition (since $\frac{g_i}{g_i+g_j} < \frac{1}{2}$).

(2) The limiting β occurs at the inlet under the flow upset condition. This is because the momentum transport between channels tends to increase the value on $\frac{g_i}{g_i+g_j}$ along the channel.

(3) The minimum value of $\frac{g_i}{g_i+g_j}$ depends on the upset flow ratio at the inlet. Generally, the higher the flow upset ratio, the smaller the value of $\frac{g_i}{g_i+g_j}$.

In our application, a step flow upset inlet condition is used where the higher flow rate $\frac{N-1}{2}$ channels at the inlet is 1.1 times larger than that for the center channel and the lower flow rate at the inlet for the rest of the channels is 0.9 times lower than that for the center channel. Therefore, β_{max} in this case can be calculated by the following formula:

$$\beta_{max} = \frac{g_i A_i}{s(g_i+g_j)\Delta x}$$

$$= \frac{0.9A_i}{s(1.1+0.9)\Delta x}$$

$$= \frac{0.9 \times 0.00094}{\frac{0.122}{12} \times (1.8) \frac{5.76}{12}}$$

$$= 0.097 \qquad \text{(F.2.2.1)}$$

If the half-sized channels are used for the center channel to calculate the coupling coefficients, the limiting β occurs in the half sized channel adjacent to the high flowrate channels. Hence the β_{max} can be calculated as follows:

$$\beta_{max} = \frac{g_i A_i}{2s(g_i+g_j)\Delta x}$$

$$= \frac{1.0 \times 0.00094}{2 \times \frac{0.122}{12} (1.0+1.1) \times \frac{5.76}{12}}$$

$$= 0.046 \qquad \text{(F.2.2.2)}$$

F.2.3 Power Upset Case

In this case, the β_{max} is the same as that in the enthalpy upset case.

F.2.4 Power and Flow Upset Case

In this case, the β_{max} is the same as that in the flow upset case.

APPENDIX G

METHODS TO ANALYZE HOMOGENIZED REPRESENTATIONS, MULTI-SUBCHANNEL REPRESENTATIONS AND TO COMPUTE $N_H(z)$

The purpose of this appendix is to illustrate the method to compute the multi-subchannel results, the homogenized results and the coupling coefficients. The procedure to obtain the multi-subchannel and homogenized results is discussed in section G.1. The input data for the homogenized representations which can be determined from the input data for the multi-subchannel representations are discussed in section G.2. Finally, the code changes are briefly discussed in section G.3 on the modifications made to fulfill the computations required in this thesis.

G.1 Procedures

COBRA IIIC/MIT version is used in this thesis to analyze the coupling coefficient N_H in the energy conservation equation. The steps to accomplish this purpose are listed below:

1) Run a multi-subchannel case to obtain
   a) Multi-subchannel results - the average parameters for the multi-subchannel steps L and R

(refer to Figure 3 for subscripts L and R).

b) Coupling Coefficients - The following approximations are made so that coupling coefficients can be obtained from the multi-subchannel computation:

$$\overline{h}_L(z) = H_L(z) \qquad (G.1)$$

$$\overline{h}_R(z) = H_R(z) \qquad (G.2)$$

For instance, N_H is defined in Appendix A as:

$$N_H = \frac{\overline{H}_L - \overline{H}_R}{h_C - h_D} \qquad (A.1.9c)$$

insert (G.1) and (G.2) into (A.1.9c)

$$N_H = \frac{\overline{h}_L - \overline{h}_R}{h_C - h_D} \qquad (G.3)$$

so N_H is expressible in the multi-subchannel parameters and can be evaluated in the multi-subchannel computation.

2) Run a homogenized case which lumps N subchannels into two homogenized channels L and R. The conservation equations in this case are modified

according to equations (A.1.7), (A.2.5) and (A.3.5) so as to compute the homogenized results with the coupling coefficients evaluated in step 1.

G.2 Input Data for Homogenized Representations

The relationships between the input data for the homogenized representation and for the multi-subchannel representation are summarized as follows:

$$Q'_L = \sum_{i=A}^{C} q'_i \qquad \text{(G.2.1a)}$$

$$Q'_R = \sum_{i=D}^{F} q'_i \qquad \text{(G.2.1b)}$$

$$A_L = \sum_{i=A}^{C} A_i \qquad \text{(G.2.1c)}$$

$$A_R = \sum_{i=D}^{F} A_i \qquad \text{(G.2.1d)}$$

$$H_L = \sum_{i=A}^{C} m_i h_i \Big/ \sum_{i=A}^{C} m_i \quad \text{at inlet} \qquad \text{(G.2.1e)}$$

$$H_R = \sum_{i=D}^{F} m_i h_i \Big/ \sum_{i=D}^{F} m_i \quad \text{at inlet} \qquad \text{(G.2.1f)}$$

$$G_L = \sum_{i=A}^{C} g_i A_i \Big/ A_L \qquad \text{at inlet} \qquad \text{(G.2.1g)}$$

$$G_R = \sum_{i=D}^{F} g_i A_i \Big/ A_R \qquad \text{at inlet} \qquad \text{(E.2.1h)}$$

From the above relationships, the input data for the homogenized representation can be determined from the input data for the multi-subchannel representation.

G.3 Code Changes

Part of the code has been modified to fulfill the purpose of this thesis. The code changes in the required subroutines are listed as follows:

1) Subroutine EXPRIN - Calculate the parameters in the homogenized representation and the coupling coefficients, i.e., N_H, N_U, N_{TP}, N_{TU} and N_TF.

2) Subroutine SCHEME - Read in the coupling coefficient either in a single value form or in a discrete value form. Calculate $\overline{N}_H$.

3) Subroutines DIFFER and DIVERT - Incorporate the coupling coefficients in the conservation equations.

APPENDIX H

N_H FOR THE HOMOGENIZED CASE COUPLING TWO STRIPS OF UNEVEN NUMBERS OF SUBCHANNELS

For the multi-subchannel strip with uneven subchannel numbers, i.e., coupling two multi-subchannel strips L and R with different number of subchannels, N_L and N_R respectively, the N_H can be derived as follows:

Assume the enthalpy at the center is zero as the reference point and

$$N_{H_L} = \frac{\overline{H}_L}{\overline{h_M}^-} \quad \text{for the multi-subchannel strip L} \tag{H.1}$$

$$N_{H_R} = \frac{\overline{H}_R}{\overline{h_M}^+} \quad \text{for the multi-subchannel strip R} \tag{H.2}$$

where

$h_{M-} \equiv$ enthalpy of the half-sized subchannel in the strip L and adjacent to the strip R

$h_{M+} \equiv$ enthalpy of the half-sized subchannel in the strip R and adjacent to the strip L.

From the definition of N_H

$$N_H \equiv \frac{\overline{H_L} - \overline{H_R}}{h_{m-} - h_{m+}} \tag{H.3}$$

Insert equations H.1 and H.2 into H.3

$$N_H \equiv \frac{N_{H_L} h_{m-} - H_{H_R} h_{m+}}{h_{m-} - h_{m+}} \tag{H.4}$$

Also assume

$$h_{m+} = - h_{m-} \tag{H.5}$$

Then equation (H.4) becomes

$$N_H = \frac{N_{H_L} + N_{H_R}}{2} \tag{H.6}$$

This relationship is expected to be valid as long as N_L and N_R are large enough to make the assumption (H.5) hold and the difference between N_L and N_R is small. An heuristic criteria is suggested to limit the validity of equation (H.6):

$$\frac{|N_L - N_R|}{\min(N_L, N_R)} < 0.3$$

where $\min(N_L, N_R)$ is the smaller number between N_L and N_R.